Computational Study of Self-Assembly in Block Copolymer/Superparamagnetic Nanoparticle Composites under External Magnetic Fields

Vinay Raman

Bachelor of Technology (B. Tech) in Chemical Engineering, Indian Institute of Technology Madras, Chennai, India (2007)

Masters in Chemical Engineering Practice (M.S.C.E.P), Massachusetts Institute of Technology, Cambridge, MA, USA (2009)

Submitted to the Department of Chemical Engineering in partial fulfillment of the requirements for the degree of

Doctor of Philosophy in Chemical Engineering

Massachusetts Institute of Technology

[FEBRUARY 2014]
October, 2013

Signature of the Author..... .....
Department of Chemical Engineering, October 24, 2013

Certified by..... .....
T. Alan Hatton
Ralph Landau Professor of Chemical Engineering Practice
Thesis Supervisor

Certified by..... .....
Bradley D. Olsen
Paul M. Cook Assistant Professor of Chemical Engineering
Thesis Supervisor

Accepted by..... .....
Patrick S. Doyle
Singapore Research Professor of Chemical Engineering
Chairman, Committee for Graduate Students

Computational Study of Self-Assembly in Block Copolymer/Superparamagnetic Nanoparticle Composites under External Magnetic Fields

by

Vinay Raman

Submitted to the Department of Chemical Engineering on October 24, 2013

in Partial Fulfillment of the Requirements for the

Degree of Doctor of Philosophy in Chemical Engineering

Abstract

This computational and theoretical study investigates the self-assembly of superparamagnetic nanoparticles and block copolymers under external magnetic fields. A variety of morphological transitions are observed based on the field orientation, nanoparticle loading, and selectivity of the nanoparticles for the blocks. For symmetric block copolymers, chaining of superparamagnetic nanoparticles under in-plane magnetic fields is shown to achieve long range orientational order of the block copolymer nanodomains and is found to be dependent on nanoparticle size, volume fraction and magnetization strength. A critical selectivity of the particles for one nanodomain is observed, above which strong alignment results and below which comparatively disordered structures are formed. Higher magnetization strengths are found to

reduce equilibrium defect densities in the nematic-isotropic ordering of lamellar thin films, as corroborated by scaling arguments.

For asymmetric coil fractions forming hexagonal block copolymer nanostructure, the in-plane field induced chaining of the nanoparticles selective for the minority block, leads to the formation of stripe phases oriented parallel to the magnetic field. Furthermore, in-plane field induced chaining of nanoparticles selective for the majority block leads to alignment of hexagonal morphology with <100> direction oriented parallel to the external magnetic field. Out of plane magnetic fields induce repulsive dipolar interactions between the nanoparticles that annihilate the defects in the hexagonal morphology of the block copolymer when the nanoparticle is selective for the minority block. Honeycomb lattices are obtained using nanoparticles selective for majority block under out of plane magnetic fields for certain specific nanoparticle loadings. Commensurability of nanoparticle size and loadings with the block copolymer structure is critical in optimizing the ordering of the final composite.

Kinetics of alignment in block copolymer nanocomposites is studied using External Potential Dynamics (EPD) method, wherein an equivalent evolution equation for potential fields is solved instead of conservation equation for the monomer segments. The dynamics study reveals an interesting interplay of nanoparticle mobility, dipolar interaction strength and nanoparticle-polymer interaction strength on the rate of alignment of domains.

Thesis Supervisor: T. Alan Hatton

Title: Ralph Landau Professor of Chemical Engineering Practice

Thesis Supervisor: Bradley D. Olsen

Title: Paul M. Cook Assistant Professor of Chemical Engineering

Dedicated to My Parents

Acknowledgements

First of all, I would like to sincerely thank my advisors Prof. T. Alan Hatton and Prof. Bradley D. Olsen for their unconditional support, guidance and help during my thesis work. The interdisciplinary nature of my research necessitated support and guidance in nanotechnology as well as in soft matter especially polymers. I was fortunate to work with two advisors who are experts in their fields. While I benefitted immensely from Alan's expertise in nanotechnology especially superparamagnetic nanoparticles, my research gained a great momentum with Brad's expertise in block copolymers. Alan was instrumental in getting me started with the project in the first place, after having tried my luck at a couple other projects that did not pan out as expected. I learnt a great deal from Alan's holistic approach of looking at the problems. His comments and views always put my thoughts in perspective and was a great guiding force. His personable nature and calm demeanor is very welcoming, comforting and very encouraging.

I found Brad to be very meticulous and focus-driven advisor; needless to mention his expertise in the field of polymers/soft matter. I learnt a lot from his style of working and basically tried to emulate his approach to problem solving during my thesis. I found his approach of breaking down the whole problem into a bunch of key scientific questions and subsequently directing the research in answering those questions to be exemplary. I followed this approach throughout my research and was quite successful in achieving my goals. My understanding of polymers increased many folds just by discussing my research with him. I immensely benefitted from his hands-on style of working and the great collaborative culture of the Olsen group. His witty, humorous and easy going nature is very likeable and he is a great advisor to work with.

I would like to thank my committee comprising of Prof. Patrick S. Doyle and Prof. Arijit Bose. Their help and guidance during my committee meetings was of great help to fine tune my project.

I would like to sincerely thank both the Hatton and the Olsen group members. Their support and help is very much appreciated. I forged a great working relationship with all my group members. They were all very helpful and easy going. The working atmosphere was very welcoming and encouraging. I sincerely wish to thank my colleague and dear friend, Dr. Seok Joon Kwon of Hatton group for introducing me to the field of phase-field modeling. Discussions with him were very rewarding and we shared great experiences during our research. I convey my heartfelt thanks and my best wishes to him for his career and life. And Thanks to you all (Paul, Demetra, Xiao, Jie, Mao, Lev, and Abhinav) for making my stay at MIT memorable and fun.

I would like to thank all the Olsen group members. Mitchell Wang, Charlotte Stewart-Sloan, Bokyung Kim, Carla Thomas, Matt Glassman, Christopher Lam, and Shenchang Tang were a great support. I immensely benefitted from these gifted individuals and would forever be grateful for their great support. All the Olsen group members were very friendly and their focus and passion towards research is infectious. I feel fortunate to have worked with such smart people in my life.

I would like to thank to my friends, Chaitanya Bandi, Amith Somnath, Abhinav Akhoury, Christopher Lam, and Amar Dani, for their support. Last but not the least; I would like to thank my family (Dr. Raman Gopalan, Sriranjini Raman, and Ajay Raman) for their never-ending love and unconditional support.

Table of Contents

List of Figures

Chapter 1

Current Progress in the Computational Modeling Of Block Copolymer Nanocomposites

1.1 Introduction

Block Copolymers (BCPs) are polymers derived from more than one type of monomeric species. The simplest BCPs are linear diblock copolymers that contain polymer chains of two different types of monomeric species connected together by a covalent bond (Figure 1.1). They cannot undergo macrophase separation, since they are essentially single component systems (due to the covalent bond), unlike a blend of homopolymers. Instead they undergo microphase separation forming a variety of periodic structures (or phases) belonging to different symmetry groups such as lamellar, cylinders, gyroid phases, spheres etc (see Figure 1.1). Thermodynamic incompatibility drives the microphase separation of the diblock copolymer (AB) wherein the contacts between similar blocks (A-A, B-B) are maximized and that between dissimilar blocks (A-B) are minimized respectively. The segregation between the dissimilar blocks is characterized by Flory-Huggins parameter χ_{AB}. The diblock copolymer (AB) is characterized by two other parameters viz. N which is the overall polymerization index or degree of polymerization; and f_A, which is the coil fraction of monomeric species A, defined as $f_A = \frac{N_A}{N}$.

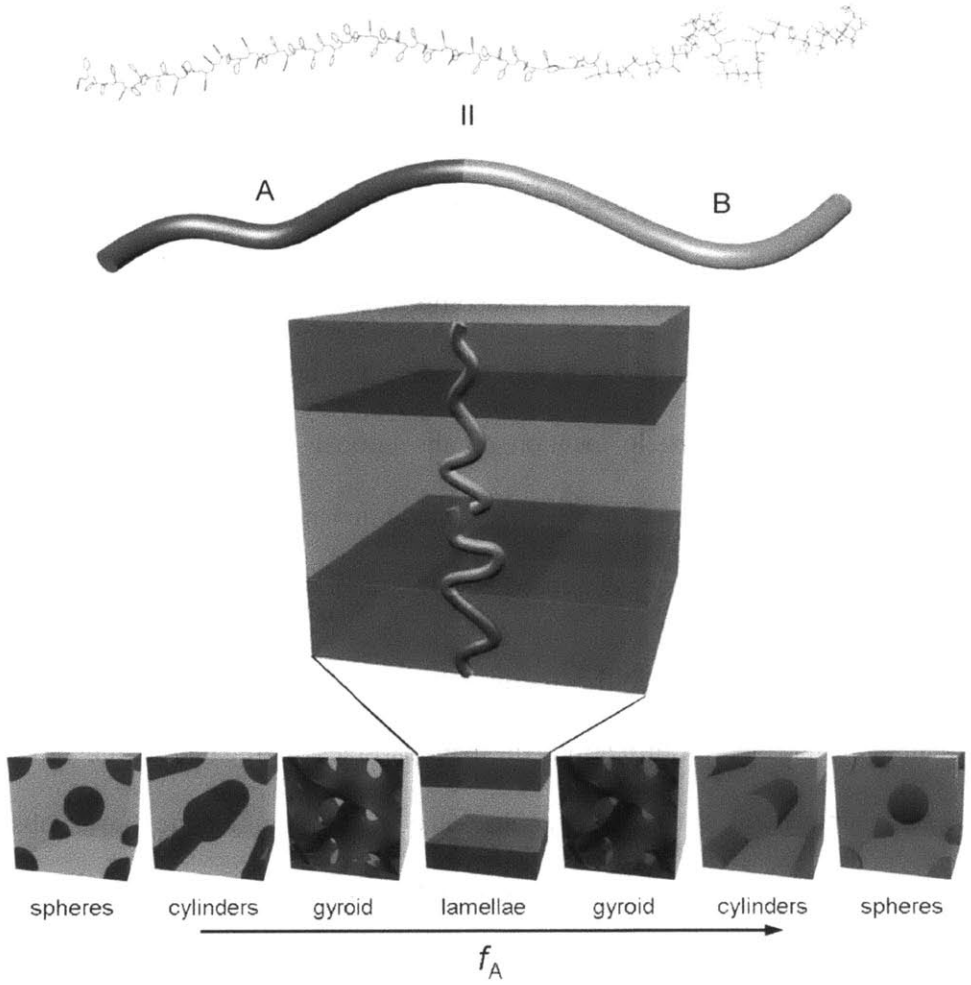

Figure 1.1. Common thermodynamically stable periodic phases of linear diblock copolymer (AB), different structures are obtained upon increasing the coil fraction f_A (*1*).

These periodic micro-domain phases can accommodate nanoparticles of specified affinity paving way for fabrication of novel hierarchically structured nanocomposite materials with properties of both the block copolymer host materials as well as those of nanoparticle inclusions. The ability to control these block copolymer morphologies at length scales of the order of domain sizes combined with the multitude of choices available in terms nanoparticle shape, size

and type, creates exciting new opportunities to engineer these nanocomposite materials for a variety of applications (*2*).

1.2 Localization of Nanoparticles in Block Copolymer Domains

The properties of block copolymer nanocomposites are highly sensitive to the location of the nanoparticles within the block copolymer domains. For instance, Bockstaller and Thomas (*3*) showed the effect of nanoparticle location on the optical properties of the block copolymer nanocomposite. It was demonstrated that nanocomposites, in which nanoparticles were segregated at the interface, showed enhanced absorption of incident light (*3*).

Nanoparticle location can stabilize the morphology of the block copolymer. Kim *et al.* (*4*) showed that, upon surface modification, the nanoparticles segregated at the block copolymer interfaces and behaved as surfactants. A decrease in lamellar thickness was observed, upon addition of such nanoparticle "surfactants" to lamellar forming block copolymer, up to a critical value of nanoparticle volume fraction, beyond which stable bicontinuous morphology was obtained.

Nanoparticle localization can also induce phase transitions in the block copolymers. Kim *et al.* (*5*) showed that localization of gold nanoparticles in the PS domains of the lamellar forming PS-b-P2VP block copolymer in resulted in higher local volume fraction of nanoparticles within the PS domains. This led to a phase transition from lamellar morphology to hexagonal morphology. The lamellar morphology was intact in those regions where the volume fraction of the Au nanoparticles was low. Thus, it is imperative to understand the mechanisms underlying the localization of the nanoparticles within block copolymer domains for an efficient design of

these novel hierarchically structured materials. The localization of the nanoparticles depends two types of nanoparticle BCP interactions viz. (1) Excluded volume interactions or Entropic interactions (2) Enthalpic interactions.

1.2.1 Entropic Effects

The excluded volume interactions between the nanoparticles and the block copolymer play a major role in the location of the nanoparticles within the block copolymer matrix and also affect their dispersion within the domains. Since the nanoparticles are hard solids, the polymer chains have to stretch around these nanoparticles, thereby causing a loss in the conformational entropy of the polymer chains. The elastic free energy cost of placing a single nanoparticle inside a polymer chain is directly proportional to the nanoparticle size (*6*),

$$\Delta E_{br} \cong P(z)\frac{4\pi R_P^3}{3} \tag{1.1}$$

where $P(z)$ is the pressure field at location z from the block copolymer interface. Hence, for larger nanoparticles, the elastic free energy cost is higher due to which they are expelled from the bulk of the block copolymers. This elastic free energy penalty can also cause morphological transitions as shown by Lee *et al.* (*7*), who observed that at fixed diblock copolymer composition, nanoparticle volume fraction and surface affinities, a phase transition is seen from lamellar morphology to cylindrical morphology with increase in nanoparticle size.

Lee *et al.* (*8*) also studied the effect of entropy on the spatial distribution of non-selective nanoparticles in a block copolymer thin film confined between two A-like surfaces. They found that nanoparticles, which are expelled from the bulk of the lamellar forming block copolymer film, segregate at the block copolymer – substrate interface. The nanoparticles at the block

copolymer – substrate mediate the interfacial interactions between the block copolymer film and the substrate and cause a reorientation of the lamellae normal to the A-like walls, which would have otherwise been oriented parallel to the substrate surface in the absence of the nanoparticles.

Excluded volume interactions between the nanoparticles and the block copolymer are significant for sufficiently high volume fractions of the nanoparticles (even for smaller sized ones) and can cause morphological transitions in the block copolymer (Figure 1.2). The effect of nanoparticle volume fraction on the Order to Order Transitions (OOT) has been studied both experimentally (*5, 9*) and theoretically (*10, 11*).

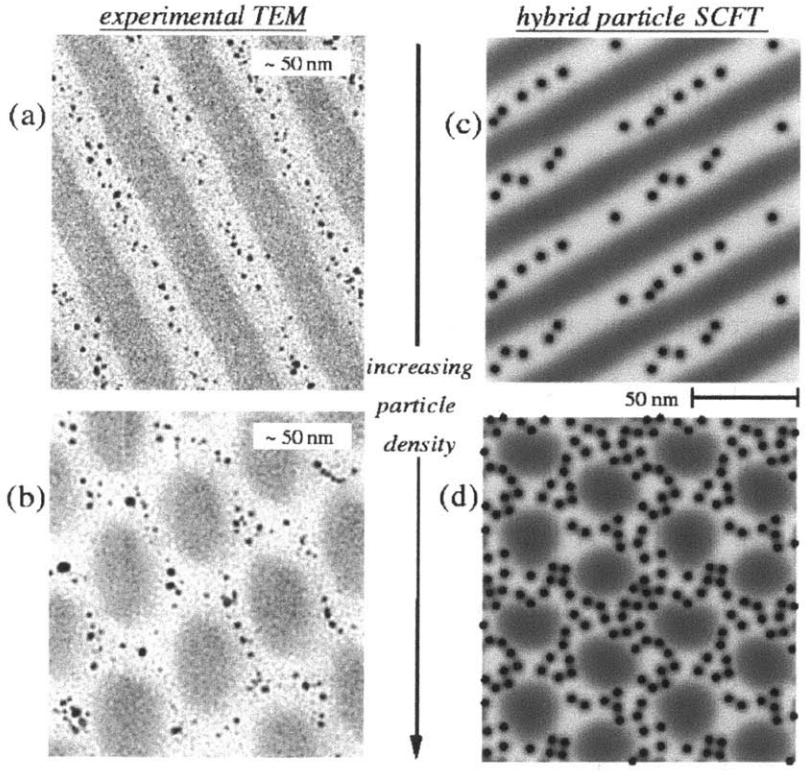

Figure 1.2. Morphological Transitions induced by increase in nanoparticle volume fraction (*11*). (a) and (b) TEM images of Au nanoparticles in the PS domains of PS-b-P2VP; (c) and (d) HPF

simulation results. Upon increasing the volume fraction of Nanoparticles, a phase transition is observed from lamellar phase to hexagonal phase.

1.2.2 Surface Modification of Nanoparticles: Enthalpic Interactions

Enthalpic interactions between the nanoparticles and the block copolymer can be tuned by chemical modification of the nanoparticle surfaces. In a composite made of block copolymer AB and nanoparticles, the nanoparticles are localized in A domains if the nanoparticle surface has favorable enthalpic interactions with A monomers and vice-versa. Hence, one of the strategies to localize the nanoparticles within one of the domains has been to coat the nanoparticle surfaces with homopolymer chains (of lower molecular weight) similar to that of the preferred domains.

Chiu *et al.* (*12*) sequestered Au nanoparticles preferentially one of the domains of poly(styrene-b-2-vinyl pyridine) (PS-b-P2VP) by coating Au nanoparticles with short chains of PS and PVP homopolymers. PS coated Au nanoparticles were localized inside the PS domains of the symmetric PS-b-P2VP block copolymer while PVP coated Au nanoparticles were localized inside the P2VP domains (Figure 1.3).

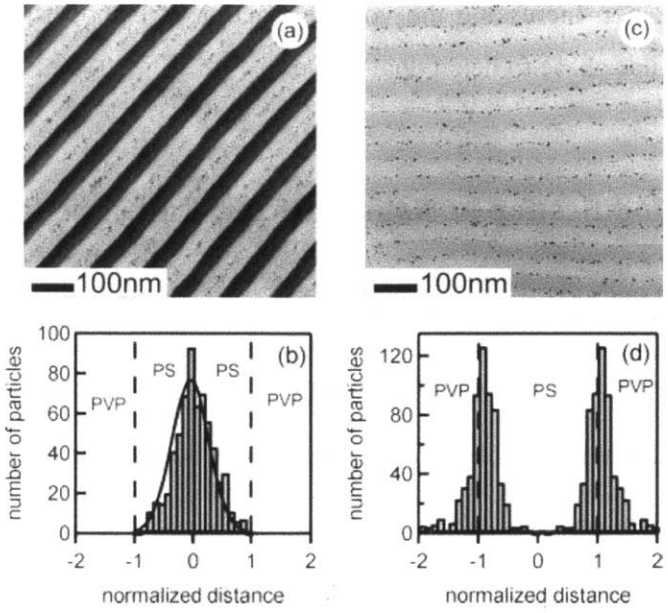

Figure 1.3. Localization of Au nanoparticles by surface functionalization, (a) and (b) PS-coated Au nanoparticles are localized inside PS domains (light regions) of PS-b-P2VP block copolymer, while in (c) and (d) PVP coated Au nanoparticles are found inside P2VP domains; Ref. (*12*).

The nature and the properties of the homopolymer ligands on the nanoparticle surface determine the enthalpic interactions between the nanoparticles and the block copolymer. The strength of these enthalpic interactions can be tuned by changing the areal chain density of the homopolymers ligands on the nanoparticles surfaces (*13, 14*). Higher areal chain density confers stronger interaction between the nanoparticle surface and the preferred domains of the block copolymer, resulting in the sequestration of the nanoparticles in the interior of the BCP domains, while lower areal chain density results in weaker nanoparticle – BCP interactions. Consequently, the nanoparticles are found at the block copolymer interface.

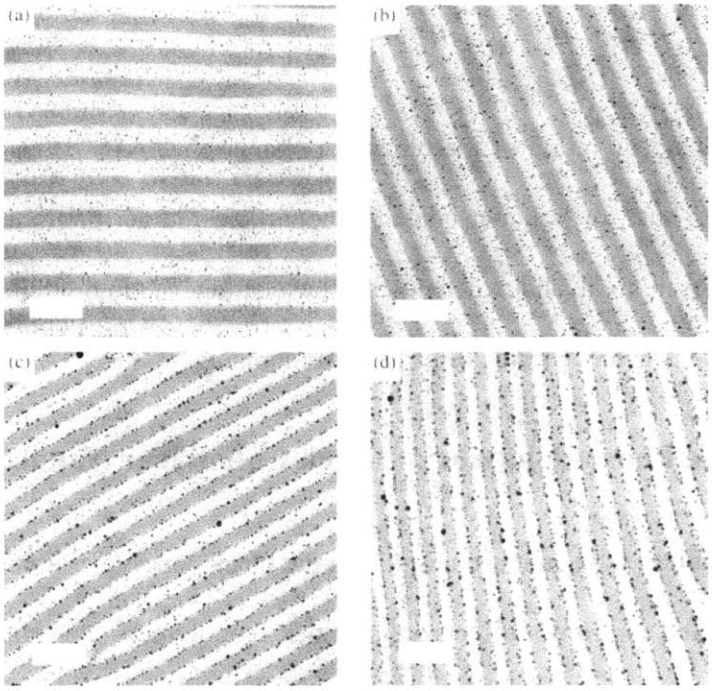

Figure 1.4. Effect of areal chain density of homopolymer ligands on the nanoparticle location in the BCP (*13*), Cross-sectional TEM image of PS-b-P2VP block copolymer with PS coated nanoparticles (M_n of PS coating = 3.4 kg/mol) with differential areal chain densities of the PS coatings (a) 1.64 chains/nm^2, (b) 1.45 chains/nm^2, (c) 1.22 chains/nm^2 and (d) 0.83 chains/nm^2. Scale bar 100 nm.

The molecular weight of the homopolymer ligands plays a major role in determining the strength of the nanoparticle- BCP enthalpic interactions (*14*) as it affects the areal chain density of homopolymer coating. The critical areal chain density, above which the polymer coated nanoparticles are located at the interior of the preferred domains and below which they are located at the block copolymer interface, decreases with increase in molecular weight of the polymer ligand. Kim *et al.* (*14*) found that the critical areal chain density scaled with molecular weight of the polymer ligands as,

$$\Sigma_C \sim R_g^{-1} \sim M_n^{-0.6} \tag{1.2}$$

where R_g is the radius of gyration of the block copolymer chain, M_n is the molecular weight of the polymer ligand. Thus, for polymer coated nanoparticles, larger the molecular weight of the polymer coating, lesser areal chain density of the coating is required for the localizing the nanoparticles within the center of the preferred BCP domains.

1.3 Predicting the Phase Behavior of Block Copolymer Nanocomposites

While the location of the nanoparticles within the block copolymer domains can be tuned by surface chemistry and entropic effects, the block copolymers do not just template the arrangement of the nanoparticles. The nanoparticles can have a significant effect on the morphology of the block copolymers (*15*). Lin *et al.* (*15*) showed that Cadmium Selenide (CdSe) nanoparticles can mediate interfacial interactions between the cylinder forming block copolymer and the substrate, and can cause an orientation of the cylindrical domains normal to the surface even when the majority block is strongly attracting to the substrate. Nanoparticles can act as surfactants and stabilize the block copolymer interface leading to stable bicontinuous morphologies (*4*). Nanoparticles can also control the ordering the block copolymers during solvent annealing by interacting with the solvent vapor (*16*). Park et al. (*16*) showed that the blending of hydrophilic Au-PEO nanoparticles with thin films of PS-b-PMMA block copolymers induced the orientation of PMMA cylindrical microdomains perpendicular to the surface, which would otherwise orient parallel to the substrate surface in the absence of the nanoparticles.

The theoretical and computational research on the self-assembly of block copolymers and nanoparticles have focused on two main aspects: (1) spatial distribution of nanoparticles in the

block copolymer, (2) morphological transitions induced by the nanoparticles. In this section, various computational studies on block copolymer nanocomposites are reviewed.

1.3.1 Spatial Distribution of Nanoparticles in Block Copolymer Domains

The work by Thompson *et al.* (*17*) was one of the first studies to employ an approach combing the SCFT technique with Density Functional Theory (DFT) of nanoparticles to predict the spatial distribution of the nanoparticles within the block copolymer melt. The non-ideal or steric free energy for excluded volume interactions between the nanoparticles, derived by P. Tarazona (*18, 19*) was used. The major prediction from this study was the effect of nanoparticle size and volume fraction on their spatial distribution in the block copolymer melt. It was found that larger nanoparticles caused greater loss in conformational entropy of the block copolymer chains compared to smaller nanoparticles for the same nanoparticle loading. As the volume fraction of the large nanoparticles was increased, they segregated to the central core of the preferred microdomain, while smaller nanoparticles, that have higher translational entropy, were found more uniformly dispersed within the preferred microdomain for same surface affinity of the nanoparticles. In a follow up study (*20*), two different types of self-assembled morphologies were predicted for block copolymer nanocomposites containing selective nanoparticles. These were termed as 'Center-Filled-Lamellar/Cylinder' (CFL/CFC) and 'Edge-Filled-Lamellar/Cylinder' (EFL/EFC). CFL morphologies were found for larger nanoparticles that were segregated to the core, while EFL morphologies were found for smaller nanoparticles.

Thus, the choice of EF or CF morphology depends on the packing considerations of the nanoparticles (entropic effect). Smaller particles can fit in side by side, squeezing the polymer at the center resulting in EF morphologies, while larger nanoparticles cannot fit in side by side and

are found sequestered in the core (*20*). When d/L > 0.3 (d being the nanoparticle diameter, and L is the domain size of the preferred domain), nanoparticles are predicted to be localized at the center of the domain, whereas they move outwards toward the interface for d/L < 0.3 (*21*).

Liu and Zhong (*22*) used Dissipative Particle Dynamics (DPD) simulations to predict the spatial distribution of a binary mixture of nanoparticles in a lamellar block copolymer. They found that nanoparticles segregated in different microdomains based on their surface affinity with the blocks. Moreover, their simulation results showed that for binary nanoparticle mixtures/lamellar copolymer systems, when both types of nanoparticles are compatible with the same block, a trilayer sheet is formed within a single domain, in which larger nanoparticles localize at the center of the domain while the smaller ones are found near interfaces forming a sheet on either side of the larger nanoparticles. Lee *et al.* (*21*) obtained similar results for binary nanoparticle mixtues/block copolymer systems. They studied both cylinder forming block copolymers and lamellar forming block copolymers using SCFT/DFT technique.

Yan *et al.* (*23*) studied the self-assembly of Janus nanoparticles of different geometries (spheres, rods and disks) and looked their interfacial segregation using DPD technique (Figure 1.5). They observed that Janus nanoparticles stabilized the block copolymer interfaces and conferred a control over the shear behavior of the composite and enhanced processing properties of the composite.

Maly *et al.* (*24*) investigated the positioning and ordering of nanoparticles in lamellar forming and cylinder forming block copolymers using DPD technique, wherein the DPD parameters were calculated from the multi-scale modeling approach, using lower scale atomistic simulations. Their results corroborated earlier studies on the effect of nanoparticle coating type

and volume fraction on their positioning in the block copolymer matrices. In addition, they also observed morphological transitions in the block copolymers upon increasing the nanoparticle volume fraction.

Most accurate predictions, till date, of the spatial distribution of nanoparticles in lamellar forming block copolymers has been provided by Matsen and Thompson (*25*) who used a SCFT technique similar to Sides *et al.* (*11*), taking into account the excluded volume interactions between the nanoparticles and the block copolymers. Since, dilute concentrations of nanoparticles were studied, inter-particle interactions were ignored and the nanoparticles were treated as true three-dimensional spheres. Their theory allowed for the bending of the interface with the nanoparticle position. One of their important findings was the strong tendency of the block copolymer interface to follow the position of the particle and its detachment from the nanoparticle.

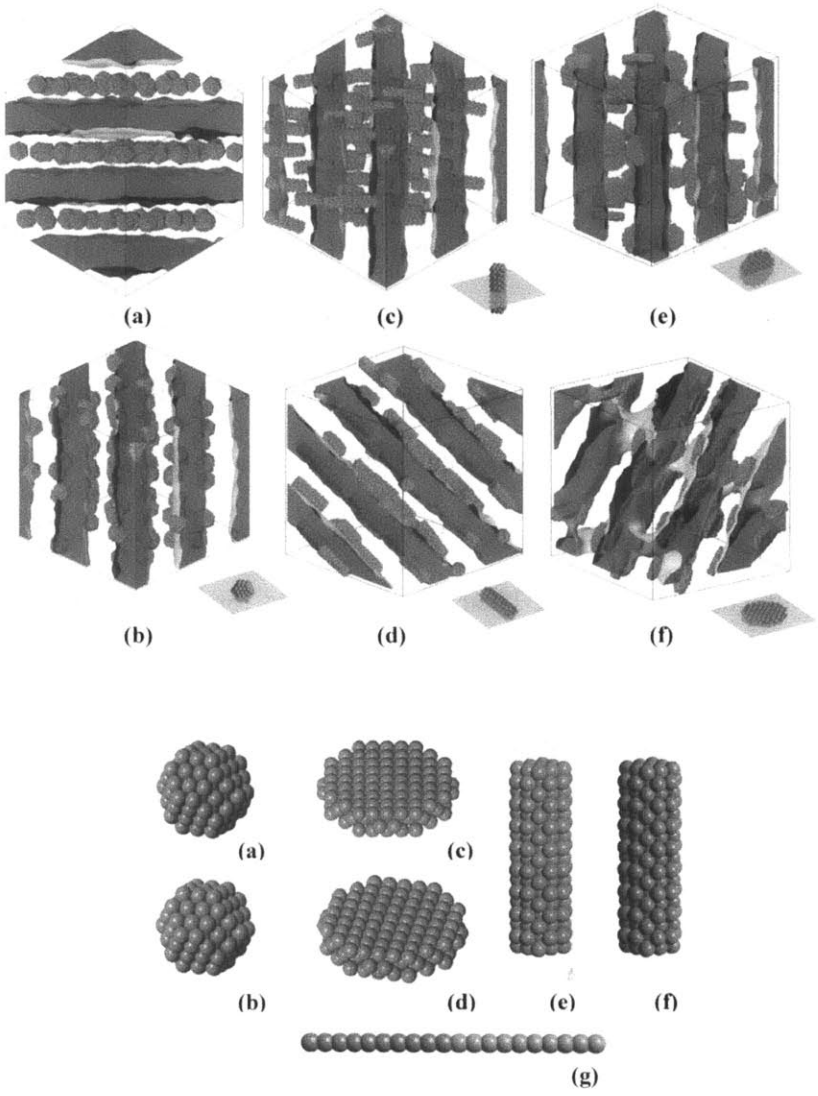

Figure 1.5. DPD study of interfacial stabilization by Janus type nanoparticles (*23*), different geometries of Janus nanoparticles were explored (a), (b) spheres, (c), (d) disks, (e), (f) rods with different types of surface chemistries.

1.3.2 Nanoparticles induced Morphological Transitions in Block Copolymers

The interplay of enthalpic stabilization of nanoparticles and entropic penalty of polymer chain stretching around the nanoparticles causes morphological transitions in block copolymers (*26*). There have been many theoretical and computational studies on the effect of nanoparticle

induced phase transitions in block copolymers (*27*). Schultz *et al.* (*28*) used Discontinuous Molecular Dynamics simulations (DMD) to predict the phase behavior of linear diblock copolymer (AB) nanoparticle mixtures. The interaction strength between the monomer species $\chi_{AB}$and the volume fraction of the nanoparticles was varied to construct the phase diagram (Figure 1.5).

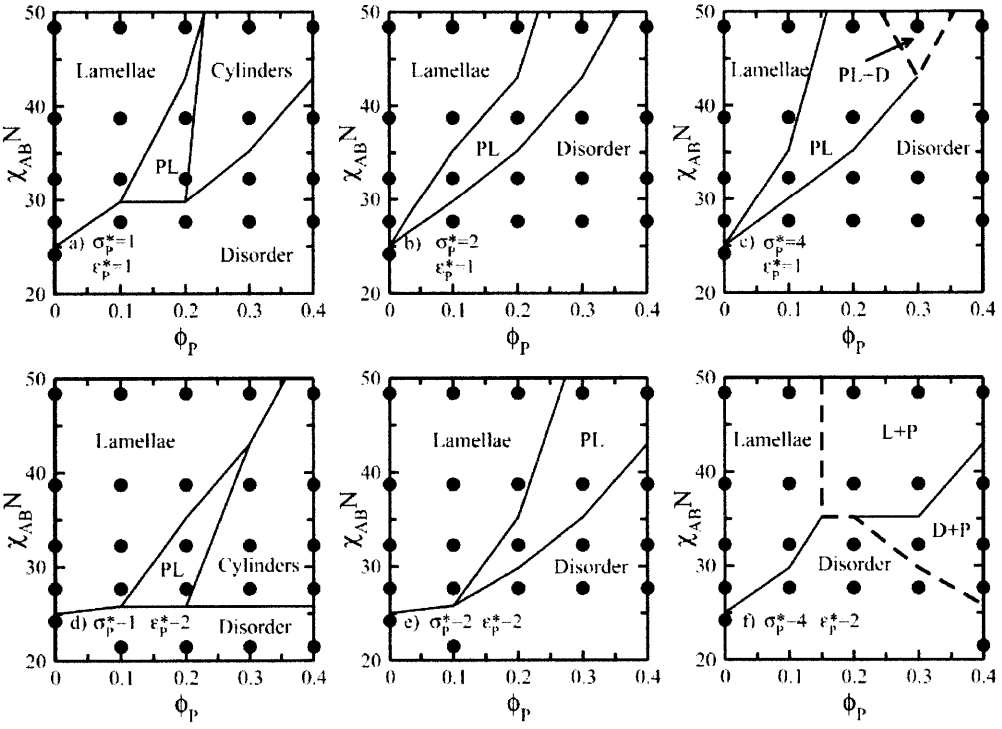

Figure 1.6. Phase diagram for a mixture of linear symmetric block copolymer (f = 0.5) and selective nanoparticles of different sizes σ_P^* and different nanoparticle – block copolymer interaction strengths (ϵ_P^*). The diameter of the nanoparticle is scaled by the diameter of the polymer bead, and $\epsilon_P^* = \frac{\epsilon_{AP}}{\epsilon_{AB}}$. Ref. (*28*).

Their simulation demonstrated the effect of the nanoparticle size and their volume fraction on the Order Disorder Transition (ODT) and Order to Order Transition (OOT) of the

block copolymers. They also showed that neutral nanoparticles were localized at the interfaces while selective nanoparticles were found in the preferred microdomains.

Xu *et al.* (*29*) studied the effect of polymer grafted nanoparticles on the phase transitions in the block copolymer using SCFT. They showed that by controlling the nanoparticle volume fraction, chain length and the grafting density of polymer coating the ordered morphologies (lamellar or hexagonal) of the composite could be controlled, and the spatial distribution of the nanoparticles could be tuned. The nonstructural transitions were attributed to the competition between entropy and enthalpy.

1.3.3 Confinement Effects on Block Copolymer Nanocomposites

The morphology of the block copolymer nanocomposites undergoes a great change upon confinement. Lee *et al.* (*8, 30*) modeled the self-assembly of block copolymer nanoparticle mixtures confined between two parallel hard walls. They considered a mixture linear symmetric diblock copolymers (AB) and hard non-selective nanoparticles confined between two A-like walls. They found that due to enthalpic and entropic interactions, the non-selective nanoparticles are driven to the block copolymer-substrate interfaces. They mediate the interfacial interactions between the block copolymer and the substrate surface, resulting in a reorientation of the lamellae from parallel to perpendicular orientation. The simulations revealed that the polymer mediated depletion attraction between the particles and walls could be used to modify the wetting properties of the substrates and affect the morphology of the composite. This simulation prediction was verified experimentally (*31*). A follow up study by the same group (*32*) used a combination of the computer simulations (SCFT/DFT) and the scaling theory to illustrate the

effect of nanoparticle localization at the block copolymer substrate interface on the wetting properties of the substrate and its subsequent effect on the morphology of the composite.

Pan *et al.* (*33*) investigated the effect of confinement by two concentric circular walls on the block copolymer nanoparticle mixtures using a combination of SCFT and Hybrid Particle-Field (HPF) technique. They observed that increase in nanoparticle concentration favored a phase transition from cylindrical phase to concentric lamellar rings phase or from concentric lamellar rings phase to cylindrical phase. When the separation distance between the concentric circular walls was sufficiently small, they effectively behaved as two parallel walls and perpendicularly oriented lamellar morphology was obtained.

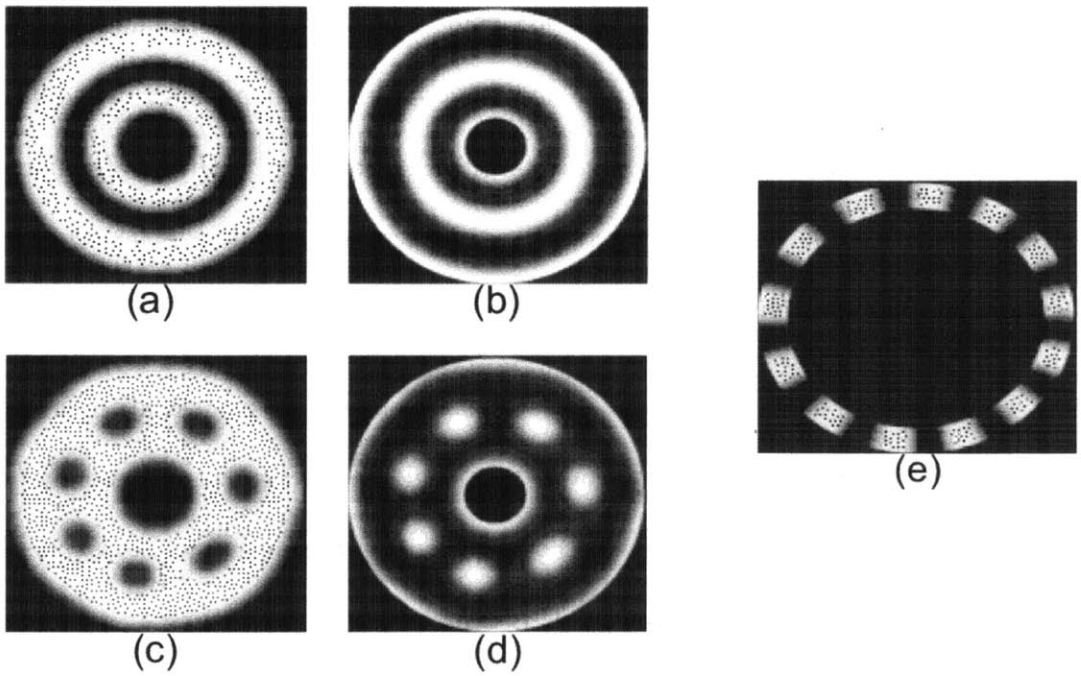

Figure 1.7. Self-assembly of block copolymer nanoparticle mixtures confined between concentric circular A-like walls, (a, b) $f = 0.55$, $r_i = 3.0\ R_g$, $r_o = 6.4\ R_g$, $\Phi_P = 0.06$ (c, d) $f = 0.55$, $r_i = 3.0\ R_g$, $r_o = 6.4\ R_g$, $\Phi_P = 0.23$, (e) $f = 0.55$, $r_i = 5.0\ R_g$, $r_o = 6.4\ R_g$, $\Phi_P = 0.05$; Ref. (*33*).

1.4 Methods to Simulate Self-Assembly in Block Copolymer Nanocomposites

There have been many techniques to simulate the self-assembly in block copolymer nanocomposites. They range from full scale atomistic simulations to continuum methods as mentioned in the previous sections. We briefly overview some of the most popular computer simulation techniques used for block copolymer nanocomposites in this section.

1.4.1 Self-Consistent Field Theory/ Density Functional Theory (SCFT/DFT) Technique

This technique was introduced by Thompson *et al.* (*17, 20*). It combines the SCFT technique for polymers and DFT technique for nanoparticles. A typical simulation considers a mixture of linear diblock copolymer (AB) and solid spherical nanoparticles of radius R. Each diblock copolymer chain consists of N segments with a volume of ρ_o^{-1}. The coil fraction of the A block is denoted by f, while the interactions between the two blocks is represented by dimensionless Flory-Huggins interaction parameter χ_{AB}.

The essence of the "Field theory" is the transformation of the many-body interactions that each monomer segments have with each other to a single interaction that the monomer segment has with the average potential energy field created by the other monomer segments. The free energy of the block copolymer nanocomposite is expressed as,

$$F = F_e + F_d + F_p \tag{1.3}$$

The free energy comprises of three terms, (1) Enthalpic interaction energy (F_e), (2) Diblock Entropic free energy (F_d), (3) Particle Entropic free energy (F_p). The enthalpic (F_e) is given by,

$$F_e = \frac{1}{V}\int d\vec{r}\{\chi_{AB}N\varphi_A\varphi_B + \chi_{AP}N\varphi_A\varphi_P + \chi_{BP}N\varphi_B\varphi_P\} \quad (1.4)$$

V is the volume of the system, $\chi_{AP}$and $\chi_{BP}$are parameters for interaction of the nanoparticles with monomer segments A and B respectively. φ_A, φ_B, and $\varphi_P$are the volume fractions of monomers A, B and the nanoparticles respectively.

The free energy for diblock entropic energy is obtained from the overall partition function of system and the "mean" potential energy fields created by monomers segments A, and B (w_A and w_B),

$$F_d = (1-\Phi_P)ln\left(\frac{V(1-\Phi_P)}{Q_d}\right) - \frac{1}{V}\int d\vec{r}\{w_A\varphi_A + w_B\varphi_B\} \quad (1.5)$$

Q_d is the overall partition function of the block copolymer subject to potential fields w_A and w_B. It is obtained from the solution of modified diffusion equations for chain propagators (see Chapter 2, Hybrid Particle Feld technique section for more details). Φ_P is the overall volume fraction of the nanoparticles.

Finally, the particle entropic free energy is expressed as,

$$F_p = \frac{\Phi_P}{\alpha}ln\left(\frac{V\Phi_P}{Q_P\alpha}\right) - \frac{1}{V}\int d\vec{r}\{w_P\rho_P\} + \frac{1}{V}\int d\vec{r}\{\rho_P\Psi_{hs}(\bar{\varphi}_P)\} \quad (1.6)$$

$Q_P$is the overall partition function of the nanoparticle subjected to the external potential field w_P. $\bar{\varphi}_P$ is the locally averaged volume fraction of the nanoparticles. The local volume fraction of the nanoparticles is obtained from,

$$\varphi_P(\vec{r}) = \frac{4\alpha}{3\pi R^3}\int_{|r'|<R} dr'\rho_P(r+r') \quad (1.7)$$

The parameter α ratio of nanoparticle volume to the volume single block copolymer chain expressed as,

$$\alpha = \frac{4\pi R^3 \rho_o}{3N} = \frac{4\pi}{3}\left(\frac{R}{R_o}\right)^3 \bar{N}^{1/2} \tag{1.8}$$

The relevant length scale of the system is the natural size of the polymer, given by $R_o = aN^{1/2}$ and $\bar{N}(= a^6\rho^2 N)$ is the invariant polymerization index of the block copolymer. The statistical Kuhn length (or the dimension of the single monomer segment) is given by a. F_p essentially describes the steric free energy between the nanoparticles using the Carnahan – Starling approximation, derived by Tarazona (*18, 19*).

The simulation involves calculation of the mean fields w_A, $w_B$and $w_P$using saddle point approximation applied to the free energy functional (equation 1.3) subjected to the incompressibility constraint,

$$\varphi_A(\vec{r}) + \varphi_B(\vec{r}) + \varphi_P(\vec{r}) = 1 \tag{1.9}$$

This yields a set of equations that are solved self-consistently to obtain the equilibrium structures.

1.4.2 Hybrid Particle- Field (HPF) Technique

This technique, introduced by Sides *et al.* (*11*), is the first one to respect the nanoparticles as discrete entities while taking into account all the excluded volume interactions and entropic interactions (monomer/monomer, monomer/nanoparticle). This is accomplished by the use of cavity functions, which simulate the hard sphere nature of the nanoparticles. The cavity functions

are means to represent discontinuities in the continuous potential energy field created by the monomer segments at the nanoparticle locations. We extensively employ this technique in this thesis and more details about its theory and implementation can be found in the next chapter.

1.4.3 Dissipative Particle Dynamics (DPD)

This simulation technique was first developed to simulate hydrodynamic behavior, by Hoogerbrugge and Koelman (*34, 35*). The simulation method monitors the trajectories of 'soft spheres' whose motion is governed by simple collision rules. Polymers are modeled using bead-spring type particles. However, the link between the parameters in this method and the Flory Huggins χ parameters was first established by Groot and Warren (*36*). Following their seminal paper, the DPD technique was widely accepted as one of the popular techniques for simulating polymeric fluids. The DPD technique has also been widely used for simulating block copolymers and block copolymer nanocomposites (*22-24, 37-39*).

We briefly overview the essential features this useful technique in this section. In DPD method, the polymers are modeled as bead-spring type particles. The time evolution of all the particles is governed by Newton's equation of motion. For every time step, the set of particle position vectors and velocities $\{r_i, v_i\}$ are evolved using a modified version of velocity-verlet algorithm (*40*),

$$r_i(t + \Delta t) = r_i(t) + \Delta t.\, v_i(t) + \frac{1}{2}(\Delta t)^2.\, f_i(t) \tag{1.20a}$$

$$\tilde{v}_i(t + \Delta t) = v_i(t) + \lambda.\, \Delta t.\, f_i(t) \tag{1.20b}$$

$$f_i(t + \Delta t) = f_i\big(r_i(t + \Delta t), \tilde{v}_i(t + \Delta t)\big) \tag{1.20c}$$

$$v_i(t+\Delta t) = v_i(t) + \frac{1}{2}.\{f_i(t) + f_i(t+\Delta t)\} \tag{1.20d}$$

The masses of the particles are assumed to be equal to 1, so the forces acting on the particles are equal to their accelerations. If the parameter λ is chosen to be equal to 0.5, the velocity-Verlet algorithm is obtained. But in DPD, λ=0.65 is chosen for accurate temperature control (*37*).

The force $f_i(t)$ in the equations 1.20(a-d), is given by the sum of a conservative force, a drag force and a pair-wise additive random force and a spring force (for polymeric beads),

$$f_i(t) = \sum_j F_{ij}^C + F_{ij}^D + F_{ij}^R + F_{ij}^S \tag{1.21}$$

The particles are modeled as soft spheres and the conservative force F_{ij}^C is given by,

$$F_{ij}^C = -a_{ij}(1 - |r_{ij}|)\hat{r}_{ij}, \qquad if\ |r_{ij}| < 1$$

$$0, \qquad if\ |r_{ij}| > 1 \tag{1.22}$$

a_{ij} is the maximum repulsion between the particles I and j and $r_{ij} = r_i - r_j$, $\hat{r}_{ij} = \frac{r_{ij}}{|r_{ij}|}$. The drag forces and random forces are modeled as,

$$F_{ij}^R = \gamma\omega_{ij}(r)\hat{r}_{ij}\frac{\zeta}{\sqrt{\Delta t}} \tag{1.23}$$

$$F_{ij}^D = -\frac{1}{2}\sigma^2\omega_{ij}^2.(v_{ij}.\hat{r}_{ij})\hat{r}_{ij} \tag{1.24}$$

ζ is a random variable with zero mean and variance 1, and $\sigma^2 = 2\gamma k_B T$, the weighting function $\omega_{ij}(r) = (1 - r_{ij})$ for $r_{ij} < 1$ and equal to zero for $r_{ij} > 1$. The choice of the weighting functions is based on the conservation of the angular momentum for the particles.

In order to map the real polymer onto this model (*36-38*), the compressibility of the polymer is matched by using appropriate values of the repulsion parameter between 'like' particles/beads, a_{ii},

$$a_{ii}\rho = 75\mathrm{k}_B T \tag{1.25}$$

The Flory Huggins χ parameter is matched to the repulsion parameter between 'unlike' particles/beads (*37*), a_{ij},

$$a_{ij} \cong a_{ii} + 3.27\chi_{ij} \; for \; \rho = 3 \tag{1.26a}$$

$$a_{ij} \cong a_{ii} + 1.45\chi_{ij} \; for \; \rho = 5 \tag{1.26b}$$

The reasoning for the choice of these parameters and logic behind this formalism can be found here (*36, 37*).

In addition to these forces, the beads comprising a polymer chain are tied together using a harmonic spring, which is represented by,

$$F_{ij}^{S} = -Cr_{ij} \tag{1.27}$$

C is the spring constant, (= 0 if beads i and j are not connected).

In the simulation, the radius of interaction (R_c), the particle mass (m) and temperature (T) are chosen to be equal 1, and the unit of time is given by,

$$\tau = R_c\sqrt{m/k_BT} \tag{1.28}$$

In case of block copolymer nanocomposites, the size of the nanoparticles and the monomer segments (polymer beads) are different. Hence in the DPD method, all the particles will not have the same sizes and the radius of interaction between the particles of different types will differ (*23*).

1.4.4 Cell Dynamics Simulations (CDS) of Time Dependent Ginzburg-Landau Model (TDGL)

The TDGL model is a microscale method for studying the structural evolution of the block copolymer. It is based on Cahn-Hilliard-Cook model for polymeric systems (*41*). The TDGL model was extended by (*42*) to include the nanoparticles. CDS is a unique and effective method to solve partial differential equations involving Laplacians. This technique was introduced by Oono and Puri (*43*). More details about this technique can be found in Chapter 2.

1.4.5 Other Techniques

In addition to the aforementioned widely used techniques, there have been other computational/theoretical techniques such as (1) Discontinuous Molecular Dynamics simulations (*28*), (2) Monte-Carlo simulations of coarse-grained polymer models (*44*), (3) Strong-segregation theory for block copolymer nanocomposites (*45*) and Potential Distribution Theorem (*46*).

1.5 Treatment of Particle-Particle Interactions

In most of the aforementioned computational studies on the block copolymer nanocomposites, the treatment of the interparticle interactions is almost always absent, primarily due to the fact that most of these studies have involved dilute concentrations of nanoparticles, wherein the interparticle interactions can be ignored to avoid computational costs (*47*). Furthermore, only a few computational/theoretical studies respect the nanoparticles as discrete entities and accommodate for excluded volume interactions between nanoparticles and the block copolymer (*11, 33, 45*).

Particle-particle interactions have to be considered explicitly in order to accurately predict the phase behavior of block copolymer nanoparticle mixtures. Especially, long range interparticle interactions can have a drastic effect on the morphology of the block copolymer (*48*). The role of long range interparticle interactions on the morphology of the block copolymer nanocomposites warrants a detailed study as it opens up another dimension to control the morphology of the block copolymer nanocomposite. The various interactions that exist between particles and the strategies to control these interparticle interactions can be reviewed here (*49*).

1.6 Thesis Goals

The main goal of this thesis is to investigate the effect of dipolar interactions on the morphology of the block copolymer nanocomposite computationally and theoretically. The following chapters consider a mixture of linear diblock copolymer (AB) and superparamagnetic nanoparticles under uniform external magnetic fields. Both thermodynamics of phase separation and kinetics of the self-assembly is given a detailed treatment. This thesis is the first study to

perform mesoscale SCFT simulations for block copolymer superparamagnetic nanoparticle composites considering the nanoparticles as hard spheres and accounting for the excluded volume interactions between the nanoparticles and block copolymers explicitly. The long ranged interparticle interactions are most accurately represented in a bid to delineate their effect on the phase transitions in the block copolymer nanocomposite.

1.7 Conclusions

This chapter provides an overview of the computational and theoretical studies on block copolymer nanocomposites done in the literature so far. The major thrust of all the computational studies has been to predict the spatial distribution of the nanoparticles and phase transitions in the block copolymer due to the complex interplay of enthalpic and entropic interactions between the block copolymer and the nanoparticles. While some studies have accounted for interparticle interactions, most do little justice in accurately representing the exact nature of the interparticle interactions. The paradigm of using the interparticle interactions to control the self-assembly of these nanocomposites and to exploit the symmetries of nanoparticle structures to modify the phase behavior of the block copolymer is relatively new and warrants a detailed study.

1.8 References

1. S. B. Darling, Directing the self-assembly of block copolymers. *Progress in Polymer Science* **32**, 1152-1204 (2007).
2. M. R. Bockstaller, R. A. Mickiewicz, E. L. Thomas, Block Copolymer Nanocomposites: Perspectives for Tailored Functional Materials. *Advanced Materials* **17**, 1331 (2005).

3. M. R. Bockstaller, E. L. Thomas, Proximity Effects in Self-Organized Binary Particle - Block Copolymer Blends. *Physical Review Letters* **93**, 166106 (2004).

4. B. J. Kim, G. H. Fredrickson, C. J. Hawker, E. J. Kramer, Nanoparticle Surfactants as a Route to Bicontinuous Block Copolymer Morphologies. *Langmuir* **23**, 7804-7809 (2007).

5. B. J. Kim, J. J. Chiu, G. R. Yi, D. J. Pine, E. J. Kramer, Nanoparticle-Induced Phase Transitions in Diblock-Copolymer Films. *Advanced Materials* **17**, 2618-2622 (2005).

6. V. Pryamitsyn, V. Ganesan, Strong Segregation Theory of Block Copolymer–Nanoparticle Composites. *Macromolecules* **39**, 8499-8510 (2006).

7. J. Y. Lee, R. B. Thompson, D. Jasnow, A. C. Balazs, Effect of Nanoscopic Particles on the Mesophase Structure of Diblock Copolymers. *Macromolecules* **35**, 4855-4858 (2002).

8. J.-Y. Lee, R. B. Thompson, D. Jasnow, A. C. Balazs, Entropically Driven Formation of Hierarchically Ordered Nanocomposites. *Physical Review Letters* **89**, 155503 (2002).

9. S.-W. Yeh, K.-H. Wei, Y.-S. Sun, U. S. Jeng, K. S. Liang, CdS Nanoparticles Induce a Morphological Transformation of Poly(styrene-b-4-vinylpyridine) from Hexagonally Packed Cylinders to a Lamellar Structure. *Macromolecules* **38**, 6559 (2005).

10. Q. Pan, C. Tong, Y. Zhu, Self-Consistent-Field and Hybrid Particle-Field Theory Simulation of Confined Copolymer and Nanoparticle Mixtures. *ACS Nano* **5**, 123 (2011).

11. S. W. Sides, B. J. Kim, E. J. Kramer, G. H. Fredrickson, Hybrid Particle-Field Simulations of Polymer Nanocomposites. *Physical Review Letters* **96**, 250601 (2006).

12. J. J. Chiu, B. J. Kim, E. J. Kramer, D. J. Pine, Control of Nanoparticle Location in Block Copolymers. *Journal of the American Chemical Society* **127**, 5036 (2005).

13. B. J. Kim, J. Bang, C. J. Hawker, E. J. Kramer, Effect of Areal Chain Density on the Location of Polymer-Modified Gold Nanoparticles in a Block Copolymer Template. *Macromolecules* **39**, 4108-4114 (2006).

14. B. J. Kim, G. H. Fredrickson, E. J. Kramer, Effect of Polymer Ligand Molecular Weight on Polymer-Coated Nanoparticle Location in Block Copolymers. *Macromolecules* **41**, 436 (2007).

15. Y. Lin, A. Boker, J. He, K. Sill, H. Xiang, C. Abetz, X. Li, J. Wang, T. Emrick, S. Long, Q. Wang, A. Balazs, T. P. Russell, Self-directed self-assembly of nanoparticle/copolymer mixtures. **434**, 55-59 (2005).

16. S. C. Park, B. J. Kim, C. J. Hawker, E. J. Kramer, J. Bang, J. S. Ha, Controlled ordering of block copolymer thin films by the addition of hydrophilic nanoparticles. *Macromolecules* **40**, 8119-8124 (2007).

17. R. B. Thompson, V. V. Ginzburg, M. W. Matsen, A. C. Balazs, Predicting the Mesophases of Copolymer-Nanoparticle Composites. *Science* **292**, 2469-2472 (2001).

18. P. Tarazona, A density functional theory of melting. *Molecular physics* **52**, 81-96 (1984).

19. P. Tarazona, Free-energy density functional for hard spheres. *Physical Review A* **31**, 2672 (1985).

20. R. B. Thompson, V. V. Ginzburg, M. W. Matsen, A. C. Balazs, Block Copolymer-Directed Assembly of Nanoparticles: Forming Mesoscopically Ordered Hybrid Materials. *Macromolecules* **35**, 1060 (2002).

21. J. Y. Lee, R. B. Thompson, D. Jasnow, A. C. Balazs, Self-assembly of a binary mixture of particles and diblock copolymers. *Faraday discussions* **123**, 121-131 (2003).

22. D. Liu, C. Zhong, Cooperative Self-Assembly of Nanoparticle Mixtures in Lamellar Diblock Copolymers: A Dissipative Particle Dynamics Study. *Macromolecular rapid communications* **27**, 458-462 (2006).

23. L.-T. Yan, N. Popp, S.-K. Ghosh, A. Boker, Self-assembly of Janus nanoparticles in diblock copolymers. *ACS Nano* **4**, 913-920 (2010).

24. M. Maly, P. Posocco, S. Pricl, M. Fermeglia, Self-assembly of nanoparticle mixtures in diblock copolymers: Multiscale molecular modeling. *Industrial & Engineering Chemistry Research* **47**, 5023-5038 (2008).

25. M. W. Matsen, R. B. Thompson, Particle Distributions in a Block Copolymer Nanocomposite. *Macromolecules* **41**, 1853 (2008).

26. B. J. Kim, J. J. Chiu, G. R. Yi, D. J. Pine, E. J. Kramer, Nanoparticle-Induced Phase Transitions in Diblock-Copolymer Films. *Advanced Materials* **17**, 2618 (2005).

27. L.-T. Yan, X.-M. Xie, Computational modeling and simulation of nanoparticle self-assembly in polymeric systems: Structures, properties and external field effects. *Progress in Polymer Science* **38**, 369-405 (2013).

28. A. J. Schultz, C. K. Hall, J. Genzer, Computer Simulation of Block Copolymer/Nanoparticle Composites. *Macromolecules* **38**, 3007 (2005).

29. G.-K. Xu, X.-Q. Feng, S.-W. Yu, Controllable nanostructural transitions in grafted nanoparticle-block copolymer composites. *Nano Research* **3**, 356-362 (2010).

30. J. Y. Lee, Z. Shou, A. C. Balazs, Modeling the Self-Assembly of Copolymer-Nanoparticle Mixtures Confined between Solid Surfaces. *Physical Review Letters* **91**, 136103 (2003).

31. Y. Lin, H. Skaff, T. Emrick, A. Dinsmore, T. Russell, Nanoparticle assembly and transport at liquid-liquid interfaces. *Science* **299**, 226-229 (2003).

32. J. Y. Lee, Z. Shou, A. C. Balazs, Predicting the morphologies of confined copolymer/nanoparticle mixtures. *Macromolecules* **36**, 7730-7739 (2003).

33. Q. Pan, C. Tong, Y. Zhu, Self-Consistent-Field and Hybrid Particle-Field Theory Simulation of Confined Copolymer and Nanoparticle Mixtures. *ACS Nano* **5**, 123-128 (2010).

34. P. Hoogerbrugge, J. Koelman, Simulating microscopic hydrodynamic phenomena with dissipative particle dynamics. *EPL (Europhysics Letters)* **19**, 155 (1992).

35. J. Koelman, P. Hoogerbrugge, Dynamic simulations of hard-sphere suspensions under steady shear. *EPL (Europhysics Letters)* **21**, 363 (1993).

36. R. D. Groot, P. B. Warren, Dissipative particle dynamics: Bridging the gap between atomistic and mesoscopic simulation. *The Journal of chemical physics* **107**, 4423 (1997).

37. R. D. Groot, T. J. Madden, Dynamic simulation of diblock copolymer microphase separation. *The Journal of chemical physics* **108**, 8713 (1998).

38. R. D. Groot, T. J. Madden, D. J. Tildesley, On the role of hydrodynamic interactions in block copolymer microphase separation. *The Journal of chemical physics* **110**, 9739 (1999).

39. L. He, L. Zhang, H. Liang, The effects of nanoparticles on the lamellar phase separation of diblock copolymers. *The Journal of Physical Chemistry B* **112**, 4194-4203 (2008).

40. M. P. Allen, D. J. Tildesley, *Computer Simulation of Liquids*. (Clarendon, Oxford, 1987).

41. Q. H. Zeng, A. B. Yu, G. Q. Lu, Multiscale modeling and simulation of polymer nanocomposites. *Progress in Polymer Science* **33**, 191-269 (2008).

42. V. V. Ginzburg, F. Qiu, M. Paniconi, G. Peng, D. Jasnow, A. C. Balazs, Simulation of Hard Particles in a Phase-Separating Binary Mixture. *Physical Review Letters* **82**, 4026-4029 (1999).

43. Y. Oono, S. Puri, Study of phase-separation dynamics by use of cell dynamical systems. I. Modeling. *Physical Review A* **38**, 434-453 (1988).

44. F. A. Detcheverry, H. Kang, K. C. Daoulas, M. Müller, P. F. Nealey, J. J. de Pablo, Monte Carlo simulations of a coarse grain model for block copolymers and nanocomposites. *Macromolecules* **41**, 4989-5001 (2008).

45. V. Pryamitsyn, V. Ganesan, Strong Segregation Theory of Block Copolymer - Nanoparticle Composites. *Macromolecules* **39**, 8499 (2006).

46. J. Jin, J. Wu, A theoretical study for nanoparticle partitioning in the lamellae of diblock copolymers. *The Journal of chemical physics* **128**, 074901 (2008).

47. M. W. Matsen, R. B. Thompson, Particle distributions in a block copolymer nanocomposite. *Macromolecules* **41**, 1853-1860 (2008).

48. G. He, A. C. Balazs, Modeling the Dynamic Behavior of Mixtures of Diblock Copolymers and Dipolar Nanoparticles. *Journal of Computational and Theoretical Nanoscience* **2**, 99 (2005).

49. A. Yethiraj, Tunable colloids: control of colloidal phase transitions with tunable interactions. *Soft Matter* **3**, 1099-1115 (2007).

Chapter 2

Simulation Methods: Theory and Algorithms

2.1 Introduction

There has been tremendous interest in polymer nanocomposites over the last few decades due to their enhanced properties (*1*). Computational modeling of polymer nanocomposites has received great attention recently, due to difficulties in manipulating the fabrication of novel functional composites by empirical approaches. The structure-property relationships of polymer nanocomposites are being studied in great detail, and there is a growing need for precise estimation of properties given their structure and vice-versa. This has sparked interest in development of novel computational methods for studying the thermodynamics and kinetics of formation of polymer nanocomposites, the molecular origins of their enhanced properties, and their rheological behavior.

This thesis focuses on the hierarchical structure of block copolymer nanocomposites, and hence involves multi-scale modeling at different length and time scales. The nanoparticles are modeled as discrete entities, while the block copolymer is modeled as a continuum. The bridging of two length and time scales is accomplished by a hybrid technique (*2*) that combines the continuum field theories of the block copolymer with the Brownian dynamics simulations of the nanoparticles. Both thermodynamics and alignment kinetics of block copolymer nanocomposites, subjected to external magnetic fields, are studied. First, the thermodynamic equilibrium structures are predicted using Hybrid Particle-Field technique (HPF) introduced by

Sides et al. (*2*). Second, the alignment kinetics are probed using External Potential Dynamics (EPD) method introduced by Maurits and Fraaije (*3*). The EPD method is extended to include "hard spherical" nanoparticles using a cavity function approach (*2, 4*).

2.2 Theory

2.2.1 Hybrid Particle-Field (HPF) Theory

We use the real-space Hybrid Particle-Field (HPF) approach (*2*), to model the self-assembly of a diblock copolymer nanoparticle mixture in the melt state. We consider a mixture of linear diblock copolymer AB (of coil fraction *f*) and superparamagnetic nanoparticles of radius R_P, where the local volume fraction of the particles is given by,

$$\varphi_P(\vec{r}) = \sum_{j=1}^{N_P} h\left(\left|\vec{r} - \vec{r}_j\right|\right) \tag{2.1}$$

where $h\left(\left|\vec{r} - \vec{r}_j\right|\right)$ represents the cavity function (*2*) that excludes the polymer chains from the inside of the particles upon the enforcement of the local incompressibility constraint, $\varphi_A + \varphi_B + \varphi_P = 1$. The total number of nanoparticles (N_P) is known from the total volume fraction of the nanoparticles (Φ_p). The cavity function is given by (*5*),

$$h\left(\left|\vec{r} - \vec{r}_j\right|\right) = \frac{1}{2}\left(1 + \tanh\left(\frac{\epsilon - \left(\left|\vec{r} - \vec{r}_j\right| - R_p\right)}{\epsilon}\right)\right) \tag{2.2}$$

where ϵ is the thickness of the diffuse layer around the nanoparticle, over which the local volume fraction of the nanoparticle decays smoothly from 1 to 0 and R_p is the radius of the nanoparticle. Another form for the cavity function $\left(\frac{1}{2}\left(1 + cos\left(\frac{\pi\left(\left|\vec{r} - \vec{r}_j\right| - R_p\right)}{\epsilon}\right)\right)\right)$ that assumes a

smoothly decaying cosine profile (*6*) was also tested in this study and it was shown not to change the qualitative nature of the results. Smooth profiles for cavity functions with finite width are known to have better convergence results (*7*) and also partly take into the account the nature of the 'soft' surface due to the ligands attached on the nanoparticle surface that controls the relative affinity of the nanoparticle for each of the blocks in the diblock copolymer.

In the SCFT/HPF theory, the dimensionless free energy of the symmetric diblock copolymer in real-space is given by (*8*),

$$\frac{NF_{AB}}{\rho_o k_B TV} = -(1-\Phi_P)ln\left(\frac{Q_{AB}}{V(1-\Phi_P)}\right)$$

$$+\frac{1}{V}\int d\vec{r}\begin{pmatrix}\chi_{AB}N\varphi_A\varphi_B + \chi_{AP}N\varphi_A\varphi_P + \chi_{BP}N\varphi_B\varphi_P - w_A\varphi_A - w_B\varphi_B \\ -\Xi\cdot(1-\varphi_A-\varphi_B-\varphi_P)\end{pmatrix}$$

(2.3)

F_{AB} is the total free-energy of the symmetric diblock-copolymers (AB) with fixed nanoparticle (P) positions in a system of volume V, N is the polymerization index of the block-copolymer, ρ_o is the total monomer number density, Φ_P is the total volume fraction of the nanoparticles, T is the absolute temperature of the system, k_B is the Boltzmann constant, χ_{MN} is the Flory-Huggins interaction parameter for species (M, N), $\varphi_A(\vec{r})$, $\varphi_B(\vec{r})$, and $\varphi_P(\vec{r})$ are the local volume fractions of block A, block B and nanoparticles, respectively. We use flexible Gaussian chain model to describe the single chain statistics in which Q_{AB} is the overall partition function of the single diblock copolymer chain given by,

$$Q_{AB} = \int d\vec{r}\, q(\vec{r},1) = \int d\vec{r}\, q(\vec{r},s)q^+(\vec{r},s) \qquad (2.4)$$

The positions of the monomer segments within the symmetric block copolymer are indicated by the scaled contour variable, s, which ranges from 0 to 1 (referring to the two ends of the polymer). $q(\vec{r},s)$ and $q^{+}(\vec{r},s)$ are the probabilities of finding the segment s at position $\vec{r}$ with either end of the diblock copolymer chain free. $w_A(\vec{r})$ and $w_B(\vec{r})$, are the mean chemical potential fields experienced by the polymer segments of A and B, respectively, at position $\vec{r}$, and $\Xi(\vec{r})$ is the Lagrange multiplier which enforces the incompressibility constraint on the free-energy minimization. The Kuhn statistical lengths of the two blocks are assumed to be equal. The chain probabilities are the solutions to the modified diffusion equations given by,

$$\frac{\partial q(\vec{r},s)}{\partial s} = \nabla^2 q(\vec{r},s) - w(\vec{r})q(\vec{r},s) \tag{2.5}$$

$$\frac{\partial q^{+}(\vec{r},s)}{\partial s} = -\nabla^2 q^{+}(\vec{r},s) + w(\vec{r})q^{+}(\vec{r},s) \tag{2.6}$$

with initial conditions $q(\vec{r},0) = 1$ and $q^{+}(\vec{r},1) = 1$, where the chemical potential field $w(\vec{r})$ is given by,

$$w(\vec{r}) = \begin{Bmatrix} w_A(\vec{r}), 0 \leq s \leq 0.5 \\ w_B(\vec{r}), 0.5 < s \leq 1 \end{Bmatrix} \tag{2.7}$$

Minimization of the free energy (equation 2.3) with respect to the variables, $\varphi_A(\vec{r})$, $\varphi_B(\vec{r})$, $w_A(\vec{r})$, $w_B(\vec{r})$ and $\Xi(\vec{r})$ yields the self-consistent field equations given by,

$$w_A(\vec{r}) = \chi_{AB} N \varphi_B(\vec{r}) + \chi_{AP} N \varphi_P(\vec{r}) + \Xi(\vec{r}) \tag{2.8}$$

$$w_B(\vec{r}) = \chi_{AB} N \varphi_A(\vec{r}) + \chi_{BP} N \varphi_P(\vec{r}) + \Xi(\vec{r}) \tag{2.9}$$

$$\varphi_A(\vec{r}) = \frac{(1-\Phi_P)V}{Q_{AB}} \int_{s=0}^{0.5} ds.\, q(\vec{r},s)q^+(\vec{r},s) \tag{2.10}$$

$$\varphi_B(\vec{r}) = \frac{(1-\Phi_P)V}{Q_{AB}} \int_{s=0.5}^{1} ds.\, q(\vec{r},s)q^+(\vec{r},s) \tag{2.11}$$

$$\varphi_A + \varphi_B + \varphi_P = 1 \tag{2.12}$$

The positions of the nanoparticles are evolved using Brownian Dynamics; the updates for nanoparticle positions given by,

$$\Delta\vec{r}_j = \beta D \Delta t. \left\{\vec{F}_{j,poly} + \vec{F}_{j,dipolar}\right\} + \vec{R}_j \tag{2.13}$$

where $\vec{R}_j$ is the Gaussian noise (given by fluctuation-dissipation theorem), which gives the displacement of the nanoparticle j due to Brownian motion, $\beta = \frac{1}{k_B T}$, D is the diffusivity of the nanoparticle, and $\vec{F}_{j,poly}$ is the force due the polymer on the nanoparticle given by,

$$\vec{F}_{j,poly} = \frac{\rho_o}{N} \int d\vec{r}\, \{\chi_{AP} N \varphi_A(\vec{r}) + \chi_{BP} N \varphi_B(\vec{r}) + \Xi(\vec{r})\} \frac{\partial}{\partial \vec{r}_j} h\left(\left|\vec{r} - \vec{r}_j\right|\right) \tag{2.14a}$$

$$\vec{F}_{j,dipolar} = -\frac{\partial V_{dip}}{\partial \vec{r}_j} \tag{2.14b}$$

$\vec{F}_{j,dipolar}$ is the dipolar force due to the magnetic dipole moments. Here V_{dip} is the dipolar energy given by (*9*),

$$\frac{V_{dip}}{k_B T} = \lambda d_p^3 \sum_{i=1}^{N_P} \sum_{j \neq i}^{N_P} \frac{\left(\vec{n}_i.\vec{n}_j - 3.(\vec{n}_i.\hat{r}_{ij}).(\vec{n}_j.\hat{r}_{ij})\right)}{\left|\vec{r}_i - \vec{r}_j\right|^3} \tag{2.15}$$

where $\vec{n}_i$ is the unit dipole moment vector of the particle *i*. The vector is assumed to be in the direction of the magnetic field because the Neel relaxation times of superparamagnetic nanoparticles are much shorter than the time-scales for particle translational motion and polymer relaxation. The dimensionless magnetization strength of the nanoparticle is given by,

$$\lambda = \frac{m^2}{4\pi\mu_o d_p^3 k_B T} \tag{2.16}$$

where m is the magnetic moment of the nanoparticle, d_p is the particle diameter, and $\mu_o$is the permittivity of free space. The long-range nature of the magnetic dipolar potential energy ($\sim 1/r^3$) results in errors when nanoparticles are considered only within a finite cut-off radius for calculation of dipolar forces; these errors can be minimized by using the Ewald summation rule (*10*).

2.2.2 External Potential Dynamics (EPD)

The External Potential Dynamics (EPD) method is used to simulate the dynamics of block copolymers. This technique was introduced by Maurits and Fraaije (*3*) and has been successfully applied to study the dynamics of block copolymers, and vesicle formation in amphiphilic block copolymers (*11, 12*). The EPD method involves the derivation of an equivalent evolution equation for the potential fields, which are conjugate to the densities (or volume fractions) of the monomer segments, from the continuity equations for the densities. The main characteristic of the density functional theory is the bijective property of the density functional, $\rho[U]$, which implies a one-to-one transformation from the potential energy space (U) and the density (ρ) space. This renders flexibility in evolving the dynamics in either space

without compromising on the physics of the system (*3*). It also allows for calculation of the non-local transport coefficient for the Rouse-type dynamics of monomer segments.

. We consider a mixture of linear diblock copolymer AB (of coil fraction *f*) and superparamagnetic nanoparticles of radius R_P whose local volume fraction is given by equation 2.1. The local monomer volume fractions ($\varphi_{I=A,B}$) obey the evolution equation,

$$\frac{\partial \varphi_I(\vec{r})}{\partial t} + \nabla_r . \vec{J}_I = 0 \tag{2.17}$$

Where the density current $\vec{J}_I$ for Rouse-type dynamics is given by,

$$\vec{J}_I = -\mathrm{D}_I \sum_J \int dr' P_{IJ}(r,r') \nabla_{r'} \mu_J(r') \tag{2.18}$$

The chemical potential $\mu_J(r')$ is functional derivative of the free energy with respect to the volume fraction φ_J,

$$\mu_J(r') = \frac{\delta F}{\delta \varphi_J} \tag{2.19}$$

$P_{IJ}(r,r')$ is the non-local transport coefficient for the dynamics of the monomer segment of type I at location (r) influenced by monomer segment of type J at location (r'). It is a two-body correlator and is expressed as (*3*),

$$P_{IJ}(r,r') = -\frac{\delta \varphi_I(r)}{\delta w_J(r')} \tag{2.20}$$

Provided an expression for the free-energy (F) of the system in terms of densities and conjugate potential fields exists, the evolution equation for monomer densities can be effectively transformed into an equivalent equation for the evolution of potential fields (w_J) given by,

$$\frac{\partial w_I}{\partial t} = -D_I \nabla^2 \left\{ \frac{\delta F}{\delta \varphi_I} + \eta_I \right\} \tag{2.21}$$

This transformation (equation 2.21) is applicable for Rouse-type dynamics (*3*). D_I is the diffusion constant of monomer segment of type I and η_I is the Gaussian white noise obeying fluctuation dissipation theorem,

$$\langle \eta_I(r,t) \rangle = 0 \tag{2.22a}$$

$$\langle \eta_I(r,t) \eta_J(r',t') \rangle = \beta \delta(r - r') \delta(t - t') \tag{2.22b}$$

The Gibbs free energy for the block copolymer-nanoparticle composite is given by,

$$\frac{NF_{AB}}{\rho_o k_B T V} = -(1 - \Phi_P) ln\left(\frac{Q_{AB}}{V(1 - \Phi_P)}\right)$$

$$+\frac{1}{V}\int d\vec{r} \begin{pmatrix} \chi_{AB} N \varphi_A \varphi_B + \chi_{AP} N \varphi_A \varphi_P + \chi_{BP} N \varphi_B \varphi_P - w_A \varphi_A - w_B \varphi_B \\ + \frac{k_H}{2} . (\varphi_A + \varphi_B + \varphi_P - 1)^2 \end{pmatrix}$$

(2.23)

The term $\frac{k_H}{2} . (\varphi_A + \varphi_B + \varphi_P - 1)^2$ in the free energy (equation 2.23) accounts for the finite compressibility of the composite. Thus, in the model the overall volume fraction $\varphi_A + \varphi_B + \varphi_P$ deviates from 1, and the penalty for the deviation is given by the compressibility parameter k_H.

Upon substitution of equation 2.23 in equation 2.21, we obtain,

$$\frac{\partial w_A}{\partial t} = -D_A \nabla^2 \{\chi_{AB} N \varphi_B + \chi_{AP} N \varphi_P - w_A + k_H.(\varphi_A + \varphi_B + \varphi_P - 1) + \eta_A\} \tag{2.24a}$$

$$\frac{\partial w_B}{\partial t} = -D_B \nabla^2 \{\chi_{AB} N \varphi_A + \chi_{BP} N \varphi_P - w_B + k_H.(\varphi_A + \varphi_B + \varphi_P - 1) + \eta_B\} \tag{2.24b}$$

Equations 2.24a and 2.24b are solved by Runge-Kutta 4th order method. We invoke the Gaussian chain model to describe the single chain statistics, wherein the chain propagators satisfy the modified diffusion equations 2.5 and 2.6. The volume fractions are calculated from equations 2.10 and 2.11.

2.2.3 Time Dependent Ginzburg-Landau (TDGL) Method

The TDGL method is based on Cahn-Hilliard-Cook (CHC) non-linear diffusion equation for binary blends and is part of general class of models called as phase-field models. The blend composition is the order parameter of this model and the structural evolution of the blend is monitored by the time-evolution of the order parameter using a conservation equation. The TDGL model has also been applied to block copolymers using additional terms in the free energy model that accounts for the connectivity of the blocks (*13-16*).

The dynamics of micro-phase separation for the diblock copolymer can be described by the following TDGL equation for the conserved order parameter (*13, 15*),

$$\frac{\partial \psi(r,t)}{\partial t} = M \nabla^2 \left\{\frac{\delta F}{\delta \psi}\right\} + \eta(r,t) \tag{2.25}$$

Where M is the mobility associated with the order parameter $\psi(r,t)$ defined as the difference in the volume fractions of the two monomer segments,

$$\psi(r,t) = \varphi_A(r,t) - \varphi_B(r,t) \tag{2.26}$$

$\eta(r,t)$ is the Gaussian white noise obeying fluctuation-dissipation theorem (*16*). The free energy functional includes a short range interactions term, a long-range term (*17*) and a polymer-particle coupling interaction term (*18*),

$$F = F_S(\psi) + F_L(\psi) + F_{cpl}\left(\psi, \vec{R}_i\right) \tag{2.27}$$

The short-range term has the following form,

$$F_S(\psi) = \int d\vec{r}\, g(\psi) + \frac{D}{2}|\nabla\psi|^2 \tag{2.28}$$

The term $g(\psi)$ represents the mixing free energy of homogenous blend of disconnected homopolymers A and B, while the gradient term represents the free energy penalty for variations in ψ and D is the diffusion coefficient. The function $g(\psi)$ is given by (*17*),

$$g(\psi) = \frac{1}{2}(-\tau + \alpha(1-2f)^2)\psi^2 + \frac{1}{3}\sigma\psi^3 + \frac{1}{4}\nu\psi^4 \tag{2.29}$$

Where α, σ, ν are phenomenological constants (derived from the vertex functions given by Liebler (*19*) and τ is related to the Flory-Huggins interaction parameter χ,

$$\tau = 8f(1-f)\rho_o\chi - \frac{2s(f)}{f(1-f)N} \tag{2.30}$$

f is the A coil fraction $\left(=\frac{N_A}{N_A+N_B}\right)$, $\rho_o$is the monomer density, N = N_A+ N_B is overall polymerization index of the block copolymer, and *s(f)* is constant of order unity (*17*). The long-range interaction term represents the chain connectivity of the two blocks and is given by (*17*),

$$F_L(\psi) = \frac{\beta}{2}\int d\vec{r}'d\vec{r}G(\vec{r}-\vec{r}')\psi(\vec{r})\psi(\vec{r}') \tag{2.31}$$

β is the strength of long-range interactions and $G(\vec{r}-\vec{r}')$ is the solution to the equation $\nabla^2 G(r) = -\delta(r)$. The parameters α, σ, ν, and β are chosen to obtain a desired phase.

The polymer-particle coupling interaction term is given by (*18*),

$$F_{cpl}(\psi, \vec{R}_i) = \int d\vec{r}\sum_i V(\vec{r}-\vec{R}_i)(\psi(\vec{r},t)-\psi_{Si})^2 \tag{2.32}$$

$\psi_{Si}$is the order parameter at the nanoparticle surface (1 or -1 for preference to A or B block respectively), The function $V(\vec{r}-\vec{R}_i)$ can take the following form,

$$V(\vec{r}-\vec{R}_i) = V_o e^{-\left(\frac{|\vec{r}-\vec{R}_i|}{R_P}\right)} \tag{2.33}$$

Where V_O is the strength of polymer-nanoparticle interaction, R_P is the nanoparticle radius, and $\vec{R}_i$ is the position vector of the nanoparticles which is evolved using Brownian dynamics equation as follows,

$$\frac{\partial \vec{R}_i}{\partial t} = M_P\left(\vec{f}_i - \frac{\partial F}{\partial \vec{R}_i}\right) + \zeta_i \tag{2.34}$$

M_P is the mobility of the nanoparticle, $\vec{f_i}$ is the force on the nanoparticle due to particle-particle interactions (equation 2.15), $\frac{\partial F}{\partial \vec{R_i}}$ is the force on the nanoparticle due to the polymer and ζ_i is the Gaussian white noise obeying fluctuation-dissipation theorem.

2.3.4 Dynamic Self Consistent Field Theory (DSCFT)

We consider a mixture of linear *compressible* diblock copolymer (AB) and superparamagnetic nanoparticles of radius R_P in the melt state. The overall volume fraction of the nanoparticles is given by Φ_P while the local volume fraction of nanoparticles is modeled using cavity functions (*2*). The volume fraction distributions of the monomer segments obey the continuity equations,

$$\frac{\partial \varphi_A}{\partial t} + \nabla . J_A = 0 \tag{2.35}$$

where J_A is the flux of monomer A, given by,

$$J_A(r,t) = -\int_V d\vec{r}\, \Lambda(\vec{r},\vec{r}')\nabla\mu_A(\vec{r}',t) \tag{2.36}$$

The Onsager coefficient $\Lambda(\vec{r},\vec{r}')$ determines the effect of chemical potential gradient at position $\vec{r}'$ on the flux at $\vec{r}$. For local coupling (in incompressible melt), the Onsager coefficient is modeled as a delta function, with its dependence only on local volume fractions of monomer segments,

$$\Lambda(r,r') = DN\varphi_A(r)\varphi_B(r)\delta(r-r') \tag{2.37}$$

This simplifies, the equation for $J_A(r,t)$ as,

$$J_A(r,t) = DN\varphi_A(r)\varphi_B(r)\nabla\mu_A(r,t) \tag{2.38}$$

where D is the single chain diffusion constant and N is the polymerization index of the polymer chain. For more complex cases, the Onsager coefficient is related to the pair correlation function ($P_o(r,r')$) between positions r and r' given by,

$$\Lambda(r,r') = DN\varphi_A(r)\varphi_B(r)P_o(r,r') \tag{2.39}$$

Appropriate models of the pair-correlation function can be used to model Rouse dynamics or reptation dynamics (*20, 21*).

For *compressible* systems we have two equations (I = A, B) instead of one, given below,

$$\frac{\partial\varphi_I}{\partial t} = L_I\nabla.(\varphi_I\nabla\mu_I) \tag{2.40}$$

L_I is a mobility coefficient; the chemical potential $\mu_{A,B}\left(=\frac{\delta F}{\delta\varphi_{A,B}}\right)$ can be found out by equilibrium statistical thermodynamics (*22-24*). For a given volume fraction distribution of monomer segments, we find external potentials U_I (I = A, B) that cause them to be equilibrium distributions. Thus we have,

$$U_I + \frac{\delta F_D}{\delta\varphi_I} = 0 \tag{2.41}$$

where F_D is the free-energy of the block copolymer (the free-energy of interactions between the nanoparticles is independent of monomer volume fractions) from which the chemical potentials can be obtained as $\frac{\delta F_D}{\delta\varphi_I} = -U_I$.

For the given system, the free energy F_D is given by,

$$\frac{NF_D}{\rho_o k_B T V} = -(1-\Phi_P)\ln\left(\frac{Q_{AB}}{V(1-\Phi_P)}\right) + \frac{1}{V}\Big[\int d\vec{r}\,\{\chi_{AB}N\varphi_A\varphi_B + \chi_{AP}N\varphi_A\varphi_P + \chi_{BP}N\varphi_B\varphi_P - w_A\varphi_A - w_B\varphi_B\} + \int d\vec{r}\,\frac{\kappa_H}{2}(\varphi_A+\varphi_B+\varphi_P-1)^2\Big] \quad (2.42)$$

We introduce the Helfand penalty function ($\kappa_H$is the Helfand parameter) to account for the compressibility effects (*25-27*) on the block copolymer around the hard nanoparticles. The penalty function represents the free-energy cost of fluctuations in overall density of the system around the mean bulk density. Thus, the chemical potentials are obtained as,

$$\frac{\mu_A}{k_B T} = -\frac{U_A}{k_B T} = \chi_{AB}N\varphi_B + \chi_{AP}N\varphi_P - w_A^* + \kappa_H(\varphi_A+\varphi_B+\varphi_P-1) \quad (2.43a)$$

$$\frac{\mu_B}{k_B T} = -\frac{U_B}{k_B T} = \chi_{AB}N\varphi_A + \chi_{BP}N\varphi_P - w_B^* + \kappa_H(\varphi_A+\varphi_B+\varphi_P-1) \quad (2.43b)$$

This reduces the evolution equations to the following,

$$\frac{\partial\varphi_A}{\partial\tau} = L_A\nabla.[\varphi_A\nabla\{\chi_{AB}N\varphi_B + \chi_{AP}N\varphi_P - w_A^* + \kappa_H(\varphi_A+\varphi_B+\varphi_P-1)\}] \quad (2.44a)$$

$$\frac{\partial\varphi_B}{\partial\tau} = L_B\nabla.[\varphi_B\nabla\{\chi_{AB}N\varphi_A + \chi_{BP}N\varphi_P - w_B^* + \kappa_H(\varphi_A+\varphi_B+\varphi_P-1)\}] \quad (2.44b)$$

Equations (2.44a and 2.44b) are solved using Runge-Kutta 4th order technique.

The main assumptions of this model are as follows,

1. Chain conformations are represented by Gaussian chain statistics, modeled using path integral formalism

2. Short range interactions are modeled using χ parameters

3. Monomer density distribution governed by simple diffusion equation (relaxation dynamics), with driving force being the gradient the local chemical potential; Hydrodynamic effects are ignored. In other words, the time-scales for fluctuations in the density field (or the volume fraction of monomer segments) is much longer than the time-scales for the chain level dynamics

We start with an initial random distribution of monomer volume fractions. The chemical potentials are obtained using an inverse algorithm (equation 2.41), and then evolution equations are solved to obtain the volume fraction distribution of monomer segments at the next time step. The procedure is repeated. The positions of the nanoparticles are evolved using Brownian dynamics.

2.3 Implementation of Hybrid Particle-Field Theory

Hybrid Particle-Field theory involves solution of SCFT equations (2.8 to 2.12) for every nanoparticle move. In order to get to the final equilibrium structure of the composite, the local equilibrium of polymer segments around the nanoparticle is maintained with every move of the nanoparticles. The nanoparticle positions are evolved using Brownian dynamics (equation 2.14).

For a given distribution of nanoparticles the SCFT equations are solved using the following algorithm,

Step 1: Input the converged potential fields w_A and w_B from the previous BD step; this is used as the initial guess for the converging the SCFT equations for the new particle positions.

Step 2: Calculate the chain propagators by solving the modified diffusion equations (2.5 and 2.6). Calculate Q_{AB}, the overall partition function of the block copolymer.

Step 3: Calculate the volume fractions of the monomer segments for the new chain propagators using equations (2.10 and 2.11).

Step 4: Update the potential fields w_A and w_B and the pressure field $\Xi(\vec{r})$ using the following recipe,

$$w_A^{n+1} = w_A^n + \lambda_m(\chi_{AB}N\varphi_B + \chi_{AP}N\varphi_P + \Xi - w_A^n) \tag{2.45a}$$

$$w_B^{n+1} = w_B^n + \lambda_m(\chi_{AB}N\varphi_A + \chi_{BP}N\varphi_P + \Xi - w_B^n) \tag{2.45b}$$

$$\Xi = \frac{1}{2}\left\{w_A^{n+1} + w_B^{n+1} - \chi_{AB}N\left(1 - \varphi_P\right) - \left(\chi_{AP}N + \chi_{BP}N\right)\varphi_P\right\} \tag{2.45c}$$

Where n is the SCFT iteration number, λ_m is the update parameter, typically chosen as 0.1 to maintain stability of the numerical algorithm. There are other alternate recipes for faster convergence and better stability (*28, 29*).

Step 5: Calculate the free-energy, for the updated potential fields and volume fractions, using equation 2.3 and check for convergence,

$$\left\|w_{A,B}^{n+1} - w_{A,B}^n\right\| < 10^{-4} \tag{2.46}$$

If equation 2.46 is satisfied, then calculate the new positions of the nanoparticles by using the Brownian dynamics equation 2.13.

If equation 2.46 is not satisfied, then repeat steps 2-5 until convergence is achieved

Step 6: Check for incompressibility constraint,

$$\|1 - \varphi_A - \varphi_B - \varphi_P\| < 10^{-4} \tag{2.47}$$

Perform optimum number of SCFT iterations to achieve both convergence (equation 2.46) and to satisfy incompressibility constraint (equation 2.47).

2.3.1 Pseudo-Spectral Operator Splitting Method

The most computationally intensive step in SCFT simulations is the solution of modified diffusion equations (2.5 and 2.6) for calculating the forward (q) and backward chain propagators (q^+). Pseudo-spectral operator splitting method is an unconditionally stable, fast and second order accurate ($O(\Delta s^2)$) and is one of best ways to solve problems involving periodic boundary conditions (*30*). In equation 2.5 (and similarly in equation 2.6), we can identify the linear operator as, $\mathcal{L} = \nabla^2 - w$, hence the solution for the forward propagator can be written as,

$$q(r, s + \Delta s) = e^{\Delta s \mathcal{L}} q(r, s) \tag{2.48}$$

We use the Baker-Campbell-Hausdorff (*29, 30*) identity to simplify the linear operator as follows,

$$e^{\Delta s \mathcal{L}} = \left\{ e^{-\frac{\Delta s}{2} w} e^{\Delta s \left\{ \frac{\partial^2}{\partial x^2} + \frac{\partial^2}{\partial y^2} + \frac{\partial^2}{\partial z^2} \right\}} e^{-\frac{\Delta s}{2} w} \right\} + O(\Delta s^3) \tag{2.49}$$

Equation 2.49 is solved by spectral collocation alternating between real and reciprocal spaces,

$$q(r,s+\Delta s)=e^{\Delta s\mathcal{L}}q(r,s)=\left\{e^{-\frac{\Delta s}{2}w}F^{-1}\left[e^{-\Delta s.k^2}F\left[e^{-\frac{\Delta s}{2}w}q(r,s)\right]\right]\right\} \quad (2.50)$$

Where $F[\Psi]$ implies Fourier transform of function Ψ and k is the wave vector in Fourier space.

2.3.2 Gaussian Quadrature

To calculate the volume fraction of monomer segments A and B using equations 2.10 and 2.11, we use 4[th] order Gaussian quadrature (*30*),

$$\int_0^1 g(s)ds=\Delta s\begin{Bmatrix}\frac{55}{24}g(s_1)-\frac{1}{6}g(s_2)+\frac{11}{8}g(s_3)+g(s_4)\\+g(s_5)+\cdots+g(s_{N_s-5})+g(s_{N_s-4})\\+\frac{11}{8}g(s_{N_s-3})-\frac{1}{6}g(s_{N_s-2})+\frac{55}{24}g(s_{N_s-1})\end{Bmatrix}+O(\Delta s^4) \quad (2.51)$$

Trapezoidal rule was used for calculating the integral for calculation of overall partition function Q.

2.4 Implementation of TDGL Model

Cell dynamics (*31*) methodology is employed to solve the TDGL model (equation 2.25) on a 2D lattice. In cell dynamics method, the evolution of the order parameter (equation 2.25) is expressed as (in the absence of nanoparticles),

$$\psi(r,t+\Delta t)=\psi(r,t)+\Delta t.\{\ll\Gamma\gg-\Gamma\}-\beta\Delta t.\psi(r,t) \quad (2.52)$$

$$\Gamma=-\mathrm{D}\{\ll\psi\gg-\psi\}+(-\tau+\alpha(1-2f)^2)\psi+\sigma\psi^2+\nu\psi^3 \quad (2.53)$$

where $\ll \psi \gg -\psi$ is the discretized version of the Laplacian $\nabla^2\psi$. The choice of $\ll \psi \gg$ discretization determines the isotropy of the observed morphologies (*31, 32*), and is chosen as,

$$\ll \psi \gg = \frac{1}{6}\sum_{NN}\psi + \frac{1}{12}\sum_{NNN}\psi \tag{2.54}$$

where NN refers to nearest neighbors and NNN refers to next nearest neighbors. Other forms of discretized Laplacian can also be used (*33*). The main advantage of this technique is that this is a semi-group discretization of the original Cahn Hilliard equation and hence it allows for much larger time step. Consequently, late stages of phase separation can be explored by this method. A small time step reduces this scheme to a simple Euler scheme (*33*).

2.5 Implementation of Dynamic Self Consistent Field Theory Model

In DSCFT, the main computational step is the calculation of the chemical potentials $\frac{\delta F_D}{\delta \varphi_I}$.

For a given $\hat{\varphi}_A, \hat{\varphi}_B$fields, the chemical potentials (μ_A, μ_B), seen in equation 2.43, are obtained using the routine shown in Figure 2.1. Initially, the pressure fields, the chemical potentials and the volume fractions for the monomer segments are assigned to be zero. Then, the potential fields V_A and V_B are calculated. Subsequently, the volume fractions are obtained, after the solution of modified diffusion equations (2.5 and 2.6), using equation 2.10 and equation 2.11. Then, a check for convergence is performed, $\|\varphi_A - \hat{\varphi}_A\| < \epsilon$, if the calculated volume fractions do not match the target volume fractions then the chemical potentials, and the pressure field are updated and the volume fractions are calculated again for the new potential fields (V_A and V_B). This procedure is repeated until the solution converges. Although, an exact expression for the pressure field $(k_H(\hat{\varphi}_A + \hat{\varphi}_B + \hat{\varphi}_P - 1))$ is known, we let the pressure fields evolve to that final

value starting from zero. This is done for the sake of numerical efficiency and to avoid convergence to unphysical solutions, which is the case when local pressure fields become too large in the nanoparticle locations.

Once the chemical potentials are obtained, the volume fractions of monomer segments are evolved using equation 2.44. Runge-Kutta 4th order technique is used to numerically integrate equation 2.44. The choice of the time-step for the equation 2.44 and time-step for Brownian dynamics depends on the relative mobilities of the nanoparticles and the monomer segments,

$$\frac{\Delta t_{BCP}}{\Delta t_{NP}} = \frac{M_{BCP}}{M_{NP}} \tag{2.56}$$

Thus, the relative mobilities are varied in the simulation by changing the time-steps for updates.

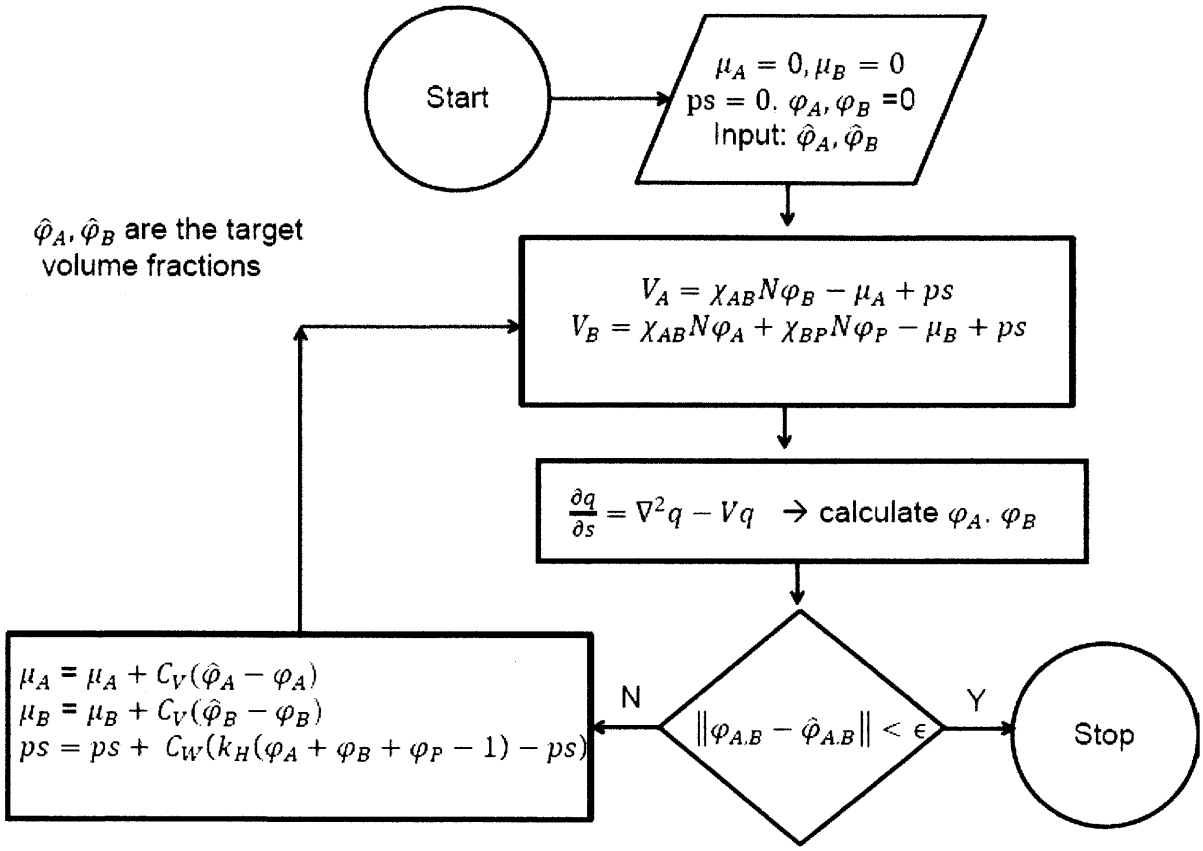

Figure 2.1. Constrained optimization routine to calculate the chemical potentials μ_A, μ_B, the convergence tolerance is set at, $\epsilon = 10^{-3}$.

2.6 References

1. R. A. Vaia, E. P. Giannelis, Polymer Nanocomposites: Status and Opportunities. *MRS Bulletin* **26**, 394-401 (2001)doi:10.1557/mrs2001.93).
2. S. W. Sides, B. J. Kim, E. J. Kramer, G. H. Fredrickson, Hybrid Particle-Field Simulations of Polymer Nanocomposites. *Physical Review Letters* **96**, 250601 (2006).

3. N. Maurits, J. Fraaije, Mesoscopic dynamics of copolymer melts: From density dynamics to external potential dynamics using nonlocal kinetic coupling. *The Journal of chemical physics* **107**, 5879 (1997).

4. D. Meng, Q. Wang, Hard-surface effects in polymer self-consistent field calculations. *The Journal of Chemical Physics* **126**, 234902-234910 (2007).

5. Z. Ma, R. K. Y. Li, Effect of particle surface selectivity on composite nanostructures in nanoparticle/diblock copolymer mixture dilute solution. *Journal of Colloid and Interface Science* **363**, 241-249 (2011).

6. Q. Y. Tang, Y. Q. Ma, Self-Assembly of Rod-Shaped Particles in Diblock-Copolymer Templates. *J. Phys. Chem. B* **113**, 10117-10120 (2009).

7. M. W. Matsen, R. B. Thompson, Particle Distributions in a Block Copolymer Nanocomposite. *Macromolecules* **41**, 1853 (2008).

8. R. B. Thompson, V. V. Ginzburg, M. W. Matsen, A. C. Balazs, Block Copolymer-Directed Assembly of Nanoparticles: Forming Mesoscopically Ordered Hybrid Materials. *Macromolecules* **35**, 1060-1071 (2002).

9. J. P. Huang, Z. W. Wang, C. Holm, Computer simulations of the structure of colloidal ferrofluids. *Physical Review E* **71**, 061203 (2005).

10. Z. W. Wang, C. Holm, Estimate of the cutoff errors in the Ewald summation for dipolar systems. *J. Chem. Phys.* **115**, 6351-6359 (2001).

11. X. He, F. Schmid, Dynamics of spontaneous vesicle formation in dilute solutions of amphiphilic diblock copolymers. *Macromolecules* **39**, 2654-2662 (2006).

12. E. Reister, M. Müller, Formation of enrichment layers in thin polymer films: The influence of single chain dynamics. *The Journal of chemical physics* **118**, 8476 (2003).

13. G. H. Fredrickson, F. S. Bates, Dynamics of Block Copolymers: Theory and Experiment. *Annual Review of Materials Science* **26**, 501-550 (1996).

14. V. V. Ginzburg, F. Qiu, A. C. Balazs, Three-dimensional simulations of diblock copolymer/particle composites. *Polymer* **43**, 461-466 (2002).

15. K. Kawasaki, K. Sekimoto, Concentration dynamics in polymer blends and block copolymer melts. *Macromolecules* **22**, 3063-3075 (1989).

16. D. A. Vega, C. K. Harrison, D. E. Angelescu, M. L. Trawick, D. A. Huse, P. M. Chaikin, R. A. Register, Ordering mechanisms in two-dimensional sphere-forming block copolymers. *Physical Review E* **71**, 061803 (2005).

17. T. Ohta, K. Kawasaki, Equilibrium morphology of block copolymer melts. *Macromolecules* **19**, 2621-2632 (1986).

18. Q. H. Zeng, A. B. Yu, G. Q. Lu, Multiscale modeling and simulation of polymer nanocomposites. *Progress in Polymer Science* **33**, 191-269 (2008).

19. L. Leibler, Theory of Microphase Separation in Block Copolymers. *Macromolecules* **13**, 1602-1617 (1980).

20. M. Müller, F. Schmid, in *Advanced Computer Simulation Approaches for Soft Matter Sciences II,* C. Holm, K. Kremer, Eds. (Springer Berlin Heidelberg, 2005), vol. 185, chap. 136794, pp. 1-58.

21. E. Reister, M. Müller, K. Binder, Spinodal decomposition in a binary polymer mixture: Dynamic self-consistent-field theory and Monte Carlo simulations. *Physical Review E* **64**, 041804 (2001).

22. J. G. E. M. Fraaije, Dynamic density functional theory for microphase separation kinetics of block copolymer melts. *The Journal of Chemical Physics* **99**, 9202-9212 (1993).

23. R. Hasegawa, M. Doi, Adsorption Dynamics. Extension of Self-Consistent Field Theory to Dynamical Problems. *Macromolecules* **30**, 3086-3089 (1997).

24. H. Morita, T. Kawakatsu, M. Doi, Dynamic Density Functional Study on the Structure of Thin Polymer Blend Films with a Free Surface. *Macromolecules* **34**, 8777-8783 (2001).

25. E. Helfand, Block Copolymer Theory. III. Statistical Mechanics of the Microdomain Structure. *Macromolecules* **8**, 552-556 (1975).

26. N. M. Maurits, B. A. C. van Vlimmeren, J. G. E. M. Fraaije, Mesoscopic phase separation dynamics of compressible copolymer melts. *Physical Review E* **56**, 816-825 (1997).

27. Q. Wang, Effects of interaction range and compressibility on the microphase separation of diblock copolymers: Mean-field analysis. *The Journal of Chemical Physics* **129**, 054904-054906 (2008).

28. M. W. Matsen, Fast and accurate SCFT calculations for periodic block-copolymer morphologies using the spectral method with Anderson mixing. *Eur. Phys. J. E* **30**, 361-369 (2009).

29. K. O. Rasmussen, G. Kalosakas, Improved numerical algorithm for exploring block copolymer mesophases. *J. Polym. Sci. Pt. B-Polym. Phys.* **40**, 1777-1783 (2002).

30. T. L. Chantawansri, S.-M. Hur, C. J. Garcia-Cervera, H. D. Ceniceros, G. H. Fredrickson, Spectral collocation methods for polymer brushes. *The Journal of Chemical Physics* **134**, 244905-244914 (2011).

31. Y. Oono, S. Puri, Computationally efficient modeling of ordering of quenched phases. *Physical review letters* **58**, 836-839 (1987).

32. Y. Oono, S. Puri, Study of phase-separation dynamics by use of cell dynamical systems. I. Modeling. *Physical Review A* **38**, 434-453 (1988).

33. P. I. C. Teixeira, B. M. Mulder, sComment on ``Study of phase-separation dynamics by use of cell dynamical systems. I.nModeling". *Physical Review E* **55**, 3789-3791 (1997).

Chapter 3

Orientational Ordering of Symmetric Block Copolymers Using Chaining of Superparamagnetic Nanoparticles under External Magnetic Fields

Reprinted (adapted) with permission from, "Long-Range Ordering of Symmetric Block Copolymer Domains by Chaining of Superparamagnetic Nanoparticles in External Magnetic Fields", V. Raman, A. Bose, B. D. Olsen, T. A. Hatton, Macromolecules 45 (23), 9373-9382

3.1 Introduction

Controlling the order in block copolymer films is an active area of research given the need for precise orientational and translational order of block copolymer domains for applications such as nanolithography (*1*), optoelectronics (*2-4*), functional thin films (*5*) and nanoporous membranes (*6, 7*). A variety of techniques (*1, 8-10*) have been developed to align block copolymers both in bulk and in thin films, including chemical patterning, topographical patterning, electric field alignment, magnetic field alignment, zone casting, directional crystallization, and solvent annealing. Techniques such as chemical patterning (chemoepitaxy) (*11-14*) and topographical patterning (graphoepitaxy) (*15-18*) use a top-down lithographic step to create the guiding patterns on substrates commensurate with the natural periodicity of the block copolymer, and then self-assemble the copolymer within the lithographic pattern. These

techniques have shown great promise for patterning long-range ordered arrays on surfaces (*19, 20*) and for the fabrication of structures useful in patterning microelectronics (*21*).

Shear alignment provides an alternative to epitaxial techniques that enables control over nanodomain orientation without lithographic patterning. Mechanical shear has proven to be a very useful technique for nanodomain alignment both in bulk (*22-28*) and in thin films (*29, 30*). Electric fields provide a complementary alignment technique (*31-34*) capable of aligning nanostructures perpendicular to the film interface. Due to the low dielectric contrast between most polymers, relatively high electric field strengths of up to 30 kV/cm (near the dielectric breakdown limit) are often required (*35*) to align block copolymer thin films. Magnetic field alignment of block-copolymers has also been explored (*36*), motivated by the ability to align samples without contacting the film surface. This technique relies on the difference in magnetic susceptibility between the two blocks. The low contrast in diamagnetic susceptibilities for most block-polymers necessitates high magnetic fields of the order of 5-8 T, achievable mostly by NMR magnets. Several block-copolymers have been aligned successfully using this technique by exploiting complex and specific magnetic moieties (*37*) that increase the contrast in diamagnetic susceptibilities. Solvent annealing (*38-41*), another powerful technique to achieve translational order over large areas, has been applied to align block-copolymers that interact with the solvent. Directional crystallization (*42*) and zone casting (*43*) may also be combined with external fields to achieve 3D ordering of the domains (*44*).

In contrast to the alignment of block copolymers achieved directly using an external field, ordering of block copolymers by exploiting the interactions between a nanoparticle and the block copolymer may be attainable through combining elements of both epitaxial and field-driven approaches. Nanoparticles, which have been traditionally used as fillers to improve the properties

of the polymer-nanocomposites (PNCs) (*45*), have been used to mediate the interfacial interactions (*46*), or interact favorably with the solvent vapor during solvent annealing (*42*), leading to the control of domain orientation. Their effect on ordering can be enhanced by using an external field which can manipulate their position and orientation similar to the orientational ordering of ferronematic liquid crystals under magnetic fields (*47*), as demonstrated using a single rod shaped nanoparticle whose orientation was controlled using an external magnetic field (*48*). However, it is often desirable to use spherical nanoparticles due to their ease of production and precise control of size distribution. In this context, superparamagnetic nanoparticles become ideal candidates for enabling magnetic field alignment in block copolymers with low contrast in magnetic susceptibility. Superparamagnetic nanoparticles align in the direction of an in-plane magnetic field to form long chains (*49*). When sequestered in one of the blocks, these chains could orient the blocks and align them in the direction of the external magnetic field. In addition to ordering, it has been shown in homopolymer/superparamagnetic nanoparticle blends that the mechanical and electronic properties of the composite material are enhanced (*50, 51*) due to the hard, metallic nature of the nanoparticles. For example, chained particles can create pathways for efficient electron transfer resulting in suppression of electron-hole recombination in photovoltaic devices. Recent work on polymer nanocomposites (*52*) has shown that the anisotropy of the nanoparticle assembly can be better tuned by external triggers such as magnetic fields to reinforce the mechanical properties of the polymer matrix.

A generalizable method for aligning block copolymers with superparamagnetic nanoparticles requires a detailed understanding of self-assembly of nanoparticles and block copolymers that includes inter-particle interactions that lead to particle chaining. The spatial arrangement of the nanoparticles within the block copolymer domains is, in itself, an extensive

area of research (*53, 54*), and is known to depend on a variety of parameters such as the surface affinity of the particles, particle size, and incompatibility of the blocks. We extend this framework of self-assembly of non-interacting nanoparticles and diblock copolymers to explore the effect of magnetic dipolar interactions on their self-assembly using the Hybrid-Particle-Field (HPF) technique (*55*), a combination of Self-Consistent Field Theory (SCFT) and Brownian Dynamics, which is a robust technique that allows for accommodating the characteristics of individual particles like size, shape, and anisotropic particle-particle interactions.

This chapter explores the effect of nanoparticle size, magnetization strength, nanoparticle selectivity, and nanoparticle concentration on the chaining of superparamagnetic nanoparticles in the direction of an in-plane external magnetic field to achieve long-range orientational ordering of symmetric diblock copolymer domains in which they are selectively embedded.

3.2 Simulation Methodology

All simulations were performed in two dimensions with periodic boundary conditions. Initially a fixed number of nanoparticles were placed randomly in the simulation box of size $32R_g$. The box size (L) was chosen to be commensurate with the natural periodicity of the diblock copolymer in order to avoid simulation artifacts and was sufficiently large to include a sufficient number of lamellae in the box to show significant orientational ordering. Simulations were performed with random initial guesses (*56*) for the potential fields $w_A(\vec{r})$ and $w_B(\vec{r})$. Accuracy and numerical stability were maintained by using 201 collocation points along the polymer contour length (Δs =0.005), and 256 collocation points for calculating the SCFT equations ($\Delta x = \Delta y = 0.125R_g$). An extended Trapezoidal rule (*57*) was used to calculate the volume fraction of the two monomers which were then used to calculate the new chemical potential fields $w_A(\vec{r})$, and $w_B(\vec{r})$ using the mixing rule prescribed by Rasmussen *et al.* (*58*). The

procedure repeated until $\|F_{AB}^{n+1} - F_{AB}^{n}\| < 10^{-4}$. The tolerance for F_{AB} ensured that the diblock copolymer was relaxed locally with respect to the nanoparticle positions. This reduced errors in the calculation of the forces on the nanoparticles due to the polymer fields. Further lowering of this tolerance ($< 10^{-4}$) had little effect on the morphology of the structure. Once the polymer fields had relaxed to within this tolerance, the forces on the nanoparticles were calculated. The nanoparticle positions were subsequently updated using the Brownian Dynamics (BD) with $\beta D \Delta t$ assumed to be $0.02R_g^2$. For the new set of nanoparticle positions, the SCFT equations were solved again using the above procedure. Free-energy minimization was followed as long as the mean square displacement for the nanoparticle moves was above $10^{-4}R_g$, at which point the morphology was very close to the final equilibrium and the tolerance was further decreased for the calculation of final morphologies. Final equilibrium morphology was attained when $\|F_{AB}^{n+1} - F_{AB}^{n}\| < 10^{-6}$, $\|1 - \varphi_A - \varphi_B - \varphi_P\| < 10^{-4}$ and the mean-square displacement of the nanoparticles was less than $10^{-4}R_g$. Further lowering of these tolerances had little effect on the morphologies obtained.

In this work, the nanoparticle positions $(\vec{r}_j)$ were treated as continuous and the nanoparticle shape and volume were allowed to fluctuate due to mapping of the particle shape onto the discretized collocation grid. When the nanoparticles jumped several lattice points, the total density of the system deviated from 1, which required higher number of SCFT iterations to meet the convergence criteria. This slow convergence problem was circumvented by providing initial guesses for the pressure field based on the new positions of the nanoparticle instead of the old positions, while the converged chemical potential fields, from the previous BD step, were used for the initial guess for these fields. The initial guesses for the pressure field were generated

at the beginning of each SCFT iteration sequence in the following manner. A control simulation of a nanoparticle in a homopolymer melt, with no interaction between the polymer and the nanoparticle, was performed. The pressure field obtained from this simulation gave an estimate for the effect of the particle on the pressure field. During the HPF simulation, after each BD step, an initial guess of pressure field was then obtained by subtracting the particle contribution from the converged pressure field at each of the old particle positions, and adding the pressure field back in, at each of the new particle positions. This had the effect of producing an initial condition for the pressure field that accounted for particle displacement. The chemical potential fields were then calculated based on this initial guess for the pressure field using mixing rule of Rasmussen *et al.* (*58*) and both fields were iterated until convergence. By this method, the residual high pressures in the regions occupied previously by the nanoparticles were automatically changed to low pressures (indicating the absence of nanoparticles) as the nanoparticles moved to different positions, and vice versa. In this manner, rapid convergence of the simulation was achieved.

Each numerical experiment was repeated 3-5 times with different random initial conditions for the nanoparticle positions to ensure reproducibility. Parallel algorithms (*59*) were used to solve the modified diffusion equations on a GPU-based computer, enabling a 15-20 fold speed-up using advanced parallel algorithms tailored specifically for GPU calculations.

3.3 Results

3.3.1 Effect of Dipolar Interaction Strength

Figure 3.1 illustrates the ability of anisotropic nanostructures (chains) of the superparamagnetic nanoparticles sequestered in block A (bright regions) to align the diblock copolymer in the direction of the in-plane external magnetic field. Although the formation of well-ordered lamellar domains with few defects is the thermodynamically favored equilibrium morphology both with and without nanoparticles, SCFT simulations of particle-free lamellar phases often result in relatively disordered structures as shown in Figure 3.1a due to the relatively small energy penalty paid for defect formation and the large kinetic barriers to structural rearrangement. The addition of superparamagnetic nanoparticle chains breaks the rotational symmetry of lamellar orientation, enforcing a preferred orientation and producing a much more ordered structure.

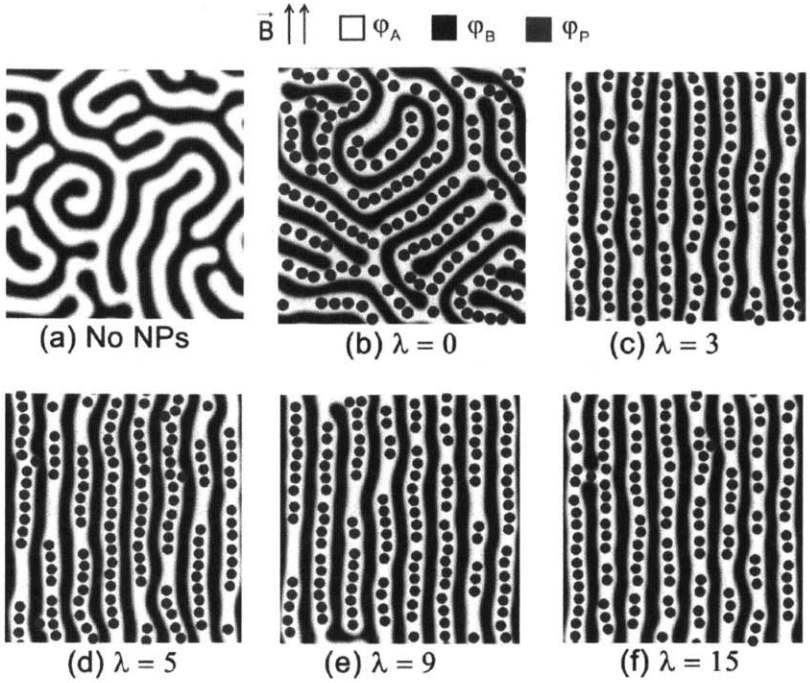

Figure 3.1. Complete alignment of the block copolymer observed at long times (10 000 BD moves), with similar final equilibrium morphology obtained for all nonzero magnetization strengths, $\Phi_P = 0.1$, $R_P = 0.51R_g$, $\chi_{AP}N = 0$, $\chi_{BP}N = 30$, $\chi_{AB}N = 20$, $L = 32R_g$, (a) without nanoparticles/magnetic field, (b) $\lambda = 0$, (c) $\lambda = 3$, (d) $\lambda = 5$, (e) $\lambda = 9$, (f) $\lambda = 15$, magnetic field applied along the y-axis. Bright regions are rich in block A ($\varphi_A \geq 0.5$); dark regions are rich in block B ($\varphi_B \geq 0.5$). Nanoparticles, represented by blue circles ($\varphi_P \geq 0.5$), are seen in block A.

To understand the effect of magnetization strength, the segregation strength between the blocks ($\chi_{AB}N = 20$) and the surface affinities of the nanoparticles toward the two blocks were kept fixed ($\chi_{AP}N = 0$, $\chi_{BP}N = 30$). This segregation can be achieved experimentally using surface ligands on the nanoparticle that are selective for one block but nonselective for the other. The magnetization, characterized by the dimensionless parameter λ, was varied from 3 to 15 to span the typical experimental range, and the nanoparticle size (RP) was kept fixed at 0.51Rg in this set of simulations. Magnetite nanoparticles of diameters 13 and 16 nm have λ values of

about 2.92 and 5.43, respectively, at room temperature (298 K). Much higher values of λ can be attained by decreasing the temperature or using other magnetic compounds, such as Co, as the working material.67 Values of $\lambda > 1$ indicate that the dipole–dipole interaction energy is greater than the thermal energy of the individual nanoparticles which would disrupt the alignment; hence, the nanoparticle chains formed are stable throughout the diblock copolymer alignment process. Magnetite nanoparticles of size 13 nm or higher are known to form chains of indefinite length for $\lambda = 2.69$ (*49, 60*).

At equilibrium, the magnetization strength over the range $3 \leq \lambda \leq 15$ had little effect on the final morphology of the aligned diblock copolymers (Figure 3.1c–e), which looked very similar. However, the final equilibrium morphology with the preferred alignment was obtained in fewer simulation steps at higher magnetization strengths, the faster alignment being due to the stronger driving forces under these higher magnetization strengths. The mechanism of block copolymer alignment by superparamagnetic nanoparticles is governed by the tendency of nanoparticle chains to resist bending against the magnetic field direction. The bending energy penalty encourages the nanoparticles to form straight chains along the direction of the magnetic field and redistributes the polymer segments around the nanoparticles depending on the surface interactions with the diblock copolymer, as illustrated in Figure 3.2. This creates an added energy penalty for defect formation, reducing the number of defects observed at higher magnetic field strengths.

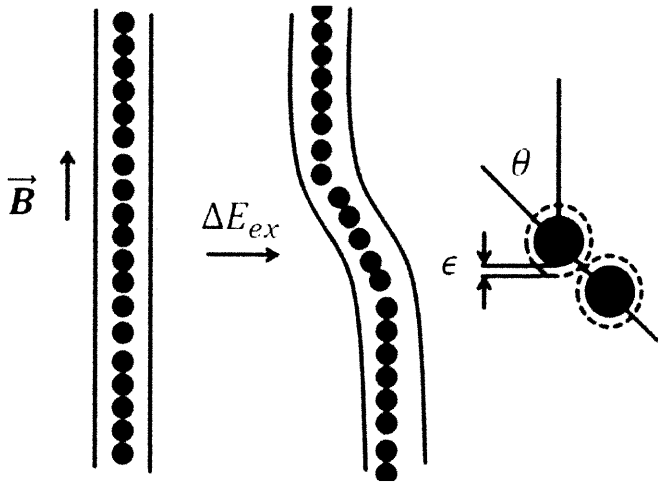

Figure 3.2. Schematic of energy penalty due to deformation of nanoparticle chains in external magnetic fields; d_P is the nanoparticle diameter, and ε is the width of the diffuse layer around the nanoparticle.

3.3.2 Scaling Analysis

Scaling analysis can be used to quantify the effect of the magnetization strength on the number density of defects in the equilibrium structure. It is assumed that each diblock copolymer domain contains a single nanoparticle chain and that the persistence length of the nanoparticle chain is sufficiently long to result in long-range orientational ordering. Under these assumptions, the magnetic dipolar-energy penalty of deformation per unit length of a single-nanoparticle chain is directly proportional to the magnetization strength of the nanoparticles.

The magnetic dipolar interaction energy between two superparamagnetic nanoparticles at their closest distance of separation ($|\vec{r}_i - \vec{r}_j| \sim d_P + 2\epsilon$) is given by,

$$\frac{E_{mag}(\theta)}{k_B T} = \frac{\lambda d_p^3 (1-3\cos^2\theta)}{(d_P+2\epsilon)^3} \tag{3.1}$$

where θ is the angle formed by the unit dipoles of the nanoparticles with the $|\vec{r}_i - \vec{r}_j|$ vector. Since the number of the nanoparticles in the edge dislocation is not known *a priori*, the dipolar

energy is scaled by the number of nanoparticles per unit length ($\sim 1/(d_P + 2\epsilon)$). The magnetic dipolar energy penalty for chain deformation ($E_{mag}(\theta) - E_{mag}(\theta = 0^o)$) is thus obtained as

$$\frac{\Delta E_{ex}}{k_B T} \sim (n-1).\frac{3\lambda d_p^3(1-\cos^2\theta)}{(d_P+2\epsilon)^3} \tag{3.2}$$

where n is the number of nanoparticles in the deformed chain (for a constant defect length, this is inversely proportional to the effective particle diameter, ($d_P + 2\epsilon$)). Therefore, the dipolar energy cost on deforming a single nanoparticle chain in the presence of a magnetic field scales directly with the magnetization strength. This results in less deformation of chains at higher magnetization strengths and hence better alignment of the diblock copolymer domains. Analogies can be drawn between these 2D simulations and monolayers of diblock copolymers, wherein there is an equilibrium number of dislocations below the ODT (*61*). These dislocations are point defects in 2D, and the equilibrium dislocation density scales with temperature as,

$$n_D \sim e^{-\frac{E_D}{k_B T}} \tag{3.3}$$

where E_D is the energy required to create the dislocation. A scaling relationship can be derived for n_D as a function of magnetization strength (λ), by assuming that only edge dislocations are present and only single-nanoparticle chains are considered. For almost all the simulations involving single-nanoparticle chains only edge dislocations were observed at long times, since the energy penalty on deforming a nanoparticle chain to form a +½ or -½ disclination would be very high. For a typical edge dislocation the single nanoparticle chain is deformed with respect to the magnetic field direction (i.e. the *y* axis) by an angle of 60° or 120°. Thus, the deformation of a nanoparticle chain contributes an excess energy (ΔE_{ex}) to the energy of dislocation (E_D) given by,

$$E_D^n = E_D + 2\Delta E_{ex} \tag{3.4}$$

Considering two nanoparticle chains per edge-dislocation (and assuming $\epsilon/d_p \ll 1$), the excess dislocation energy ΔE_{ex} is obtained by substituting $\theta = 60$ or 120°. Thus, the equilibrium number density of dislocations in the diblock copolymer scales as,

$$n_D \sim e^{-a\lambda} \tag{3.5}$$

This analysis implies that higher magnetic field strengths lower the equilibrium dislocation density, but that the effect of increasing magnetic field strength on orientational order should be relatively minor thermodynamically, since all orientations have the same energy. However, higher magnetization strengths help overcome the kinetic trapping of defect laden morphologies.

3.3.3 Effect of Nanoparticle Size

Nanoparticle size plays an important role in directing the orientational ordering of the block copolymer domains. Simulations were performed for four different nanoparticle radii with values of $0.25R_g$, $0.51R_g$, $0.63R_g$, and $1.14R_g$, giving d_P/L_0 ratios of 0.25, 0.51, 0.64, and1.15, respectively (d_P is the diameter of the nanoparticle). L_0 (=1.98Rg) is the half-domain width for the self-assembly of the diblock copolymer in the melt, with $\chi_{AB}N = 20$. The selected values of nanoparticle sizes for which $d_P/L_0 > 0.3$, and a surface affinity of the nanoparticles of $\chi_{BP}N = 30$, ensured that the nanoparticles were distributed at the center of the lamellae and that alignment was not affected by changes in interfacial curvature due to interfacial sequestration of nanoparticles (*53*).

The monodomain character of magnetite nanoparticles is preserved only up to a size of around 15–17 nm (*62*), although this is not a limitation because clusters of superparamagnetic Fe_3O_4 nanoparticles of much larger sizes (~50–200 nm) are known to exhibit superparamagnetic

behavior (*63*). Furthermore, superparamagnetic silica-coated Fe_3O_4 nanoparticle clusters of varying sizes (up to 300 nm) and high saturation magnetization (53.3 emu/g) can be synthesized using the sol–gel approach (*64*). These superparamagnetic nanoparticles are very stable, since they do not cluster through dipole–dipole interactions before the application of a magnetic field, and are ideal for BCP alignment. Figure 3.3 shows the effect of nanoparticle size on the alignment of the diblock copolymer domains.

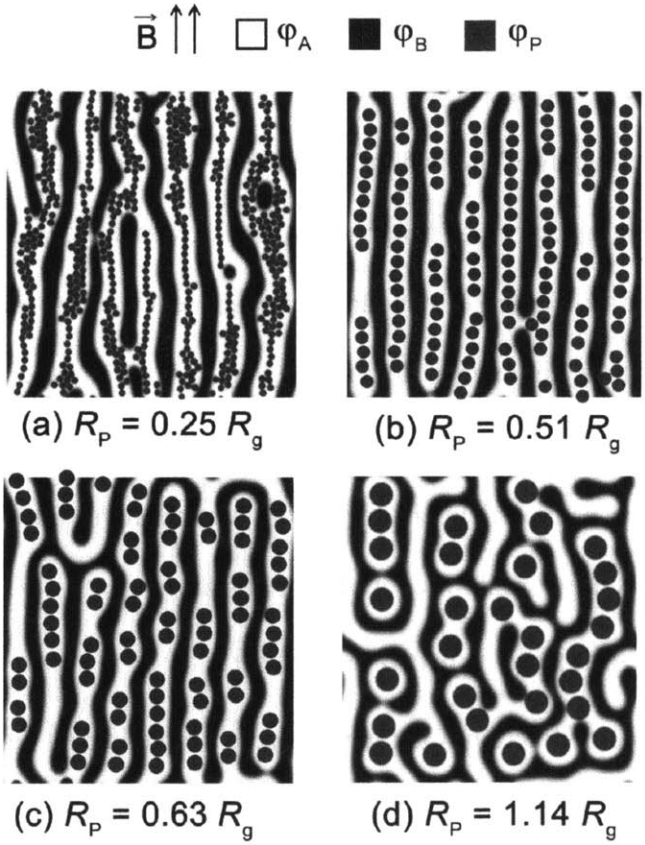

Figure 3.3. Effect of nanoparticle size on the diblock copolymer self-assembly, L = $32R_g$, Φ_P= 0.1, $\lambda = 9$, $\chi_{BP}N = 30$= 30: (a) $R_P = 0.25Rg$ (γ =0.69); (b) $R_P = 0.51R_g$ ($\gamma = 0.91$); (c) $R_P = 0.63\ R_g$ ($\gamma = 0.77$); (d) $R_P = 1.14R_g$ ($\gamma = 0.31$).

Smaller nanoparticles ($0.25R_g$) led to colloidal jamming and kinetic trapping of the diblock copolymer structure with a large number of defects in the structure, even though

macroscopic alignment occurred. Colloidal jamming was verified by a low mean-square displacement of the nanoparticles ($\sim 10^{-4} R_g \ll d_P$) with time at sufficiently long times (~10 000 BD moves). Intermediate nanoparticle sizes ($0.51R_g$ and $0.63R_g$) gave better alignment with fewer defects. When the nanoparticle size became comparable to that of the half-domain width, the curvature of the interface between the blocks was affected by the nanoparticle (Figure 3.3d), and swelling of the domains destroyed the rotational symmetry of the lamellar phase with a consequent loss of orientational order. For a given volume fraction of the nanoparticles, the number density was lower for the larger nanoparticles than for the smaller nanoparticles which reduced the persistence length of the nanoparticle chains. For these shorter persistence lengths, only local alignment, in the regions of nanoparticle chains, was seen. Higher volume fractions of larger nanoparticles did not improve nanodomain alignment because of the nanoparticle size mismatch with the diblock copolymer domain spacing. Thus, intermediate nanoparticle sizes (d_P/L_0 = 0.51, 0.64) gave better alignment and good orientational order due to both the longer persistence length of the nanoparticle chains for the same volume fraction and the absence of colloidal jamming or swelling of diblock copolymer domains.

3.3.4 Effect of Nanoparticle Volume Fraction

Nanoparticle volume fraction was found to have a large impact on the degree of ordering in superparamagnetic nanoparticle/diblock copolymer composites due to the interplay between superparamagnetic nanoparticle chain persistence length and the increasing diblock copolymer swelling with nanoparticle loading. Simulations were performed for different nanoparticle volume fractions (loadings) ranging from 0.04 to 0.18 (Figure 3.4), using an intermediate nanoparticle radius of $0.51R_g$. Low nanoparticle volume fractions resulted in poor alignment even at very long times (~10 000 BD moves), with local alignment seen only in the regions of

short nanoparticle chains due to the relatively short persistence lengths of the chains. As the particle density increased toward the concentration at which a single complete chain formed within each lamellar nanodomain ($\Phi_P \sim 0.1$) for the particle size shown in Figure 3.4), a high degree of ordering was achieved. At higher volume fractions ($\Phi_P \sim 0.18$) an order-to-order (OOT) phase transition was observed from lamellae to the hexagonal phase due to swelling of the A nanodomains, producing a structure that has an effective A block fraction much greater than the B block fraction. Sides *et al.* (*55*) observed a similar OOT due to nanoparticle loadings for non-interacting nanoparticles in their simulations, and these results were confirmed by experiments (*65*).

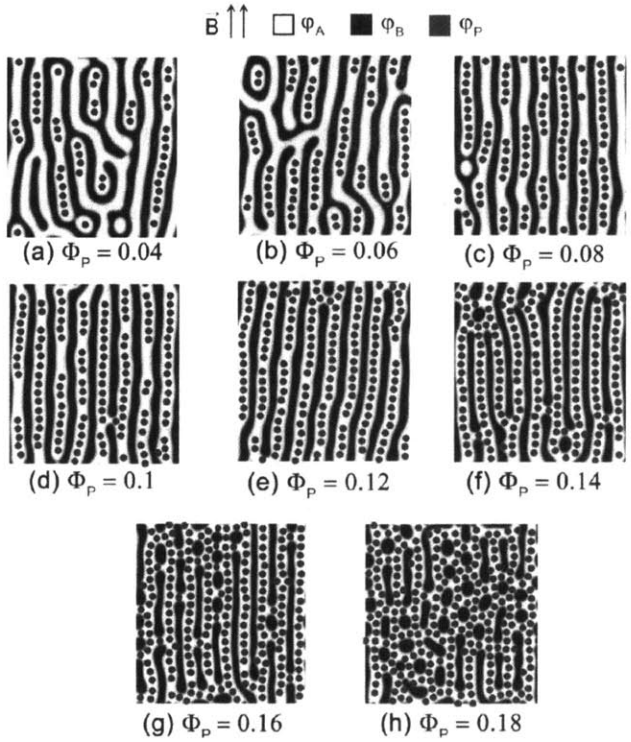

Figure 3.4. Effect of nanoparticle volume fraction on the alignment of diblock copolymer domains, $\lambda = 9$, $\chi_{BP}N = 30$, $R_P = 0.51R_g$, $L = 32R_g$: (a) $\Phi_P = 0.04$, (b) $\Phi_P = 0.06$, (c) $\Phi_P = 0.08$, (d) $\Phi_P = 0.1$, (e) $\Phi_P = 0.12$, (f) $\Phi_P = 0.14$, (g) $\Phi_P = 0.16$, (h) $\Phi_P = 0.18$.

At much higher volume fractions ($\Phi P > 0.2$) macrophase separation of the diblock copolymer and nanoparticle mixture has been predicted (*66*), and hence our simulations were limited to $\Phi P < 0.2$. Because of these competing effects, intermediate volume fractions illustrated in Figure 3.4c–e gave better alignment, albeit with some defects. At a volume fraction of 0.14 (Figure 3.4f), the onset of OOT phase transition was observed, marked by the appearance of circular defects in the lamellar structures. As the volume fraction of particles was further increased (Figure 3.4g, h), hexagonal regions were observed mixed with lamellar structures. In the absence of an applied magnetic field ($\lambda = 0$), a volume fraction of 0.18 yielded a complete hexagonal phase that corroborated results from other studies (*55*). The coexistence of lamellar and hexagonal structures in a single simulation was consistent with the Gibbs phase rule for a two-component system. The fraction of hexagonal structures in the hexagonal–lamellar coexistence region was also influenced by the strength of the magnetic field. This is evident from Figure 3.5a–d, which show the structures formed for a fixed nanoparticle volume fraction of 0.18 with different magnetization strengths. As the magnetization strength increased, stronger dipolar interactions resulted in more rigid and longer nanoparticle chains which made the lamella phase stable at even higher nanoparticle loadings; hence, more lamellar phase was observed at higher magnetization strengths than at lower magnetization strengths.

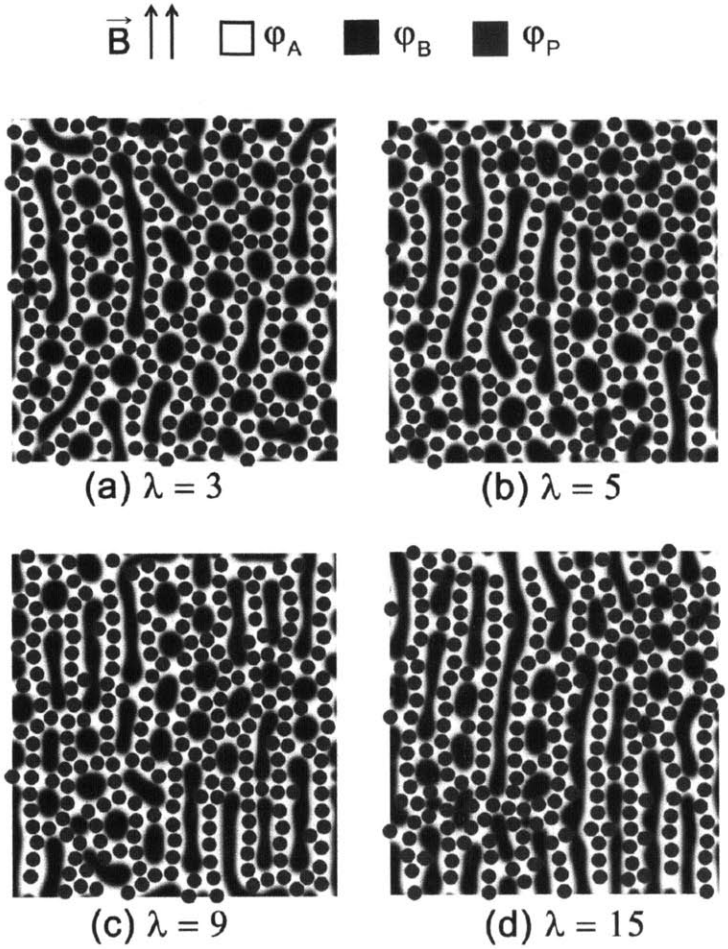

Figure 3.5. Effect of magnetization strength on the OOT: (a) $\lambda = 3$, (b) $\lambda = 5$, (c) $\lambda = 9$, (d) $\lambda = 15$. The nanoparticles (blue circles) were sequestered in block A, and their loading was kept fixed at $\Phi_P = 0.18$. The interaction strength between the nanoparticles and block B was $\chi_{BP}N = 30$, $R_P = 0.51R_g$. More of the lamellar phase was observed for higher magnetization strength.

This type of mixed lamellar–hexagonal phase was not seen with smaller nanoparticles (0.25Rg) in the presence of magnetic fields ($\lambda = 9$). For the smaller particles, the diblock copolymer domains were large enough to accommodate the nanoparticles without causing any significant entropic penalty ($\Delta F_{entropic} \sim (R_P/R_g)^3$), although swelling of the domains was observed. Moreover, colloidal jamming of the nanoparticles due to the higher number density of

nanoparticles for the same nanoparticle volume fraction structurally frustrated the diblock copolymer, preventing it from undergoing OOT and kinetically trapping the diblock copolymer domains in metastable states.

3.3.5 Effect of Nanoparticle–Diblock Copolymer Interactions

In addition to the need for a critical nanoparticle size and a critical nanoparticle loading for effective alignment of block copolymer domains, HPF simulations also suggest that particle/polymer interactions must be carefully tuned to achieve a high degree of diblock copolymer alignment. Simulations were performed keeping the interaction between nanoparticles and block A ($\chi_{AP}N = 0$) fixed while varying the interaction between the nanoparticles and the B block. Figure 3.6 shows the effect of surface interactions of the nanoparticles with block B on the alignment of the diblock copolymer. Neutral particles ($\chi_{BP}N = 0$) resulted in local alignment of the diblock copolymer perpendicular to the applied magnetic field direction, although long-range orientational order was absent. The neutral particles were present mainly at the interfaces between block copolymer nanodomains as predicted by earlier studies (*53, 67*). In addition, the nanoparticle chains tended to coincide with defect-rich regions in the lamellar structures. Similar perpendicular alignment was observed locally for $\chi_{BP}N = 10$. In this case, nanoparticles were found to reside primarily within block A, although there was some distribution of the nanoparticles between this domain and the interface. As $\chi_{BP}N$ increased, good alignment with long-range orientational order in the direction of the applied magnetic field was first observed for $\chi_{BP}N = 22$.

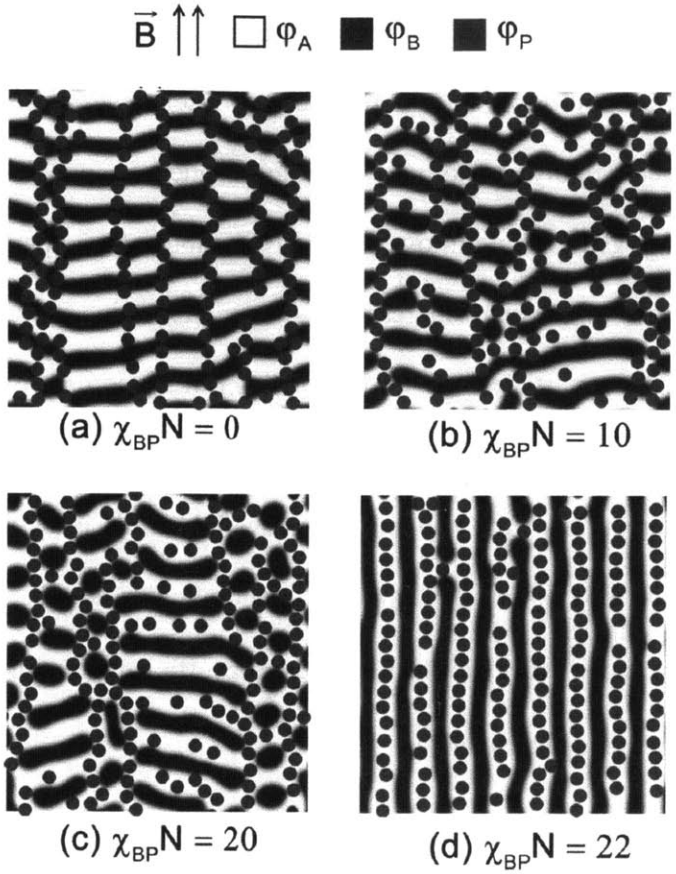

Figure 3.6. Effect of surface affinity of the nanoparticles for the blocks; λ= 9, Φ_P = 0.12, L = $32R_g$, $\chi_{AP}N$ = 0, $\chi_{AB}N$ = 20, R_P = $0.51R_g$: (a) neutral particles (γ = −0.38) and (b) $\chi_{BP}N$ = 10 (γ = −0.21) lead to perpendicular alignment, (c) mixed lamellar−cylindrical phase (γ =−0.12) is observed, (d) good alignment is observed for $\chi_{BP}N$ = 22 (γ =0.86).

With higher interaction strengths (Figure 3.6d), the nanoparticles were sequestered dominantly in the A domains, which aided larger magnetic dipolar interactions between the nanoparticles, leading to local chaining. This local chaining caused redistribution of polymer segments around the nanoparticles, thereby aligning the diblock copolymer along the direction of the chains. For nonselective particles, segregation to the interface between the two block copolymer domains was predominant as noted above and seen in previous studies (*53, 67*). These particles aligned strongly with the magnetic field but did not orient the diblock copolymers in

that direction; on the contrary, alignment perpendicular to the magnetic field direction was observed, yielding a morphology that was unique to nonselective particles. Good nonparallel alignment of the block copolymer to the superparamagnetic nanoparticle chains under the magnetic field was observed even with lower volume fractions of nanoparticles, albeit with high defect density (Figure 3.7) which increased with increase in nanoparticle loading. The segregation of neutral nanoparticles to the domain interface was driven by a relatively weak entropic potential, but simulations suggest that a strong interaction is required to reorient the nanodomains in the direction of the applied magnetic field. This leads us to hypothesize that domain alignment in the direction of the applied magnetic field is not observed for nanoparticles localized at the diblock–copolymer interface due to an insufficient coupling between the diblock copolymer field and the nanoparticle chains.

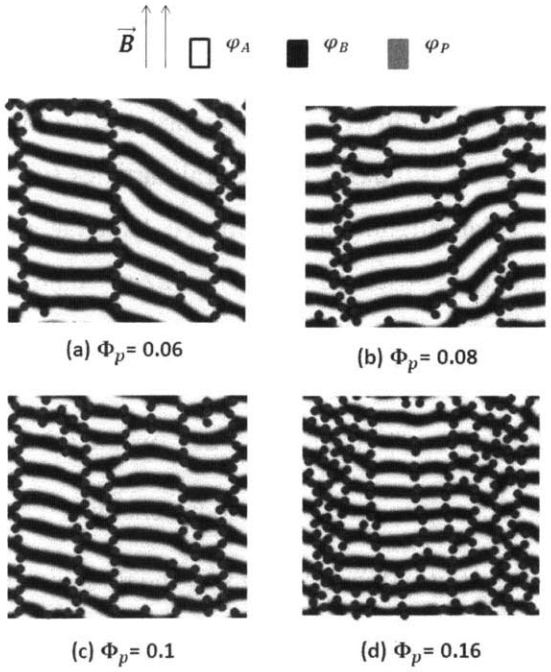

Figure 3.7. Effect of neutral nanoparticles on BCP alignment, $\lambda = 9$, $L = 32R_g$, $\chi_{BP}N = 0$, $\chi_{AP}N = 0$, $\chi_{AB}N = 20$, $R_P = 0.51R_g$; (a) $\Phi_P = 0.06$, (b) $\Phi_P = 0.08$, (c) $\Phi_P = 0.1$, (d) $\Phi_P = 0.16$.

3.3.6 Quantification of Orientational Ordering

The orientational order can also be quantified using an orientational order parameter (γ) that depends on the local nematic director angle $\phi(\vec{r})$ of the diblock copolymer domains given by (*68*),

$$\gamma = \frac{3}{2}\langle \cos^2\phi \rangle - \frac{1}{2} \tag{3.6}$$

where $\phi(\vec{r})$ is the angle between the vector normal to the interface of the blocks ($\hat{e}_n$) and the magnetic field direction ($\hat{e}_z$) at position $\vec{r}$. The value of the orientational order parameter varies between −0.5 and 1 for alignment of the diblock copolymer perpendicular to and parallel to the field direction, respectively. Figure 3.8 shows the typical variation of γ as a function of the number of Brownian dynamics (BD) moves per nanoparticle. As the nanoparticles chain along the direction of the magnetic field, the order parameter increases from around 0 (disordered initial condition) to near 1 (parallel alignment). There is little dependence of the equilibrium order parameter on the magnetic field strength.

Faster alignment and defect annihilation are expected to occur at higher magnetization strengths, since the magnitude of dipolar forces is directly proportional to the magnetization strength of the nanoparticles. Hence, at higher magnetization strengths, the chaining of superparamagnetic nanoparticles that aligns the block copolymer domains occurs faster than the formation of the block copolymer domains, leading to faster alignment with fewer defects. Our focus in this study is primarily on the equilibrium characteristics of the self-assembly process, and the quantitative aspects of the kinetics of alignment are currently being explored using Ginzburg–Landau theory (*67*)

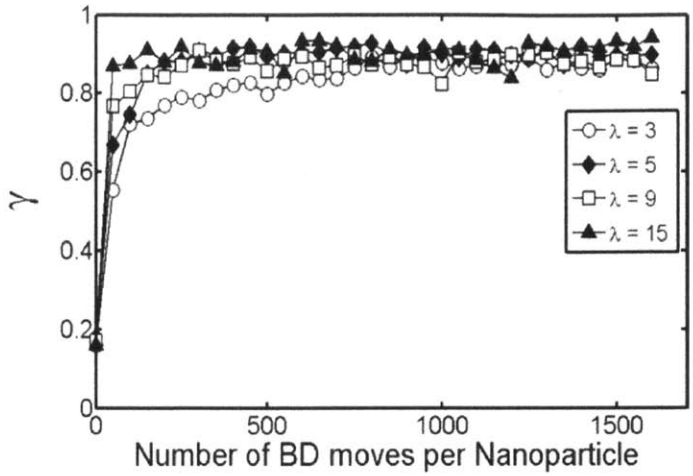

Figure 3.8. Variation of the orientational order parameter with number of BD moves per nanoparticle. As the simulation proceeds, the diblock copolymer aligns in the direction of the magnetic field, and different magnetization strengths give similar γ at long times. Qualitatively, it is seen that at higher magnetization strengths the initial rate of change in the value of γ is higher, suggesting faster alignment at higher magnetization strengths. $\chi_{BP}N = 30$, $\Phi_P = 0.12$.

.The effect of nanoparticle loading on the alignment is clearly reflected in the order parameter values shown in Figure 3.9. Good orientational ordering was observed for a limited window of nanoparticle loadings, in the range of 0.08–0.12, as evidenced by the high γ values in this region. Low values of γ were obtained at low loadings since only local alignment of superparamagnetic nanoparticle chains was observed and the number of defects in the structure increased due to the short persistence lengths of the nanoparticle chains. At high loadings, the value of γ was reduced dramatically due to the formation of mixed lamellar–hexagonal phases.

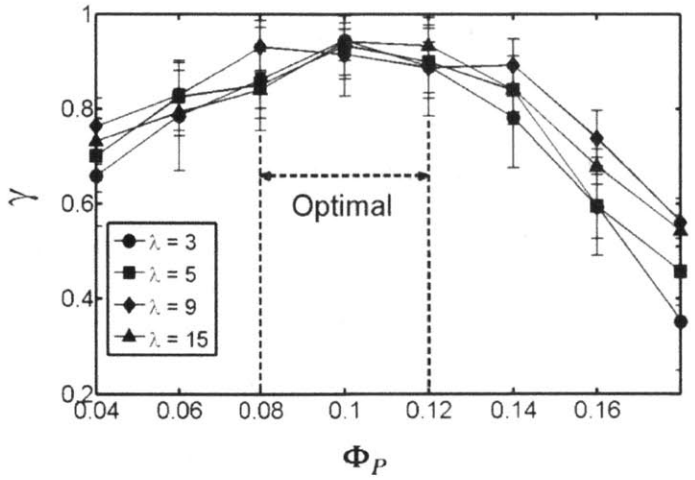

Figure 3.9. Variation of γ with nanoparticle loading (Φ_P) for different magnetization strengths; there exists an optimal range of loadings over which the best orientational order is observed with minimal defects, $\chi_{BP}N = 30$, $\chi_{AP}N = 0$, $\chi_{AB}N = 20$, $R_P = 0.51R_g$, $L = 32R_g$.

3.4 Conclusions

A new method to align symmetric diblock copolymer domains using the chaining of superparamagnetic nanoparticles in the presence of in-plane external magnetic fields is introduced and investigated numerically. Interplay of nanoparticle loadings, magnetization strengths, and nanoparticle sizes give rise to interesting phase behavior and alignment characteristics. Simulations reveal the importance of choice of nanoparticle size and loading to achieve good orientational ordering. Ideal nanoparticle loadings will allow one complete nanoparticle chain to form within each diblock copolymer nanodomain to maximize nanoparticle chain persistence length while minimizing diblock copolymer domain swelling. The nanoparticle size (R_P) must be chosen to be around $0.51R_g$ to avoid the distortions to nanodomains observed with large particle sizes and the colloidal jamming seen for small nanoparticles. Good orientational ordering is observed even at low field strengths, and the equilibrium defect density decreases with increasing field strength. Magnetic fields involved for BCP alignment with the

superparamagnetic nanoparticles are much lower than that required to align BCP using different magnetic susceptibilities of the two blocks. For liquid crystal BCPs, magnetic fields of the order of 6 T are required for BCP alignment, while the magnetic field strength required to induce superparamagnetic nanoparticle chaining is only ~1 T; therefore, nanoparticle chaining enables alignment at much lower field strengths. Finally, the selectivity of the particles is critically important, since a coupling between the block copolymer density field and the nanoparticle chain is required to produce aligned nanostructures. Strong orientational ordering of the diblock copolymer domains in the direction of the applied magnetic field is observed for $\chi_{BP}N \geq 22$.

3.5 References

1. R. A. Segalman, Patterning with block copolymer thin films. *Materials Science and Engineering: R: Reports* **48**, 191-226 (2005).
2. I. Botiz, S. B. Darling, Optoelectronics using block copolymers. *Materials Today* **13**, 42-51 (2010).
3. M. R. Bockstaller, E. L. Thomas, Optical Properties of Polymer-Based Photonic Nanocomposite Materials. *The Journal of Physical Chemistry B* **107**, 10017-10024 (2003).
4. S. B. Darling, Block copolymers for photovoltaics. *Energy & Environmental Science* **2**, 1266-1273 (2009).
5. M. R. Bockstaller, R. A. Mickiewicz, E. L. Thomas, Block copolymer nanocomposites: perspectives for tailored functional materials. *Advanced Materials* **17**, 1331-1349 (2005).

6. T. Thurn-Albrecht, R. Steiner, J. DeRouchey, C. M. Stafford, E. Huang, M. Bal, M. Tuominen, C. J. Hawker, T. P. Russell, Nanoscopic Templates from Oriented Block Copolymer Films. *Advanced Materials* **12**, 787-791 (2000).

7. S. Y. Yang, I. Ryu, H. Y. Kim, J. K. Kim, S. K. Jang, T. P. Russell, Nanoporous Membranes with Ultrahigh Selectivity and Flux for the Filtration of Viruses. *Advanced Materials* **18**, 709-712 (2006).

8. J. N. L. Albert, T. H. Epps Iii, Self-assembly of block copolymer thin films. *Materials Today* **13**, 24-33 (2010).

9. S. Darling, Directing the self-assembly of block copolymers. *Progress in Polymer Science* **32**, 1152-1204 (2007).

10. I. W. Hamley, Ordering in thin films of block copolymers: Fundamentals to potential applications. *Progress in Polymer Science* **34**, 1161-1210 (2009).

11. R. Ruiz, H. Kang, F. A. Detcheverry, E. Dobisz, D. S. Kercher, T. R. Albrecht, J. J. de Pablo, P. F. Nealey, Density Multiplication and Improved Lithography by Directed Block Copolymer Assembly *Science* **321** 936-939 (2008).

12. S. Ouk Kim, H. H. Solak, M. P. Stoykovich, N. J. Ferrier, J. J. de Pablo, P. F. Nealey, Epitaxial self-assembly of block copolymers on lithographically defined nanopatterned substrates. *Nature* **424**, 411-414 (2003).

13. X. M. Yang, R. D. Peters, P. F. Nealey, H. H. Solak, F. Cerrina, Guided Self-Assembly of Symmetric Diblock Copolymer Films on Chemically Nanopatterned Substrates. *Macromolecules* **33**, 9575-9582 (2000).

14. M. P. Stoykovich, M. Müller, S. O. Kim, H. H. Solak, E. W. Edwards, J. J. de Pablo, P. F. Nealey, Directed Assembly of Block Copolymer Blends into Nonregular Device-Oriented Structures. *Science* **308**, 1442-1446 (2005).

15. I. Bita, J. K. W. Yang, Y. S. Jung, C. A. Ross, E. L. Thomas, K. K. Berggren, Graphoepitaxy of Self-Assembled Block Copolymers on Two-Dimensional Periodic Patterned Templates *Science* **321** 939-943 (2008).

16. J. Y. Cheng, C. A. Ross, H. I. Smith, E. L. Thomas, Templated Self-Assembly of Block Copolymers: Top-Down Helps Bottom-Up. *Advanced Materials* **18**, 2505-2521 (2006).

17. R. A. Segalman, A. Hexemer, E. J. Kramer, Effects of Lateral Confinement on Order in Spherical Domain Block Copolymer Thin Films. *Macromolecules* **36**, 6831-6839 (2003).

18. R. A. Segalman, H. Yokoyama, E. J. Kramer, Graphoepitaxy of spherical domain block copolymer films. *Advanced Materials* **13**, 1152-1155 (2001).

19. J. Y. Cheng, C. A. Ross, E. L. Thomas, H. I. Smith, G. J. Vancso, Fabrication of nanostructures with long-range order using block copolymer lithography. *Applied Physics Letters* **81**, 3657-3659 (2002).

20. J. Y. Cheng, A. M. Mayes, C. A. Ross, Nanostructure engineering by templated self-assembly of block copolymers. *Nat Mater* **3**, 823-828 (2004).

21. C. Park, J. Yoon, E. L. Thomas, Enabling nanotechnology with self assembled block copolymer patterns. *Polymer* **44**, 6725-6760 (2003).

22. R. J. Albalak, E. L. Thomas, Microphase separation of block copolymer solutions in a flow field. *Journal of Polymer Science Part B: Polymer Physics* **31**, 37-46 (1993).

23. S. S. Patel, R. G. Larson, K. I. Winey, H. Watanabe, Shear Orientation and Rheology of a Lamellar Polystyrene-Polyisoprene Block Copolymer. *Macromolecules* **28**, 4313-4318 (1995).

24. V. K. Gupta, R. Krishnamoorti, J. A. Kornfield, S. D. Smith, Evolution of Microstructure during Shear Alignment in a Polystyrene-Polyisoprene Lamellar Diblock Copolymer. *Macromolecules* **28**, 4464-4474 (1995).

25. V. K. Gupta, R. Krishnamoorti, Z.-R. Chen, J. A. Kornfield, S. D. Smith, M. M. Satkowski, J. T. Grothaus, Dynamics of Shear Alignment in a Lamellar Diblock Copolymer: Interplay of Frequency, Strain Amplitude, and Temperature. *Macromolecules* **29**, 875-884 (1996).

26. T. J. Hermel, L. Wu, S. F. Hahn, T. P. Lodge, F. S. Bates, Shear-Induced Lamellae Alignment in Matched Triblock and Pentablock Copolymers. *Macromolecules* **35**, 4685-4689 (2002).

27. M. E. Vigild, C. Chu, M. Sugiyama, K. A. Chaffin, F. S. Bates, Influence of Shear on the Alignment of a Lamellae-Forming Pentablock Copolymer. *Macromolecules* **34**, 951-964 (2001).

28. B. L. Riise, G. H. Fredrickson, R. G. Larson, D. S. Pearson, Rheology and Shear-Induced Alignment of Lamellar Diblock and Triblock Copolymers. *Macromolecules* **28**, 7653-7659 (1995).

29. D. E. Angelescu, J. H. Waller, D. H. Adamson, P. Deshpande, S. Y. Chou, R. A. Register, P. Chaikin, Macroscopic Orientation of Block Copolymer Cylinders in Single-Layer Films by Shearing. *Advanced Materials* **16**, 1736-1740 (2004).

30. D. E. Angelescu, J. H. Waller, R. A. Register, P. M. Chaikin, Shear-Induced Alignment in Thin Films of Spherical Nanodomains. *Advanced Materials* **17**, 1878-1881 (2005).

31. K. Amundson, E. Helfand, D. D. Davis, X. Quan, S. S. Patel, S. D. Smith, Effect of an electric field on block copolymer microstructure. *Macromolecules* **24**, 6546-6548 (1991).

32. K. Amundson, E. Helfand, X. Quan, S. D. Smith, Alignment of lamellar block copolymer microstructure in an electric field. 1. Alignment kinetics. *Macromolecules* **26**, 2698-2703 (1993).

33. K. Amundson, E. Helfand, X. Quan, S. D. Hudson, S. D. Smith, Alignment of Lamellar Block Copolymer Microstructure in an Electric Field. 2. Mechanisms of Alignment. *Macromolecules* **27**, 6559-6570 (1994).

34. T. Xu, Y. Zhu, S. P. Gido, T. P. Russell, Electric Field Alignment of Symmetric Diblock Copolymer Thin Films. *Macromolecules* **37**, 2625-2629 (2004).

35. T. L. Morkved, M. Lu, A. M. Urbas, E. E. Ehrichs, H. M. Jaeger, P. Mansky, T. P. Russell, Local Control of Microdomain Orientation in Diblock Copolymer Thin Films with Electric Fields *Science* **273** 931-933 (1996).

36. Y. Tao, H. Zohar, B. D. Olsen, R. A. Segalman, Hierarchical Nanostructure Control in Rod-Coil Block Copolymers with Magnetic Fields. *Nano Letters* **7**, 2742-2746 (2007).

37. P. W. Majewski, M. Gopinadhan, C. O. Osuji, Magnetic field alignment of block copolymers and polymer nanocomposites: Scalable microstructure control in functional soft materials. *Journal of Polymer Science Part B: Polymer Physics*, (2011).

38. K. Fukunaga, H. Elbs, R. Magerle, G. Krausch, Large-Scale Alignment of ABC Block Copolymer Microdomains via Solvent Vapor Treatment. *Macromolecules* **33**, 947-953 (2000).

39. S. Park, D. H. Lee, J. Xu, B. Kim, S. W. Hong, U. Jeong, T. Xu, T. P. Russell, Macroscopic 10-Terabit-per-Square-Inch Arrays from Block Copolymers with Lateral Order *Science* **323**, 1030-1033 (2009).

40. S. H. Kim, M. J. Misner, T. P. Russell, Solvent-Induced Ordering in Thin Film Diblock Copolymer/Homopolymer Mixtures. *Advanced Materials* **16**, 2119-2123 (2004).

41. Y. S. Jung, C. A. Ross, Solvent-Vapor-Induced Tunability of Self-Assembled Block Copolymer Patterns. *Advanced Materials* **21**, 2540-2545 (2009).

42. S. C. Park, B. J. Kim, C. J. Hawker, E. J. Kramer, J. Bang, J. S. Ha, Controlled Ordering of Block Copolymer Thin Films by the Addition of Hydrophilic Nanoparticles. *Macromolecules* **40**, 8119-8124 (2007).

43. C. B. Tang, W. Wu, D. M. Smilgies, K. Matyjaszewski, T. Kowalewski, Robust Control of Microdomain Orientation in Thin Films of Block Copolymers by Zone Casting. *Journal of the American Chemical Society* **133**, 11802-11809 (2011).

44. T. Xu, J. T. Goldbach, T. P. Russell, Sequential, Orthogonal Fields: A Path to Long-Range, 3-D Order in Block Copolymer Thin Films. *Macromolecules* **36**, 7296-7300 (2003).

45. R. A. Vaia, J. F. Maguire, Polymer nanocomposites with prescribed morphology: Going beyond nanoparticle-filled polymers. *Chemistry of Materials* **19**, 2736-2751 (2007).

46. Y. Lin, A. Boker, J. He, K. Sill, H. Xiang, C. Abetz, X. Li, J. Wang, T. Emrick, S. Long, Q. Wang, A. Balazs, T. P. Russell, Self-directed self-assembly of nanoparticle/copolymer mixtures. **434**, 55-59 (2005).

47. F. Brochard, P. G. D. Gennes, Theory of Magnetic Suspensions in Liquid Crystals. *Journal De Physique* **31**, 691 (1970).

48. M. R. Hammond, H. Dietsch, O. Pravaz, P. Schurtenberger, Mutual Alignment of Block Copolymer-Magnetic Nanoparticle Composites in a Magnetic Field. *Macromolecules* **43**, 8340-8343 (2010).

49. R. E. Rosenweig, *Ferrohydrodynamics*. (Dover Publications, 1997).

50. A. C. Balazs, T. Emrick, T. P. Russell, Nanoparticle Polymer Composites: Where Two Small Worlds Meet *Science* **314** 1107-1110 (2006).

51. C. Xu, K. Ohno, V. Ladmiral, R. J. Composto, Dispersion of polymer-grafted magnetic nanoparticles in homopolymers and block copolymers. *Polymer* **49**, 3568-3577 (2008).

52. A.-S. Robbes, F. Cousin, F. Meneau, F. Dalmas, F. o. BouÃ©, J. Jestin, Nanocomposite Materials with Controlled Anisotropic Reinforcement Triggered by Magnetic Self-Assembly. *Macromolecules*, (2011).

53. M. W. Matsen, R. B. Thompson, Particle distributions in a block copolymer nanocomposite. *Macromolecules* **41**, 1853-1860 (2008).

54. V. Pryamitsyn, V. Ganesan, Strong Segregation Theory of Block Copolymer-Nanoparticle Composites. *Macromolecules* **39**, 8499-8510 (2006).

55. S. W. Sides, B. J. Kim, E. J. Kramer, G. H. Fredrickson, Hybrid particle-field simulations of polymer nanocomposites. *Physical Review Letters* **96**, (2006).

56. F. Drolet, G. H. Fredrickson, Combinatorial screening of complex block copolymer assembly with self-consistent field theory. *Physical Review Letters* **83**, 4317-4320 (1999).

57. T. L. Chantawansri, S.-M. Hur, C. J. Garcia-Cervera, H. D. Ceniceros, G. H. Fredrickson, Spectral collocation methods for polymer brushes. *The Journal of Chemical Physics* **134**, 244905-244914 (2011).

58. K. O. Rasmussen, G. Kalosakas, Improved numerical algorithm for exploring block copolymer mesophases. *Journal of Polymer Science Part B-Polymer Physics* **40**, 1777-1783 (2002).

59. S. W. Sides, G. H. Fredrickson, Parallel algorithm for numerical self-consistent field theory simulations of block copolymer structure. *Polymer* **44**, 5859-5866 (2003).

60. D. Andelman, R. E. Rosensweig, Modulated Phases: Review and Recent Results. *The Journal of Physical Chemistry B* **113**, 3785-3798 (2008).

61. M. R. Hammond, E. Cochran, G. H. Fredrickson, E. J. Kramer, Temperature dependence of order, disorder, and defects in laterally confined diblock copolymer cylinder monolayers. *Macromolecules* **38**, 6575-6585 (2005).

62. W. F. Brown, The Fundemental Theorem of TheTheory of Fine Ferromagnetic Particles. *Annals of the New York Academy of Sciences* **147**, 463-488 (1969).

63. R. Sondjaja, T. Hatton, A., M. K. C. Tam, Clustering of magnetic nanoparticles using a double hydrophilic block copolymer, poly(ethylene oxide)-b-poly(acrylic acid). *Journal of Magnetism and Magnetic Materials* **321**, 2393-2397 (2009).

64. Y. Deng, D. Qi, C. Deng, X. Zhang, D. Zhao, Superparamagnetic High-Magnetization Microspheres with an Fe3O4@SiO2 Core and Perpendicularly Aligned Mesoporous SiO2 Shell for Removal of Microcystins. *Journal of the American Chemical Society* **130**, 28-29 (2007).

65. B. J. Kim, J. J. Chiu, G. R. Yi, D. J. Pine, E. J. Kramer, Nanoparticle-Induced Phase Transitions in Diblock-Copolymer Films. *Advanced Materials* **17**, 2618-2622 (2005).

66. J. Huh, V. V. Ginzburg, A. C. Balazs, Thermodynamic Behavior of Particle/Diblock Copolymer Mixtures: Simulation and Theory. *Macromolecules* **33**, 8085-8096 (2000).

67. V. V. Ginzburg, F. Qiu, A. C. Balazs, Three-dimensional simulations of diblock copolymer/particle composites. *Polymer* **43**, 461-466 (2002).

68. C. Harrison, P. M. Chaikin, D. A. Huse, R. A. Register, D. H. Adamson, A. Daniel, E. Huang, P. Mansky, T. P. Russell, C. J. Hawker, D. A. Egolf, I. V. Melnikov, E. Bodenschatz, Reducing Substrate Pinning of Block Copolymer Microdomains with a Buffer Layer of Polymer Brushes. *Macromolecules* **33**, 857-865 (2000).

Chapter 4

Magnetic Field Induced Morphological Transitions in Block Copolymer/Superparamagnetic Nanoparticle Composites

4.1 Introduction

Polymer nanocomposites are an interesting class of heterogeneous materials that are known for their enhanced mechanical, optical and electrical properties; the characteristics of the nanoparticles play an important role in determining the morphology and properties of the composites (*1-5*). The need for spatial patterning and hierarchical structural control in such materials (*6*) has spurred interest in block copolymer nanocomposites, where block copolymer self-assembly into morphologies such as lamellae, spheres, and cylinders can be used to achieve a preferred spatial and orientational distribution of nanoparticles (*2, 7, 8*). The effect of morphology on the optical (*9-13*) and mechanical performance (*14*) of nanocomposites has been well documented in the literature.

The morphology of block copolymer nanocomposites depends on the interplay of nanoparticle size, nanoparticle loading and particle selectivity for the blocks (*1, 2, 15*), as is evident from the results of many theoretical (*16-22*) and experimental (*23-26*) studies on the phase behavior of block copolymer – nanoparticle mixtures. The presence of non-selective nanoparticles in the block copolymers, for example, affects the order-disorder transition (ODT) temperature (*27, 28*), effectively reducing the Flory-Huggins interaction energy of the two blocks due to the losses in conformational entropy of the polymer chains (*27*). Excluded volume interactions between the nanoparticles and the block copolymer also lead to morphological transitions due to the swelling the block copolymer domains (*29, 30*). Morphology control of composites can be achieved by tuning the enthalpic and entropic interactions between the nanoparticles and the block copolymer. Enthalpic interactions, for instance, can be tuned by functionalization of nanoparticle surfaces with selective or nonselective ligands, while entropic interactions are known to depend on the size of the nanoparticles relative to the block copolymer domain spacing (*31*). Confinement effects (*32, 33*) and substrate chemical potentials (*34*) are also known to play an important role in the self-assembly of these composite systems due to both symmetry breaking and surface segregation of polymer or nanoparticles to the confining interface (*32*). Inter-particle interactions between the nanoparticles can also affect the morphology of the composite (*35, 36*), and control of inter-particle interactions (*37*) can serve as an efficient tool to manipulate the hierarchical assembly of block copolymers, especially when long-range interactions are present.

In polymer nanocomposites with magnetic nanoparticles, uniform magnetic fields can be used to alter the orientation of magnetic nanoparticle dipoles (*38*) and consequently tune the long-range interparticle interactions. This affects the structure of nanoparticle aggregates and

subsequently the morphology of the block copolymer nanocomposite. For instance, magnetic nanoparticles are known to form chain-like aggregates due to dipolar interactions that are predicted to promote alignment of block copolymer nanostructures.(*35, 39*) He and Balazs (*35*) demonstrated using cell dynamics simulations that in-plane magnetic fields promote alignment of magnetic nanoparticles and, consequently, alignment of lamellar domains as well as cylinder forming block copolymers. Recently, we studied the effect of chaining of superparamagnetic nanoparticles on the alignment of symmetric block copolymers using hybrid particle-field theory simulations, which explicitly took into account the excluded volume interactions between the nanoparticles and the block copolymer. We delineated the role of dipolar interaction strength, nanoparticle size, nanoparticle loading and the surface interaction of the nanoparticles with the block copolymer on the morphology of the composite (*39*).

While previous modeling efforts have focused primarily on in-plane magnetic fields which lead to the formation of superparamagnetic nanoparticle chains, out of plane magnetic fields can change the nanoparticle symmetry to form hexagonal arrays due to repulsive dipolar interactions. In this chapter, we investigate the interplay of magnetic field orientation, coil fraction of the block copolymer, and nanoparticle size and loading on the morphology of the composite, specifically exploring the interplay between block copolymer and superparamagnetic nanoparticle lattice symmetry. Depending upon the symmetry of the block copolymer in two-dimensional simulations (hexagonal/dots and lamellar/stripes), the nanoparticles induce a variety of morphological transitions in the final composite.

4.2 Simulation Methodology

The effects of nanoparticle size and loading on the self-assembly of the composite system are characterized using a hybrid of self-consistent field theory (SCFT) and Brownian dynamics (*30, 39*). The block copolymer is characterized by the coil fraction, f, of the block that has the most favorable interaction with the nanoparticles. The Flory-Huggins interaction parameter between the blocks is denoted by χ_{AB}, while the selectivities of the nanoparticles for the two blocks A and B are denoted by χ_{AP} and χ_{BP}, respectively. N is the total degree of polymerization of the block copolymer chain. All the Flory-Huggins interaction parameters were kept fixed ($\chi_{AP}\mathrm{N} = 0, \chi_{BP}\mathrm{N} = 30, \chi_{AB}\mathrm{N} = 20$) in the simulations. All lengths (box size L and the nanoparticle radius, R_P) are scaled by R_g, the unperturbed radius of gyration of the block copolymer. The statistical segment lengths of the A and B blocks are assumed to be equal, and the overall nanoparticle volume fraction is denoted by Φ_P. The dipolar interactions are characterized by the parameter λ, the ratio of the dipolar interaction energy to the thermal energy ($k_\mathrm{B}\mathrm{T}$). The dipole moments are assumed to align in the direction of the applied magnetic field, a valid assumption when the external magnetic field strength is much larger than the saturation magnetization strength of the nanoparticle. Since the simulations are in 2D, the symmetric block copolymers form phases with line symmetry (referred to as stripe phases), and the asymmetric block copolymers form hexagonal phases (referred to as dot phases). For the case of assembly in thin-films, stripe phases can be identified with lamellar phases or cylinders oriented parallel to the surface of the film, while dot phases are akin to spherical phases or perpendicularly oriented cylinders.

4.3 Results

4.3.1 Influence of Dipolar Interactions on Block Copolymer Morphology

The simulations reveal that dipolar interactions have a significant influence on the morphology of the block copolymer nanocomposite. In the absence of an external magnetic field ($\lambda = 0$), the superparamagnetic nanoparticles behave like non-magnetic nanoparticles due to the absence of any remnant magnetic dipole moments. Thus, in the absence of an external magnetic field ($\lambda = 0$), nanoparticles that have selective surface interactions ($\chi_{AB}N = 0$, $\chi_{BP}N = 30$) show behavior consistent with established results for block copolymer/non-magnetic nanoparticle composites (Figure 4.1a-e). The hexagonal symmetry of the resulting morphology is preserved for low nanoparticle loadings (volume fractions) when the domains of the minority block accommodate the nanoparticles (Figure 4.1a; $f = 0.3$). However, an increase in the nanoparticle loading (Figure 4.1b) causes a morphological transition from dots to stripes, where stripes are predominantly observed at nanoparticle loadings of $\Phi_P \geq 0.1$. Similar morphological transitions from lamellar to hexagonal morphologies & vice-versa, have been reported in the literature for non-magnetic nanoparticles that interact through excluded volume only (*26, 29, 30, 40*). When the nanoparticles favor the majority block, (Figure 4.1d-e; $f = 0.7$), the increase in nanoparticle volume fraction does not affect the symmetry of the inverse hexagonal phase, although the hexagonal phase is distorted in some regions due to local structural frustration. Furthermore, superparamagnetic nanoparticles have little effect on the final morphology of the composites of symmetric block copolymer (Figure 4.1c; $f = 0.5$), in the absence of an external magnetic field ($\lambda = 0$). However, at high enough nanoparticle loadings, an order to order phase transition from

stripe phases (lamellar symmetry) to dot phases (hexagonal symmetry) is observed, similar to that reported for non-magnetic nanoparticles (*30, 40*).

With superparamagnetic nanoparticles ($\lambda = 9$), the orientation of the external magnetic field plays an important role in determining the morphology of the composite. Out of plane magnetic fields induce repulsive dipolar interactions resulting in formation of hexagonal arrays of nanoparticles. For nanoparticles selective for the minority block ($f = 0.3$), the symmetry of the block copolymer lattice and the nanoparticle lattice match. When the lattice parameter of the nanoparticle structure matches the lattice parameter of the hexagonal phase block copolymer, hexagonal symmetry of the composite is preserved with minimal or no defects in the final morphology (Figure 4.1f).

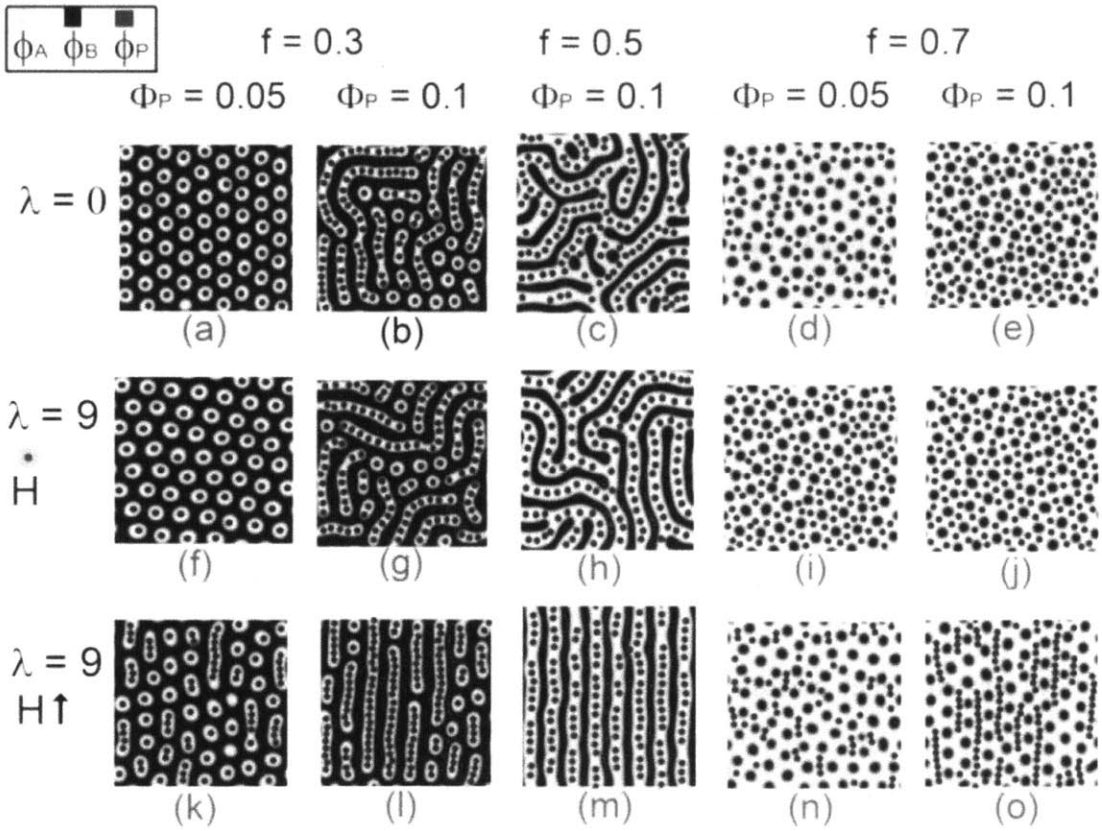

Figure 4.1. Effect of dipolar interactions on the morphology of the block copolymer nanocomposite,. R_P= 0.5 R_g, χ_{BP}N=30; (a) – (e) non-magnetic nanoparticles; (f) – (j) magnetic field ($\vec{H}$) is out of plane (along z axis); (k) – (o) magnetic field ($\vec{H}$) is in-plane (along y axis); Local volume fractions for block A (bright regions), B (dark regions) and nanoparticles (blue spheres) are represented by ϕ_A, ϕ_B,and ϕ_P respectively; λ represents ratio of dipolar interaction energy to thermal energy.

4.3.2 Conditions for Symmetry Matching in Out-of-Plane Magnetic Fields

Using geometrical arguments, we can derive the optimum overall volume fraction of the nanoparticles for symmetry match to be $\Phi_P^* = \frac{2\pi R_P^2}{\sqrt{3}L_S^2}$, where L_s is the lattice constant of the nanoparticle loaded hexagonal phase of the block copolymer. For a given number density of

superparamagnetic nanoparticles, we calculate the lattice constant of the hexagonal lattice formed by the nanoparticles in the presence of out of plane magnetic fields. For symmetry match to occur, this lattice constant has to match the lattice constant of inter-dot spacing of the hexagonal phase of the block copolymer.

The number density of the nanoparticles is

$$n'_P = \frac{n_P}{A} = \frac{\Phi_P}{\pi R_P^2} \tag{4.1}$$

In a primitive cell of a hexagonal lattice, we have 1 nanoparticle per area of $\frac{\sqrt{3}}{2}L_P^2$, where L_P is the lattice constant, which corresponds to a number density of $\left(\frac{\sqrt{3}}{2}L_P^2\right)^{-1}$.

We thus obtain the lattice constant for the nanoparticle lattice as

$$L_P = 2R_P.\sqrt{\frac{\pi}{\sqrt{3}\Phi_P}} \tag{4.2}$$

For symmetry match, we require

$$L_P = L_S \tag{4.3}$$

where L_s is the inter-dot spacing of the nanoparticle-loaded hexagonal phase of the block copolymer. We thus obtain the optimum volume fraction, at which symmetry match occurs as

$$\Phi_P^* = \frac{2\pi R_P^2}{\sqrt{3}L_S^2} \tag{4.4}$$

Assuming that nanoparticles have a minor effect on the lattice constant of the hexagonal phase of the block copolymer (consistent with simulation results), we anticipate that symmetry match should occur at an optimum volume fraction of nanoparticles, of radius R_P = 0.5 R_g, at $\Phi_P^* = 0.057$; simulations show a symmetry match at about $\Phi_P^* = 0.055$.

Although, the final nanocomposite morphology looks similar in the two relatively small simulations shown in Figures 4.1a and 4.1f, faster defect annihilation is expected in the presence of the external magnetic field due to the long-ranged nature of the dipolar interactions. Therefore, the inclusion of nanoparticles is anticipated to reduce the formation of defects when the particle loading is selected to be near this symmetry match.

4.3.3 Effect of Nanoparticle Size on Symmetry Matching Conditions

These symmetry matching conditions only apply when there is exactly one nanoparticle in each of the block copolymer minority nanodomains, which also requires commensurability between R_P and R_g. Figure 4.2 shows the effect of nanoparticle size on the morphology of an asymmetric block copolymer (f = 0.3), in the presence of repulsive dipolar interactions (out of plane magnetic fields). High surface selectivity of the nanoparticles ($\chi_{BP}N > \chi_{AB}N, \chi_{AP}N = 0$) ensures that even the smallest nanoparticles (R_P = 0.25 R_g, $d_P/L_o < 0.3$) are sequestered well within the domains of the minority block.

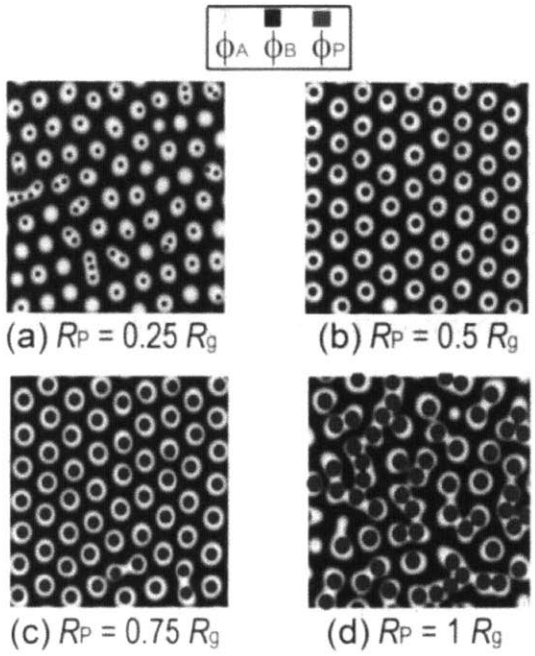

Figure 4.2. Effect of nanoparticle size on the morphology of block copolymer composite, $\vec{H}$ field is out of plane, resulting in repulsive dipolar interactions between the nanoparticles; $\lambda = 9$, $\chi_{AP}N = 0$, $\chi_{BP}N = 30$, (a) $R_P = 0.25\ R_g$, Φ_P=0.0125, (b) $R_P = 0.5\ R_g$, Φ_P=0.05, (c) $R_P = 0.75\ R_g$, Φ_P=0.1125, (d) $R_P = 1\ R_g$, Φ_P=0.2. The choice of these loadings results in equal nanoparticle number densities for all particle sizes.

However, for the same dipolar energy, the smaller nanoparticles do not give defect-free structures, since some domains accommodate more than one nanoparticle. This gives rise to structural frustration within the domains due to repulsive dipolar interactions between the nanoparticles, stretching some of the domains. Large nanoparticles ($R_P = 1\ R_g$) result in disordered structures because an individual nanoparticle cannot be incorporated within a single domain. Therefore, the optimal particle sizes are in the range $R_P \sim 0.5\text{-}0.75\ R_g$.

4.3.4 Effect of Magnetic Field on Order to Order (OOT) Phase Transitions

When the nanoparticle volume fraction is increased, the same morphological transition is observed (Figure 1g) as in the non-magnetic nanoparticle case (Figure 4.1b). However, the morphology as a function of particle loading (Figure 4.3) is unchanged from the non-magnetic nanoparticle case, as the volume fraction is increased from 0.05 to 0.11.

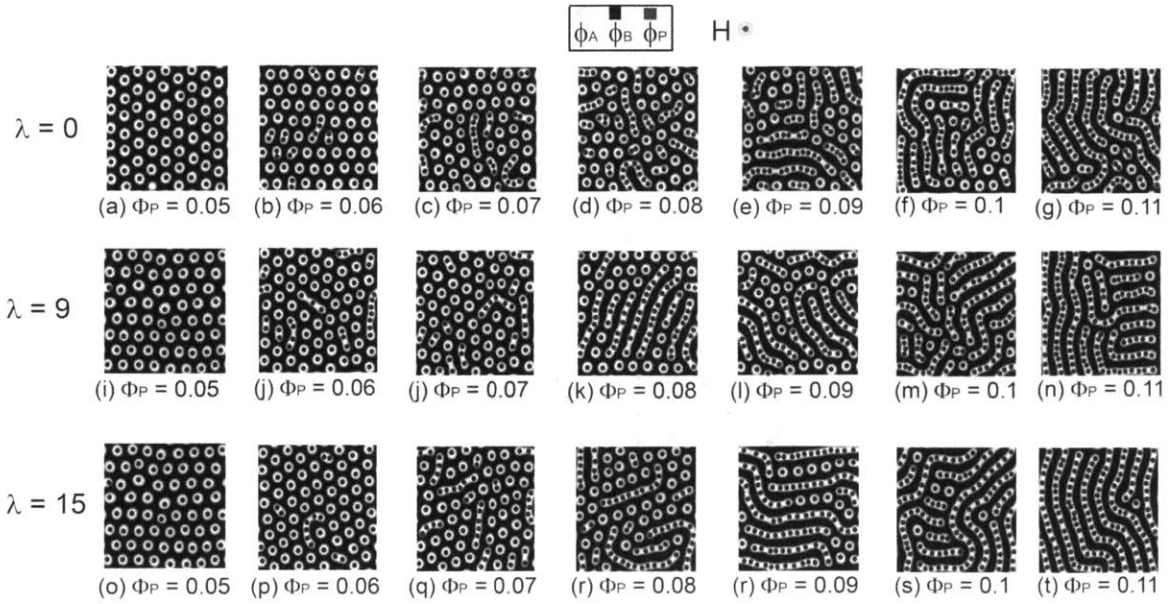

Figure 4.3. Effect of nanoparticle volume fraction on the morphological transitions in the block copolymer, $f = 0.3$, $\chi_{AP}N = 0$, $\chi_{BP}N = 30$, $\chi_{AB}N = 20$, $R_P = 0.5\ R_g$

This indicates that dipolar interactions do not have a significant effect on the Order-to-Order phase transition (OOT), which is primarily caused by the swelling of the domains on addition of nanoparticles. However, this counterintuitive result is consistent with the fact that the energy of block copolymer self-assembly dominates the dipolar interaction strength for the

values of parameters chosen in this study. Block copolymer nanocomposites with symmetric composition (f =0.5) remain in a stripe phase even with the application of an out of plane magnetic field (Figure 4.1h). For a wide variety of different particle volume fractions, the repulsive dipolar interactions do not force the phase transition from lamellar (stripes) to hexagonal phase (dots) (Figure 4.4).

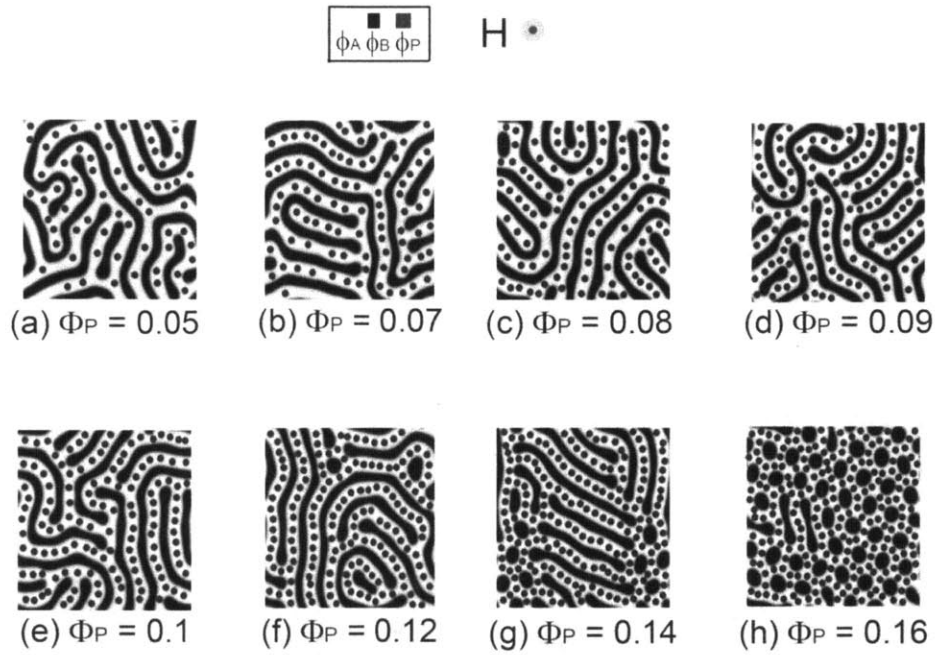

Figure 4.4. Effect of out-of-plane magnetic field on the stripe-forming phase, $f = 0.5$, $\chi_{AB}N = 20$, $\chi_{AP}N = 0$, $\chi_{BP}N = 30$, $R_P = 0.5\ R_g$, $\lambda = 9$

Since the out of plane field does not orient the nanoparticles, symmetry is not broken, and the lamellar domains may orient in any direction. Morphological transitions from stripes to dots arise only because of the swelling of the domains (as seen in Figure 4.4), as reported previously in the literature (*26, 29, 30, 39, 40*).

4.3.5 Formation of Honeycomb Nanoparticle Lattices

When the superparamagnetic nanoparticles ($\lambda = 9$) are selective for the majority block ($f = 0.7$) they occupy the interstitial spaces within the hexagonal dot morphology formed by the minority block in the presence of out-of-plane magnetic fields.

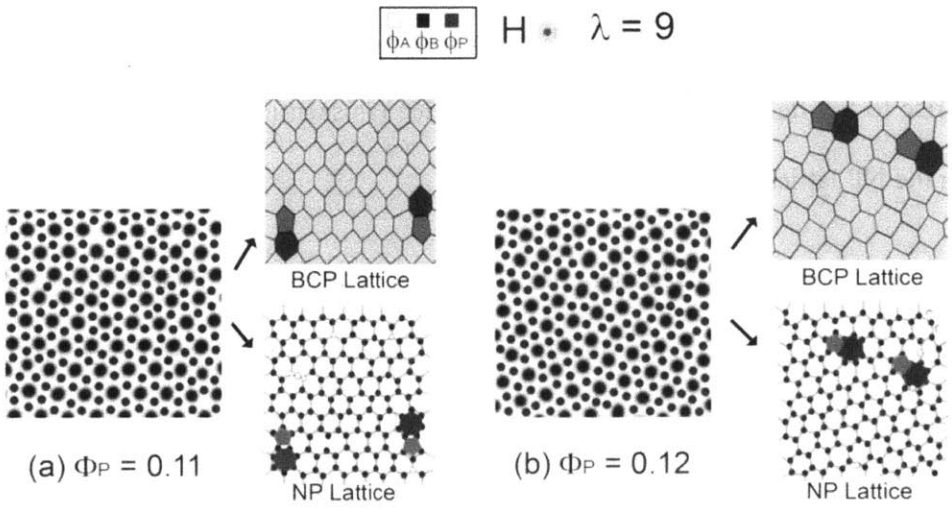

Figure 4.5. Effect of out of plane magnetic fields ($\vec{H}$), when the nanoparticles are selective for the majority block; f =0.7, $\chi_{AP}N = 0$, $\chi_{BP}N = 30$, RP = 0.5 Rg, (a) $\lambda = 9$, Φ_P=0.11, (b) $\lambda = 9$, Φ_P=0.12, Red-blue hexagon pairs denote dislocations in the block copolymer (BCP) and 5-7 defects in the nanoparticle (NP) lattice. Black empty circles denote 1-vacancy defects in the nanoparticle lattice; yellow circles denote excess nanoparticles in the interstitial spaces.

As seen in Figure 4.5, for certain specific nanoparticle volume fractions; each nanoparticle has just three nearest neighbors, and they form a honeycomb lattice. This honeycomb lattice minimizes inter-particle repulsive interactions by evenly spacing the particles throughout the block copolymer, and places particles within the majority block of the hexagonal

lattice at points farthest from the minority block domains, effectively reducing the decrease in entropy due to chain stretching in the majority block.

Defects in the block copolymer structure and the nanoparticle honeycomb lattice are collocated in the final structure. In the regions where dislocations (evident in 5-sided red and 7-sided blue polygons in the BCP lattice, Figure 4.5a) occur in the block copolymer lattice, there are 5 and 7 interstitial spaces in the block copolymer, each occupied by a single nanoparticle. This gives rise to 5-7 defects in the honeycomb lattice (as seen in 5-sided red and 7- sided blue polygons in the NP lattice, Figure 4.5a).

In addition, for $\Phi_P = 0.11$, there are 1-vacancy defects in the honeycomb lattice, shown as black empty circles (Figure 4.5a), due to an insufficient number of particles present to fill all the interstitial spaces. In contrast, when the number of nanoparticles is slightly higher than the number of interstitial spaces in the block copolymer lattice (for $\Phi_P = 0.12$) , a few of the interstitial spaces tend to accommodate two particles instead of just one, without distorting the overall symmetry of the honeycomb lattice (as seen by yellow circles in the NP lattice of Figure 4.5b).

Inter-particle repulsive interactions, induced by out-of-plane magnetic fields, are critical to the formation of honeycomb lattices: the absence of the field results in a random dispersion of the nanoparticles in the majority block domains even at particle densities optimal for honeycomb lattice formation (Figures 4.6a and 4.6b).

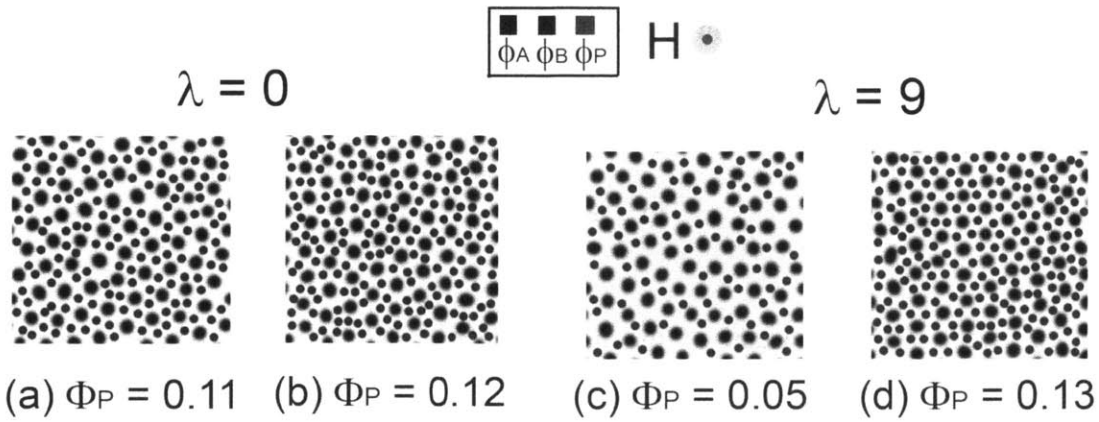

Figure 4.6. $f = 0.7$, $\chi_{AP}N = 0$, $\chi_{BP}N = 30$, $\chi_{AB}N = 20$, honeycomb lattice not formed for non-magnetic nanoparticles ($\lambda = 0$), (a) $\Phi_P^* = 0.11$, and (b) $\Phi_P^* = 0.12$; honeycomb lattices not formed for superparamagnetic nanoparticles ($\lambda = 9$), when $\Phi_P \neq \Phi_P^*$, (c) $\Phi_P = 0.05$, (d) $\Phi_P = 0.13$

Using geometrical arguments, we derive the optimum nanoparticle volume fraction at which a honeycomb lattice is formed to be $\Phi_P^* = \frac{4\pi R_P^2}{\sqrt{3}L_H^2}$, where L_H is the lattice constant of the nanoparticle loaded hexagonal phase of block copolymer. For formation of the honeycomb lattice (Figure 4.7), only one nanoparticle (blue circles) should occupy the interstitial space between the minority block domains (black dots), implying two nanoparticles for every dot.

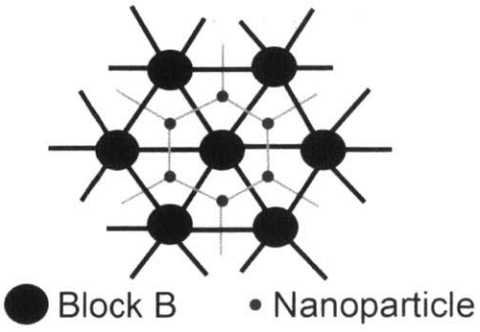

Figure 4.7. Schematic of honeycomb lattice formation, nanoparticles (blue circles) occupy the interstitial spaces of the hexagonal phase formed by the block copolymer (black dots refers to minority block B).

Under these conditions, the optimum volume fraction required for formation of a honeycomb lattice is,

$$\Phi_P^* = \frac{4\pi R_P^2}{\sqrt{3} L_H^2} \tag{4.5}$$

where L_H is the lattice constant of the nanoparticle-loaded hexagonal phase of the block copolymer.

This relationship is valid only for the case of a single nanoparticle occupying each interstitial space in the hexagonal lattice, which is dependent on the nanoparticle size. Assuming that the nanoparticles have only a minor effect on the block copolymer periodicity, we can estimate the optimum volume fraction for nanoparticles of radius R_P = 0.5 R_g to be near 0.11. Simulations reveal the formation of a honeycomb lattice for nanoparticle volume fractions of $\Phi_P = 0.11$ and $\Phi_P = 0.12$ (Figures 4.5a and 4.5b); while lower and higher volume fractions do not show a honeycomb Lattice (Figures 4.6c and 4.6d). For $\Phi_P = 0.11$ and $\Phi_P = 0.12$, most nanoparticles have three-nearest neighbors (Figure 4.5). Honeycomb lattices are not observed for larger (R_P = 0.75 R_g) or smaller nanoparticles (R_P = 0.25 R_g) even at optimum volume fractions (Figure 4.8). Larger nanoparticles (R_P = 0.75 R_g) distort the hexagonal structure of the block copolymer, while smaller nanoparticles (R_P = 0.25 R_g) are found dispersed in the majority block.

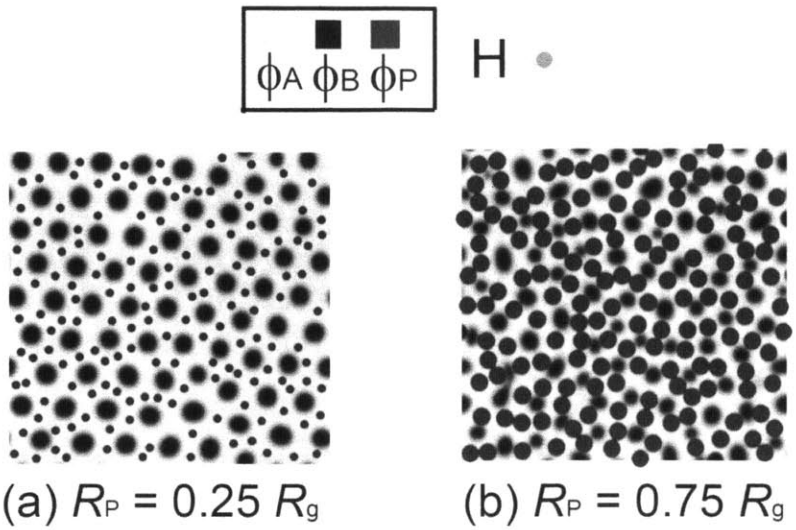

Figure 4.8. Honeycomb lattices not formed for nanoparticle sizes, $f = 0.7$, $\chi_{AP}N = 0$, $\chi_{BP}N = 30$, $\chi_{AB}N = 20$, $\lambda = 9$, (a) $R_P = 0.25\ R_g$, $\Phi_P^* = 0.03$, and (b) $R_P = 0.75\ R_g$, $\Phi_P^* = 0.27$. These volume fractions are chosen to be optimal for honeycomb lattice formation, as calculated by geometrical arguments. Therefore, particle size is also critical to lattice formation.

Therefore, both the particle size and the particle volume fraction must be commensurate with the block copolymer lattice in order to achieve optimal field-induced ordering and formation of honeycomb lattices.

4.3.6 Effect of In-Plane Magnetic Fields on Hexagonal Morphology

When the orientation of the magnetic field is changed to in-plane, the field causes chaining of nanoparticles, resulting in stretching of A domains along the field direction for $f = 0.3$ (Figure 4.1k). At higher nanoparticle volume fractions (Figure 4.1l), the persistence length of the nanoparticle chains increases, and the stripe phase is predominantly observed for $\Phi_P > 0.11$. (Figure 4.9)

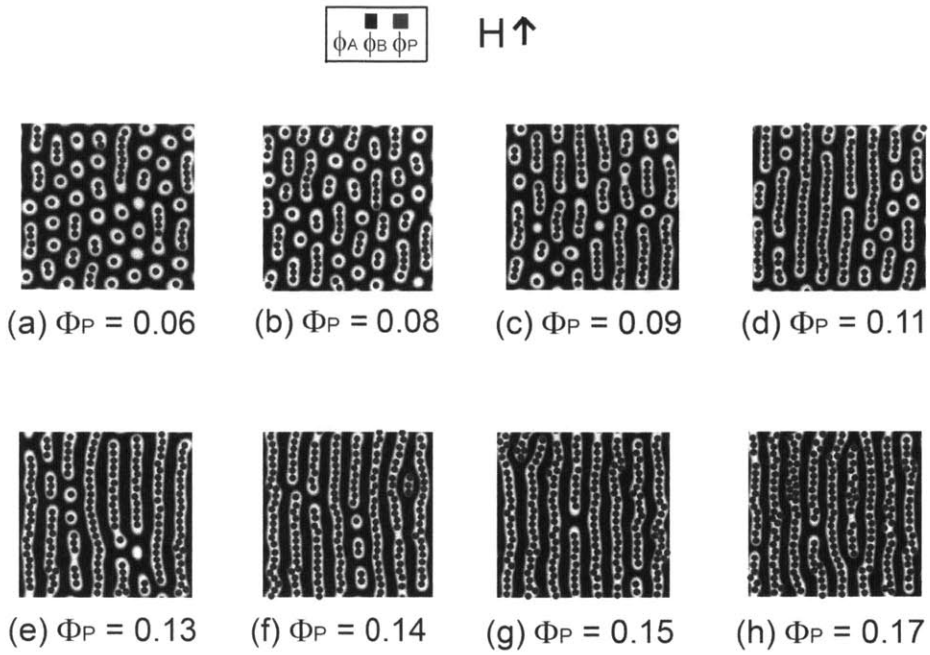

Figure 4.9. Effect of in-plane magnetic fields on the morphological transitions in the block copolymer as a function of nanoparticle loading, $f = 0.3$, $\chi_{AP}N = 0$, $\chi_{BP}N = 30$, $\chi_{AB}N = 20$, $\lambda = 9$, $R_P = 0.5\ R_g$

For $f = 0.5$ with an in-plane magnetic field (Figure 3.1m), extensive previous studies (*35, 39*) have clearly demonstrated the ability of the field to induce particle chaining and block copolymer alignment.

When the nanoparticles are selective for the majority block ($f = 0.7$), the hexagonal symmetry of the minority block is preserved in the presence of in-plane magnetic fields because the domains of the minority block are not stretched in the field direction (Figure 4.10). To accomplish this, the block copolymer lattice aligns with the <100> direction parallel to the superparamagnetic chains, resulting in control over the orientational order of the hexagonal phase. However, the addition of nanoparticles results in distortion of the hexagonal phase of the

block copolymer with a transition seen in the symmetry of block copolymer morphology from hexagonal to centered rectangular symmetry at higher nanoparticle volume fractions (Figure 4.10d).

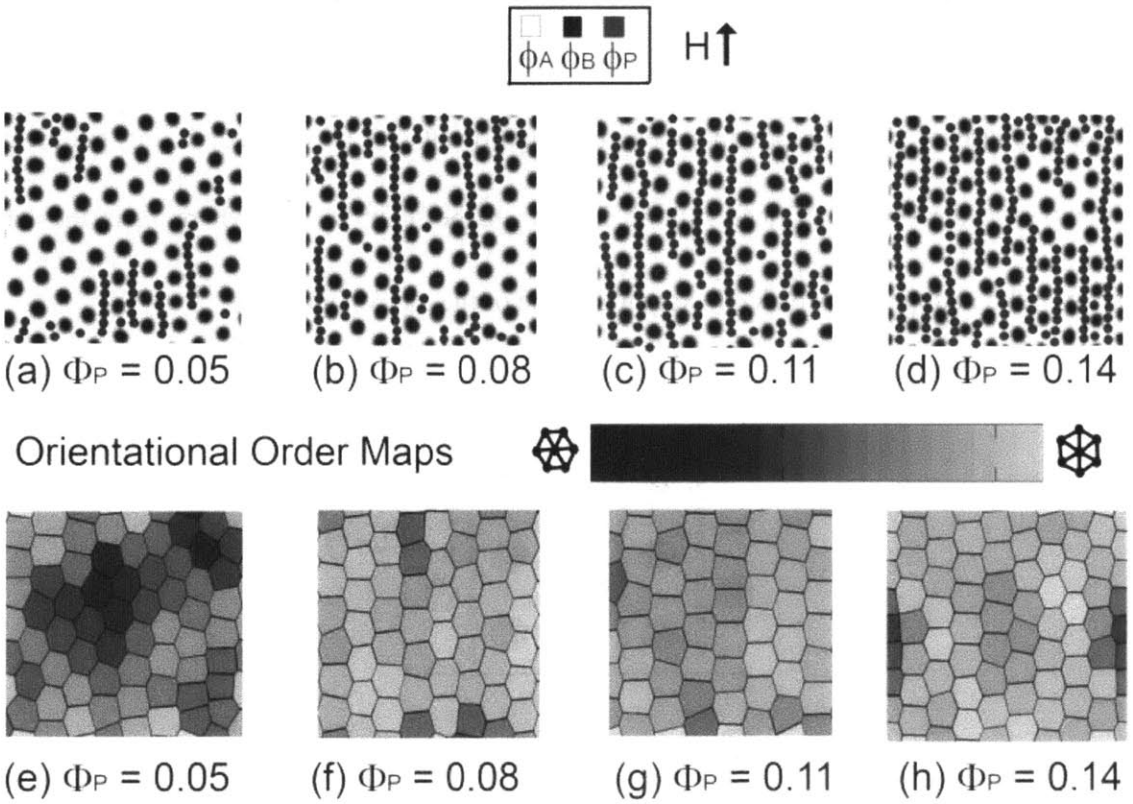

Figure 4.10. Orientational alignment of hexagonal phase of the minority block (B) by chaining of nanoparticles sequestered in the majority block (A) in the direction of external magnetic field ($\vec{H}$) along the y axis; $\lambda = 9$, $\chi_{BP}N = 30$, RP = 0.5 Rg, (a) Φ_P=0.05, (b) Φ_P=0.08, (c) Φ_P=0.1, (d) Φ_P=0.14; Red - green hexagons refer to dislocations, Voronoi maps shaded with orientational order parameter, for the corresponding volume fractions are given in (e – h).

Nevertheless, the orientation of the centered rectangular phases is in the direction of the external magnetic field along the <100> direction, evident from the orientational order maps

(Figure 4.10g). Beyond a critical volume fraction (Φ_P^{max}), structural frustration of the block copolymer due to dynamic confinement between parallel nanoparticle chains with spacing less than the lattice spacing causes complete distortion in the hexagonal phase of the block copolymer. For *single* nanoparticle chains confined between minority domains of the block copolymer matrix (Figure 4.11), the maximum volume fraction beyond which distortion of the hexagonal phase of block copolymer becomes significant can be derived. Using geometrical arguments, we derive this critical volume fraction to be $\Phi_P^{max} = \frac{\pi R_P}{\sqrt{3} L_I}$ where L_I is the lattice constant of the nanoparticle-loaded hexagonal phase of the block copolymer.

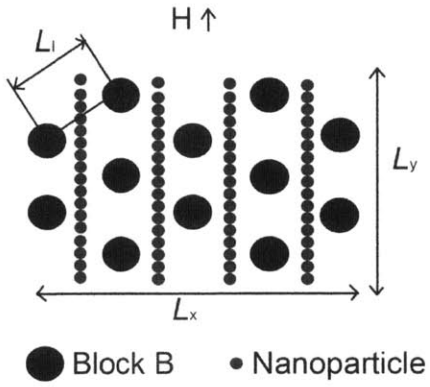

Figure 4.11. Schematic of alignment of hexagonal phase of the block copolymer (minority block B, black dots), by chaining of superparamagnetic nanoparticles (blue circles) in the presence of in-plane magnetic fields.

The number of nanoparticles is given by,

$$n_P = \frac{\Phi_P L_x L_y}{\pi R_P^2} \tag{4.8}$$

Where L_x, L_y are the dimensions of the simulation box (in units of R_g)

The number of nanoparticles required to form *single* complete chains (i.e. persistence length = L_y) is given by,

$$n_P = \frac{L_y}{2R_P} \cdot \frac{2L_x}{\sqrt{3}L_I} \tag{4.9}$$

where L_I is the lattice constant of the nanoparticle-loaded hexagonal phase of the block copolymer. From equations (4.8) and (4.9), we obtain the optimum volume fraction of the nanoparticles required to form complete chains and result in complete ordering of the hexagonal phase of the block copolymer,

$$\Phi_P^{max} = \frac{\pi R_P}{\sqrt{3}L_I} \tag{4.10}$$

Beyond this nanoparticle volume fraction (Φ_P^{max}), the nanoparticles are packed into forming multiple chains and distort the hexagonal phase of the block copolymer (Figure 4.12b).

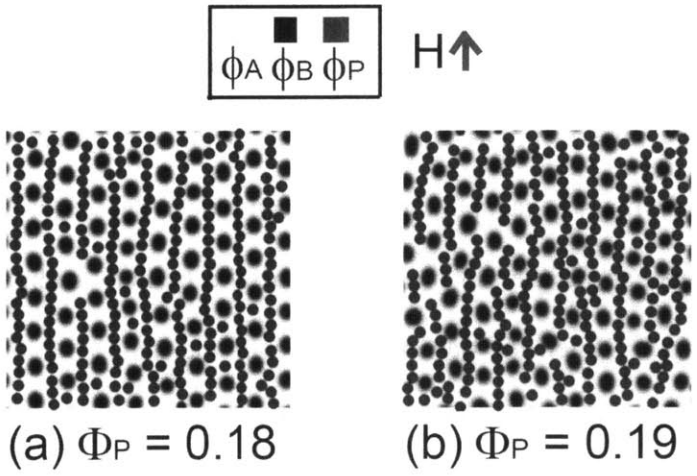

Figure 4.12. Distortion of hexagonal phase of the minority block at very high nanoparticle volume fractions, $f = 0.7$, $\chi_{AP}N = 0$, $\chi_{BP}N = 30$, $\chi_{AB}N = 20$, $\lambda = 9$, $R_P = 0.5\ R_g$. (a) $\Phi_P = \Phi_P^{max} = 0.18$, (b) $\Phi_P = 0.19 > \Phi_P^{max}$

For a nanoparticle radius of R_P = 0.5 R_g, the maximum volume fraction beyond which a complete distortion of the hexagonal/centered rectangular phases occurs is around 0.18. The alignment of the hexagonal/centered rectangular phase at this volume fraction can be seen in Figure 4.12a.

4.4 Conclusions

Dipolar interactions in superparamagnetic nanoparticles are demonstrated to have a large effect on the morphology of block copolymer nanocomposites. The materials display a variety of transitions based on field orientation, volume fraction of block copolymer, nanoparticle size, and nanoparticle loading. Matching of both the symmetry and characteristic spacing of the structures formed by the superparamagnetic nanoparticles and the block copolymers enables improvement of block copolymer ordering, while a mismatch in structures drives phase transitions between poorly ordered phases. In the case of asymmetric copolymers with nanoparticles selective for the minority block, an out of plane magnetic field may be used to drive the nanoparticles into a hexagonal lattice that can reduce defects in the block copolymers; geometrical arguments can be used to predict the specific particle loading required to achieve such a symmetry match. When the nanoparticles favor the majority block of an asymmetric block copolymer, application of an out of plane field leads to the formation of honeycomb lattices. Alternately, an in-plane field will produce superparamagnetic nanoparticle chains that can be used to orient the hexagonal phase of the block copolymer, provided the nanoparticles are selective for the majority block and are of appropriate size.

4.5 References

1. A. C. Balazs, T. Emrick, T. P. Russell, Nanoparticle Polymer Composites: Where Two Small Worlds Meet. *Science* **314**, 1107-1110 (2006).
2. M. R. Bockstaller, R. A. Mickiewicz, E. L. Thomas, Block Copolymer Nanocomposites: Perspectives for Tailored Functional Materials. *Advanced Materials* **17**, 1331 (2005).
3. M. Moniruzzaman, K. I. Winey, Polymer Nanocomposites Containing Carbon Nanotubes. *Macromolecules* **39**, 5194 (2006).
4. R. A. Vaia, E. P. Giannelis, Polymer Nanocomposites: Status and Opportunities. *MRS Bulletin* **26**, 394-401 (2001).
5. K. I. Winey, R. A. Vaia, Polymer Nanocomposites. *MRS Bulletin* **32**, 314-322 (2007).
6. R. A. Vaia, J. F. Maguire, Polymer Nanocomposites with Prescribed Morphology: Going beyond Nanoparticle-Filled Polymers. *Chemistry of Materials* **19**, 2736 (2007).
7. B. J. Kim, G. H. Fredrickson, E. J. Kramer, Effect of Polymer Ligand Molecular Weight on Polymer-Coated Nanoparticle Location in Block Copolymers. *Macromolecules* **41**, 436 (2007).
8. C. Xu, K. Ohno, V. Ladmiral, R. J. Composto, Dispersion of polymer-grafted magnetic nanoparticles in homopolymers and block copolymers. *Polymer* **49**, 3568 (2008).
9. M. Bockstaller, R. Kolb, E. L. Thomas, Metallodielectric Photonic Crystals Based on Diblock Copolymers. *Advanced Materials* **13**, 1783 (2001).
10. M. R. Bockstaller, E. L. Thomas, Proximity Effects in Self-Organized Binary Particle - Block Copolymer Blends. *Physical Review Letters* **93**, 166106 (2004).
11. G. A. Buxton, J. Y. Lee, A. C. Balazs, Computer Simulation of Morphologies and Optical Properties of Filled Diblock Copolymers. *Macromolecules* **36**, 9631 (2003).

12. A. C. Edrington, A. M. Urbas, P. DeRege, C. X. Chen, T. M. Swager, N. Hadjichristidis, M. Xenidou, L. J. Fetters, J. D. Joannopoulos, Y. Fink, E. L. Thomas, Polymer-Based Photonic Crystals. *Advanced Materials* **13**, 421 (2001).

13. Y. Fink, A. M. Urbas, M. G. Bawendi, J. D. Joannopoulos, E. L. Thomas, Block copolymers as photonic bandgap materials. *Lightwave Technology, Journal of* **17**, 1963 (1999).

14. G. A. Buxton, A. C. Balazs, Simulating the morphology and mechanical properties of filled diblock copolymers. *Physical Review E* **67**, 031802 (2003).

15. A. Haryono, W. H. Binder, Controlled Arrangement of Nanoparticle Arrays in Block-Copolymer Domains. *Small* **2**, 600 (2006).

16. J. Huh, V. V. Ginzburg, A. C. Balazs, Thermodynamic Behavior of Particle/Diblock Copolymer Mixtures: Simulation and Theory. *Macromolecules* **33**, 8085 (2000).

17. J.-Y. Lee, R. B. Thompson, D. Jasnow, A. C. Balazs, Entropically Driven Formation of Hierarchically Ordered Nanocomposites. *Physical Review Letters* **89**, 155503 (2002).

18. M. W. Matsen, R. B. Thompson, Particle Distributions in a Block Copolymer Nanocomposite. *Macromolecules* **41**, 1853 (2008).

19. V. Pryamitsyn, V. Ganesan, Strong Segregation Theory of Block Copolymer - Nanoparticle Composites. *Macromolecules* **39**, 8499 (2006).

20. A. J. Schultz, C. K. Hall, J. Genzer, Computer Simulation of Block Copolymer/Nanoparticle Composites. *Macromolecules* **38**, 3007 (2005).

21. R. B. Thompson, V. V. Ginzburg, M. W. Matsen, A. C. Balazs, Predicting the Mesophases of Copolymer-Nanoparticle Composites. *Science* **292**, 2469-2472 (2001).

22. R. B. Thompson, V. V. Ginzburg, M. W. Matsen, A. C. Balazs, Block Copolymer-Directed Assembly of Nanoparticles: Forming Mesoscopically Ordered Hybrid Materials. *Macromolecules* **35**, 1060 (2002).

23. M. R. Bockstaller, Y. Lapetnikov, S. Margel, E. L. Thomas, Size-Selective Organization of Enthalpic Compatibilized Nanocrystals in Ternary Block Copolymer/Particle Mixtures. *Journal of the American Chemical Society* **125**, 5276 (2003).

24. J. J. Chiu, B. J. Kim, E. J. Kramer, D. J. Pine, Control of Nanoparticle Location in Block Copolymers. *Journal of the American Chemical Society* **127**, 5036 (2005).

25. K. Tsutsumi, Y. Funaki, Y. Hirokawa, T. Hashimoto, Selective Incorporation of Palladium Nanoparticles into Microphase-Separated Domains of Poly(2-vinylpyridine)-block-polyisoprene. *Langmuir* **15**, 5200 (1999).

26. S.-W. Yeh, K.-H. Wei, Y.-S. Sun, U. S. Jeng, K. S. Liang, CdS Nanoparticles Induce a Morphological Transformation of Poly(styrene-b-4-vinylpyridine) from Hexagonally Packed Cylinders to a Lamellar Structure. *Macromolecules* **38**, 6559 (2005).

27. I. C. Alexander, C. B. Anna, Effect of particle size and shape on the order--disorder phase transition in diblock copolymers. *The Journal of Chemical Physics* **119**, 3529-3534 (2003).

28. M. K. Gaines, S. D. Smith, J. Samseth, M. R. Bockstaller, R. B. Thompson, K. Ã. Rasmussen, R. J. Spontak, Nanoparticle-regulated phase behavior of ordered block copolymers. *Soft Matter* **4**, 1609-1612 (2008).

29. Q. Pan, C. Tong, Y. Zhu, Self-Consistent-Field and Hybrid Particle-Field Theory Simulation of Confined Copolymer and Nanoparticle Mixtures. *ACS Nano* **5**, 123 (2011).

30. S. W. Sides, B. J. Kim, E. J. Kramer, G. H. Fredrickson, Hybrid Particle-Field Simulations of Polymer Nanocomposites. *Physical Review Letters* **96**, 250601 (2006).

31. J. U. Kim, B. O' Shaughnessy, Morphology Selection of Nanoparticle Dispersions by Polymer Media. *Physical Review Letters* **89**, 238301 (2002).

32. J. Y. Lee, Z. Shou, A. C. Balazs, Modeling the Self-Assembly of Copolymer-Nanoparticle Mixtures Confined between Solid Surfaces. *Physical Review Letters* **91**, 136103 (2003).

33. L. Zhou, Y. Ma, Phase behavior of nanoparticle copolymer films confined between polymer-grafted surfaces. *Journal of Physics Condensed Matter* **20**, 5006 (2008).

34. H. Kang, F. A. Detcheverry, A. N. Mangham, M. P. Stoykovich, K. C. Daoulas, R. J. Hamers, M. Muller, J. J. de Pablo, P. F. Nealey, Hierarchical Assembly of Nanoparticle Superstructures from Block Copolymer-Nanoparticle Composites. *Physical Review Letters* **100**, 148303 (2008).

35. G. He, A. C. Balazs, Modeling the Dynamic Behavior of Mixtures of Diblock Copolymers and Dipolar Nanoparticles. *Journal of Computational and Theoretical Nanoscience* **2**, 99 (2005).

36. C. Houyang, R. Eli, Nanoparticle aggregation in the presence of a block copolymer. *The Journal of Chemical Physics* **131**, 244904 (2009).

37. A. Yethiraj, Tunable colloids: control of colloidal phase transitions with tunable interactions. *Soft Matter* **3**, 1099-1115 (2007).

38. M. R. Hammond, H. Dietsch, O. Pravaz, P. Schurtenberger, Mutual Alignment of Block Copolymer-Magnetic Nanoparticle Composites in a Magnetic Field. *Macromolecules* **43**, 8340 (2010).

39. V. Raman, A. Bose, B. D. Olsen, T. A. Hatton, Long-Range Ordering of Symmetric Block Copolymer Domains by Chaining of Superparamagnetic Nanoparticles in External Magnetic Fields. *Macromolecules* **45**, 9373 (2012).

40. B. J. Kim, J. J. Chiu, G. R. Yi, D. J. Pine, E. J. Kramer, Nanoparticle-Induced Phase Transitions in Diblock-Copolymer Films. *Advanced Materials* **17**, 2618 (2005).

Chapter 5

Kinetics of Magnetic Field Induced Alignment of Block Copolymer Superparamagnetic Nanoparticle Composites

5.1 Introduction

In this chapter, we study the kinetics of ordering in diblock copolymer superparamagnetic nanoparticle mixtures subjected to uniform magnetic fields. We employ the external potential dynamics (EPD) method to evolve the potentials with time and calculate the volume fractions from the potentials (see chapter 2, section 2.2.2). The EPD method, introduced by Maurits and Fraaije (*1*), is a computationally efficient technique to study the phase separation dynamics of block copolymers (*2-4*), wherein the essential physics of the phase separation dynamics is preserved. In this method, the concentration/volume fraction of the monomer segments is a conserved quantity and the dynamics of the polymer chains is inherently of Rouse-type (*1*). This is the first attempt to use this technique to study the dynamics of structural evolution in block copolymer nanoparticle mixtures.

In this study, we consider a mixture of block copolymers and superparamagnetic nanoparticles. The block copolymers are modeled as continuous Gaussian chains and the nanoparticles as hard spheres. The "hard sphere" nature of the nanoparticles is imbibed in the free energy model through the finite compressibility assumption. $\left(\int d\vec{r} \left\{ \frac{k_H}{2} . (\varphi_A + \varphi_B + \varphi_P)^2 \right\} \right)$. The orientational ordering of the lamellar phase is quantified using orientational order

parameter (see chapter 3), whose temporal evolution is monitored to quantify the kinetics of alignment.

5.2 Simulation Methodology: External Potential Dynamics

All simulations are performed on a square 2D lattice of 128 by 128 grid points. The length of the simulation box is maintained at 16 R_g (all the length units are in terms of R_g, the unperturbed radius of gyration of the block copolymer). The block copolymer is characterized by the coil fraction, f, of the block that has the most favorable interaction with the nanoparticles. The Flory-Huggins interaction parameter between the blocks is denoted by χ_{AB}, while the selectivities of the nanoparticles for the two blocks A and B are denoted by χ_{AP} and χ_{BP}, respectively. N is the total degree of polymerization of the block copolymer chain. The statistical segment lengths of the A and B blocks are assumed to be equal, and the overall nanoparticle volume fraction is denoted by Φ_P. The dipolar interactions are characterized by the parameter λ, the ratio of the dipolar interaction energy to the thermal energy (k_BT). The dipole moments are assumed to align in the direction of the applied magnetic field, a valid assumption when the external magnetic field strength is much larger than the saturation magnetization strength of the nanoparticle. Periodic boundary conditions are applied in x-y directions for both the nanoparticles and the block copolymer. The use of cavity functions (*5*) maps the location of nanoparticles in the continuous space onto the finite collocation grid (see chapter 3, and 4). The conservation equation for the volume fraction of monomer segments is solved on this grid. The equivalent evolution equation for the potential fields (section 2.2.2) is solved using the Runge-Kutta 4^{th} order method. The resolution of the contour length for the modified diffusion equations was maintained at $\Delta s = 0.005$ (using 201 contour points along the polymer chain).

We briefly review the equations comprising the EPD technique. The evolution equations for the potential fields are given by (from 2.24),

$$\frac{\partial w_A}{\partial t} = -M_{Poly}\nabla^2\{\chi_{AB}N\varphi_B + \chi_{AP}N\varphi_P - w_A + k_H.(\varphi_A + \varphi_B + \varphi_P - 1) + \eta_A\}$$

(5.1a)

$$\frac{\partial w_B}{\partial t} = -M_{Poly}\nabla^2\{\chi_{AB}N\varphi_A + \chi_{BP}N\varphi_P - w_B + k_H.(\varphi_A + \varphi_B + \varphi_P - 1) + \eta_B\}$$

(5.1b)

We have assumed the diffusivities or the mobilities of both the monomer segments to be equal ($M_A = M_B = M_{poly}$), and the update equation for the nanoparticle positions is given by,

$$\Delta\vec{r}_j = M_{Par}\Delta t.\{\vec{F}_{j,poly} + \vec{F}_{j,dipolar}\} + \vec{R}_j = \Delta t_{Par}.\{\vec{F}_{j,poly} + \vec{F}_{j,dipolar}\} + \vec{R}_j$$

(5.2)

Since, the unit of length scale is common throughout (i.e. R_g), we have the following relation,

$$\frac{\Delta t_{Par}}{\Delta t_{Poly}} = \frac{M_{Par}}{M_{Poly}} = \sigma \tag{5.3}$$

σ is the ratio of mobilities (nanoparticle to polymer). Thus, the mobility of the nanoparticle is changed in the simulation by changing the time step for nanoparticle update ($\Delta t_{Par} = \sigma\Delta t_{Poly}$).

In all the simulations, the following parameters are kept constant, unless otherwise specified explicitly; (1) the radius of the nanoparticle is kept fixed at 0.5 R_g, (2) the interaction strength between the two monomer blocks ($\chi_{AB}N = 20$), (3) $\Delta t_{poly} = M_{poly}.\Delta t = 0.025$, (4) $\kappa_H N = 500$.

5.3 Results

5.3.1 Nanoparticle Dipolar Strength

Figure 5.1 illustrates the structural evolution of block copolymer superparamagnetic nanoparticle composite as a function of time. The mobility of the nanoparticles is lower than the mobility of the monomer segments and the external magnetic field is applied along the y axis.

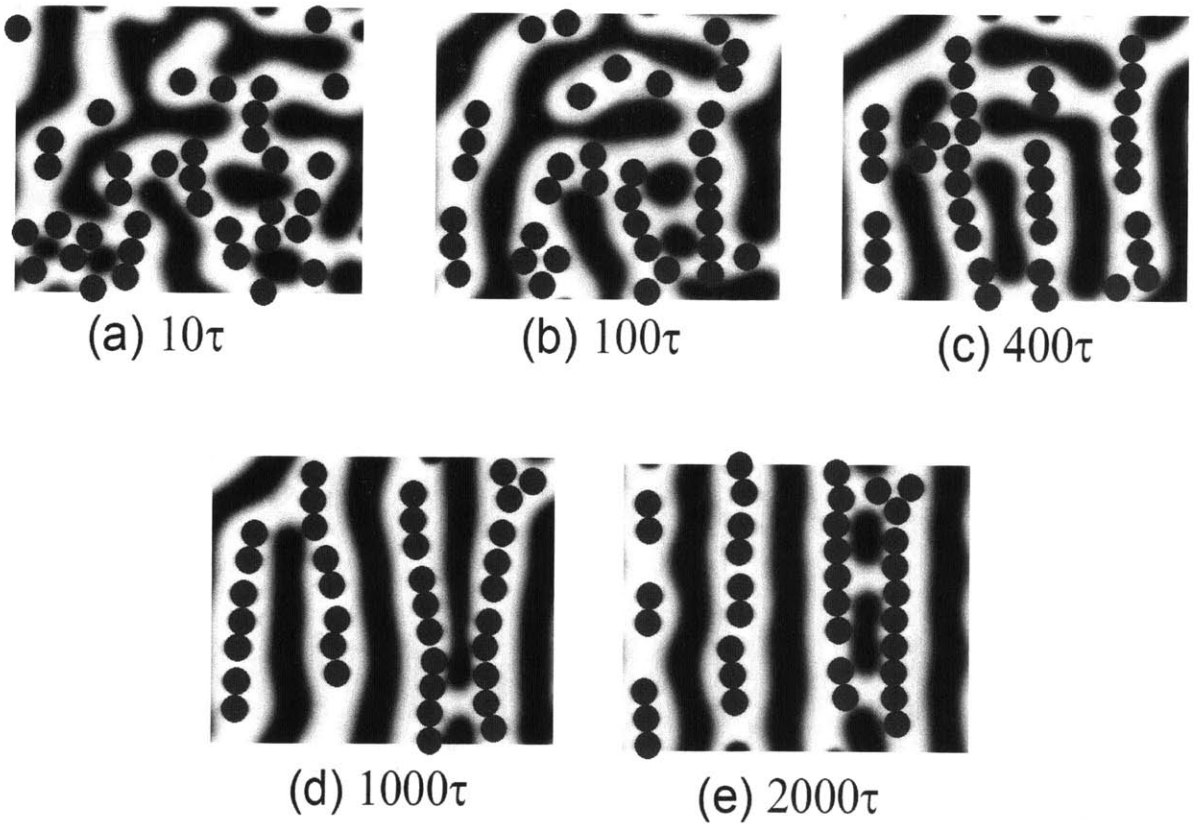

Figure 5.1. Structural evolution of block copolymer superparamagnetic nanoparticle composite subjected to external magnetic field applied along y axis; filled contour plot of volume fraction of monomer A (blue circles represent nanoparticles). $\lambda = 15$, $\chi_{AB}N = 20$, $\chi_{BP}N = 30$, R_P =0.5 R_g, Φ_P=0.11, $\tau = 2.5 * 10^2 \Delta t_{poly}$, σ=0.2, domain spacing = 4 R_g, L = 16 R_g.

The initial condition for this set of simulations is the phase separated block copolymer melt in which the nanoparticles are sequestered preferentially in block A. The lamellae have random orientation initially and the nanoparticles are magnetized to their saturation magnetization upon application of the external magnetic field.

To study the effect of dipolar interactions, the dipolar interaction parameter (λ) is varied from 3 to 15 and the structural evolution is monitored.

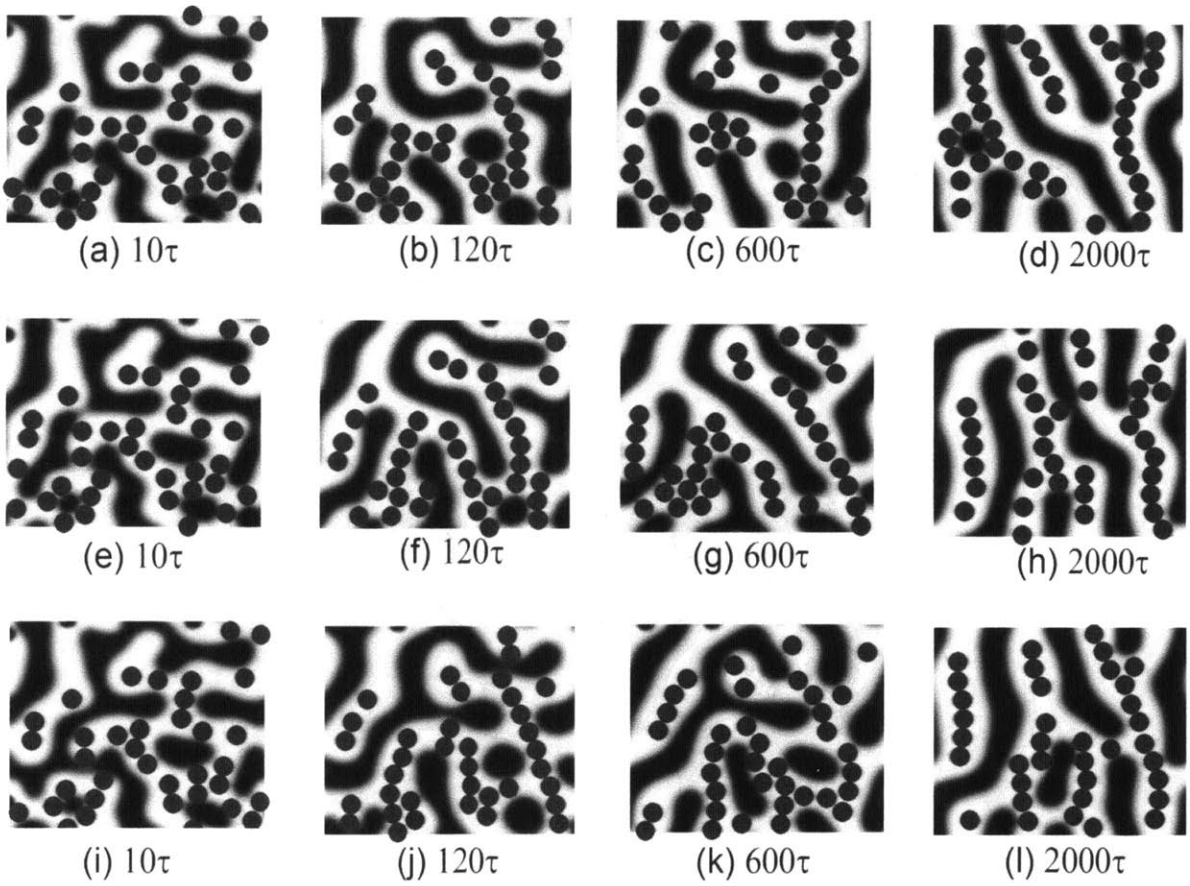

Figure 5.2. Effect of dipolar interactions on the alignment of block copolymer nanocomposite, (a) – (d) $\lambda = 3$, (e) – (h) $\lambda = 5$, (i) – (l) $\lambda = 9$, $\chi_{AB}N = 20$, $\chi_{BP}N = 30$, R_P =0.5 R_g, Φ_P=0.11, $\tau = 2.5 * 10^2 \Delta t_{poly}$, σ=0.2.

Figure 5.2 illustrates the effect of dipolar interactions on the block copolymer nanocomposite. Relatively faster alignment is seen for higher dipolar interaction strength. In order to quantify the effect of dipolar interactions on the alignment of the domains, we run simulations on a larger box size of L = 32 R_g with 256 collocation points. We plot the temporal evolution of the orientational order parameter for different dipolar interaction strengths (Figure 5.3). Faster alignment is clearly seen for $\lambda = 15$. The orientational order parameter reaches its peak value (of 0.84) within a short span of time. For $\lambda = 9$, it takes slightly longer time for the orientational order parameter to reach the peak value (of 0.82). For $\lambda = 3$, the domains get stuck in a partially aligned state and the peak value of only 0.6 reached.

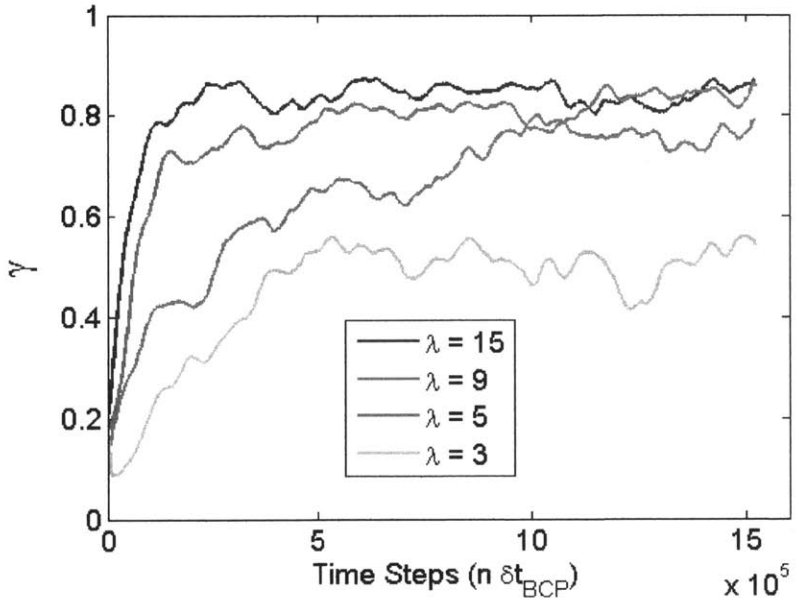

Figure 5.3. Temporal evolution of orientational order parameter (γ) for different dipolar interaction strengths, L = 32 R_g, $\chi_{AB}N$ = 20, $\chi_{BP}N$ = 30, R_P =0.5 R_g, Φ_P=0.11, $\tau = 2.5 * 10^2 \Delta t_{poly}$, σ=0.2.

5.3.2 Effect of Nanoparticle-Block Copolymer Interaction

Simulations were performed keeping the interaction between nanoparticles and block A ($\chi_{AP}N$ = 0) fixed while varying the interaction between the nanoparticles and the block B ($\chi_{BP}N$ = 22 to 50). Figure 5.4 shows temporal evolution of orientational order parameter for different block copolymer nanoparticle interaction strengths. The nanoparticle mobilities are lower than those used before (σ=0.04).

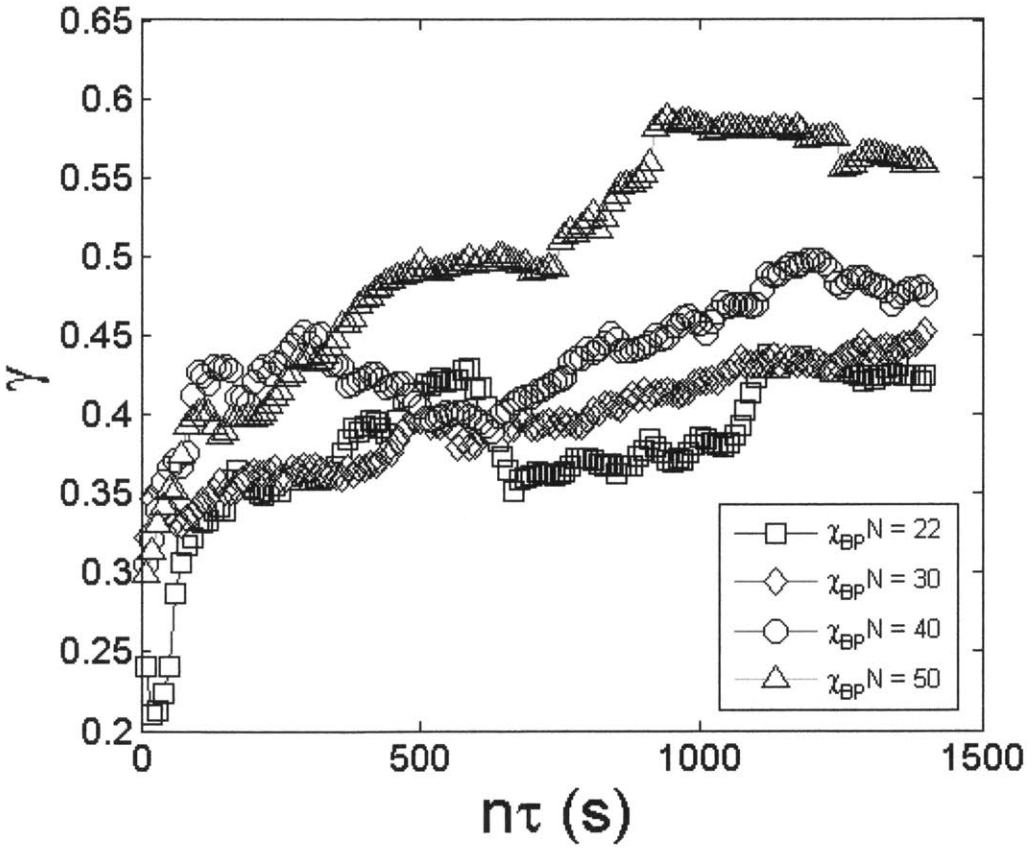

Figure 5.4. Effect of nanoparticle-block B interaction strength on the structural evolution of the block copolymer nanocomposite; higher interaction strength leads to faster alignment of lamellae along the magnetic field direction. $\lambda = 9, \chi_{AB}N = 20, \chi_{AP}N = 0, R_P = 0.5\ R_g, \Phi_P = 0.11, \tau = 2.5 * 10^2 \Delta t_{poly}$, σ=0.04.

Repulsive interactions between block B and the nanoparticles, that are stronger than repulsive interactions between block B and block A, result in effective "attraction" of the block A towards the nanoparticles. This is different from the case when $\chi_{AP}N < 0$, which indicates affinity of block A towards nanoparticle surface. Higher the nanoparticle-block B interaction strength, there is more likelihood of rearrangement of polymer segments around the nanoparticle. This causes ordering of the block copolymer domains when the nanoparticles chain along the direction of the field. From equilibrium studies, we found that there exists critical interaction strength of $(\chi_{BP}N)_{critical} = 22$ (see chapter 3, section 3.3.5) for alignment to occur.

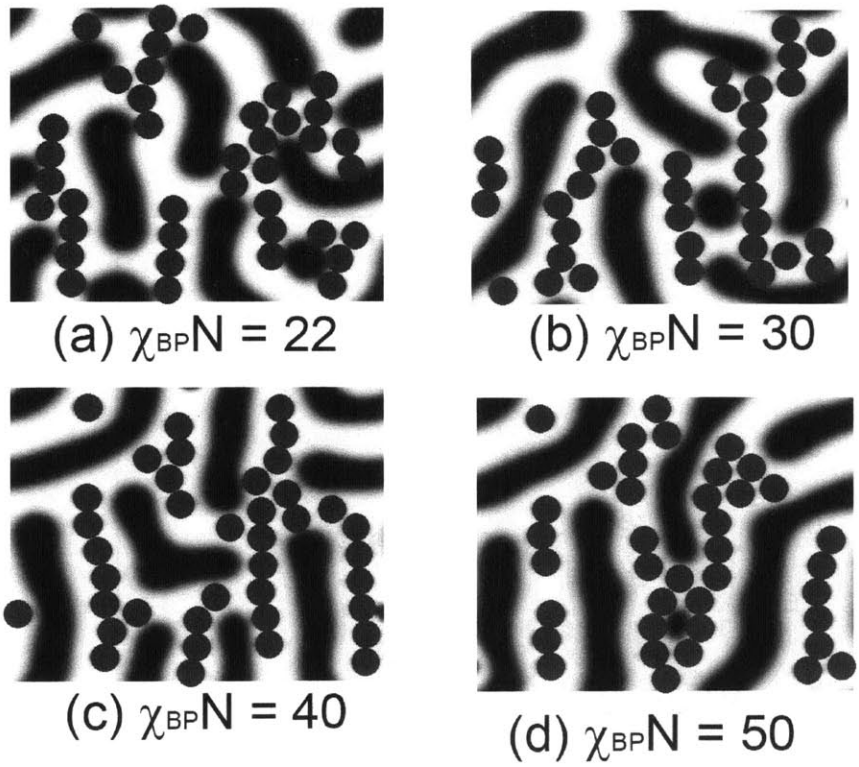

Figure 5.5. Block Copolymer nanocomposite at t = 1400τ. $\lambda = 9$, $\chi_{AB}N = 20$, $\chi_{AP}N = 0$, R_P =0.5 R_g, Φ_P=0.11,$\tau = 2.5 * 10^2 \Delta t_{poly}$, σ=0.04, (a) $\chi_{BP}N = 22$, (b) $\chi_{BP}N = 30$, (c) $\chi_{BP}N = 40$, (d) $\chi_{BP}N = 50$.

As seen from Figure 5.4, faster alignment is seen for higher interaction strength between the nanoparticle and the block B. Figure 5.5 shows the structure of the block copolymer nanocomposite at t = 1400 τ for different nanoparticle-block B interactions.

5.3.3 Effect of Nanoparticle Mobility

The nanoparticle mobility is varied by changing the time step for updates for the nanoparticle moves in Brownian dynamics simulation, provided the numerical stability considerations are met. Higher value of σ implies higher mobility of the nanoparticle. The value of σ is varied from 0.04 to 0.2. Figure 5.6 shows the effect of change in the mobility of the nanoparticles. Higher mobility of the nanoparticles (for the ranges of mobilities studied) results in faster alignment of the block copolymer.

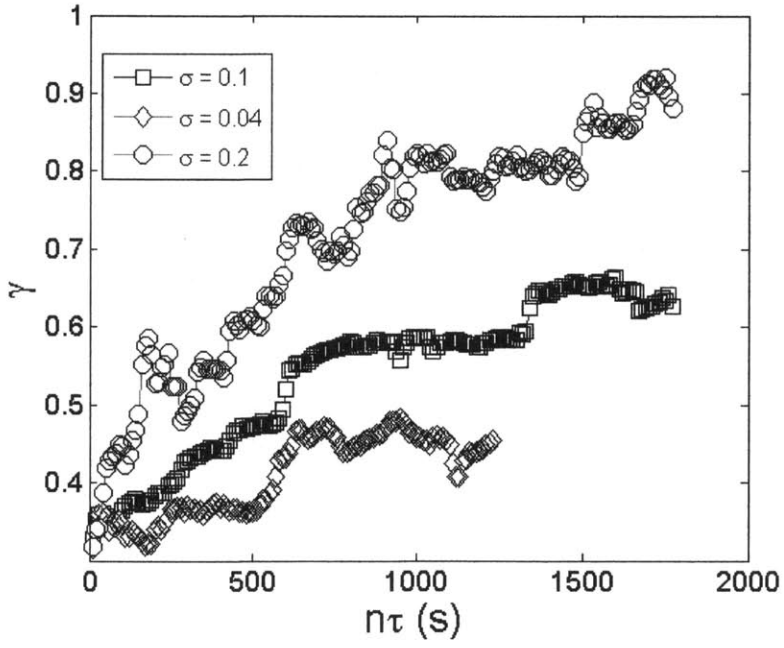

Figure 5.6. Effect of nanoparticle mobility on the alignment of block copolymer, $\lambda = 15$, $\chi_{AB}N = 20$, $\chi_{BP}N = 30$, R_P =0.5 R_g, Φ_P=0.11,$\tau = 2.5 * 10^2 \Delta t_{poly}$.

However, when the nanoparticle mobility is increased further, $\sigma = 0.4$, the nanoparticle takes bigger jumps and delays the coarsening of the block copolymer domains. As seen in Figure 5.7, we see that the block copolymer shows poor ordering for $\sigma = 0.4$.

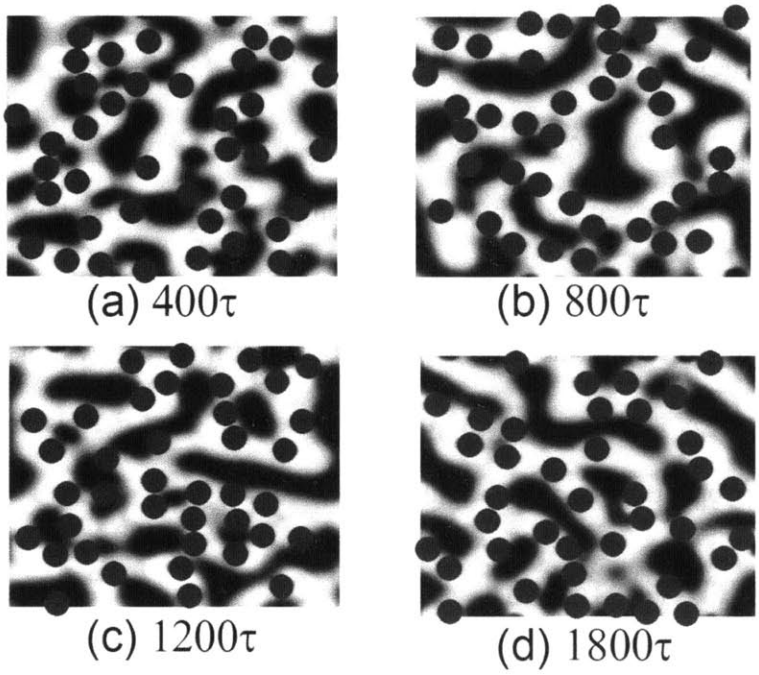

Figure 5.7. Effect of high nanoparticle mobility on block copolymer ordering, $\lambda = 15$, $\chi_{AB}N = 20$, $\chi_{BP}N = 30$, R_P =0.5 R_g, Φ_P=0.11,$\tau = 2.5 * 10^2 \Delta t_{poly}$.

These results seem to suggest that there is a critical limit up to which the nanoparticle mobility can enhance the ordering process. Beyond this limit, the mobility of nanoparticle can be detrimental to the ordering process and the ordering process is delayed due to frequent redistribution of the monomer segments brought about by the large jumps in the nanoparticle position.

5.3.4 Conclusions

The applicability of EPD technique to study ordering in block copolymer nanocomposites was demonstrated in this section. Preliminary results for relatively small box sizes seem to suggest that dipolar interaction strength plays a major role in the kinetics of alignment. Higher dipolar interaction strength leads to faster alignment, whereas higher mobility of nanoparticles is beneficial to up to a critical limit. Higher nanoparticle-block B interaction strength seems to quicken the ordering process as evident from the temporal evolution of the orientational order parameter. This study stops short of making detailed claims about the ordering and defect annihilation mechanisms due to the limitations of the small box size. A more detailed analysis using a much larger box size to accurately capture the statistics of defects annihilation will be undertaken as follow up study for a future publication.

5.4 Results from TDGL Method

For large scale simulations we use Cell Dynamics Simulation (CDS) technique as it is computationally efficient. It describes the phase separation dynamics qualitatively and preserves the essential scaling laws of domain coarsening observed in phase separating systems such as block copolymers and polymer blends (*6, 7*). We study the defect annihilation in the hexagonal phase of block copolymers and demonstrate the effect of repulsive dipolar interactions on defect annihilation dynamics. This model considers the nanoparticles as "soft spheres" and allows for non-zero order parameter (see chapter 2, section 2.2.3) inside the nanoparticles. Hence these results do not accurately capture the order to order (OOT) phase transitions due to the excluded volume interactions between the nanoparticles and block copolymers.

A square 2D lattice of 128 by 128 grid points is considered. The simulation box size is kept fixed at 64 R_g and the nanoparticle size is kept fixed at R_P = 0.5 R_g. The parameters of the simulation (see chapter 2, section 2.2.3) are chosen so as to obtain the hexagonal phase of the block copolymer,$f = 0.3,\ \alpha = 0.06,\ \tau = 0.3,\ \sigma = 0.23,\ \upsilon = 0.38,\ \beta = 0.03,\ D = 0.3$ (*8*). The noise amplitude is kept fixed at $\eta_o = 0.25$, and is calculated using the criterion mentioned in (*8*). The interaction strength between the nanoparticles and the block copolymer, and the dipolar interaction strength are varied in the set of simulations discussed in the following sections.

5.4.1 Defect Annihilation in Hexagonal Phase of Block Copolymers

In a perfect hexagonal lattice, each lattice point has 6 nearest-neighbors (NN). In a typical asymmetric block copolymer forming a hexagonal phase, the minority nanodomains form a hexagonal lattice. In polycrystalline morphology, not all the minority domains have 6 NN, while some have 5 NN, others have 7 NN. These defects occur in pairs and are termed as '5-7 defects'. We monitor the temporal evolution of total number of such defects, using Voronoi tessellation of the morphologies (*8*), and study the rate at which the total number of defects decreases at various stages of domain coarsening/ordering process.

5.4.1.1 Effect of Nanoparticle Dipolar Interaction Strength

For a typical asymmetric block copolymer (f = 0.3) forming a hexagonal phase (in 2D), the defect scaling follows $1/3^{rd}$ law during initial stages of coarsening while $1/5^{th}$ scaling law is observed during the late stages. A typical scaling law for defect annihilation is expressed as,

$$f_d = Ae^{-\frac{1}{\Gamma}} \tag{5.4}$$

f_d is the defect concentration (number of defects per unit area), A is an arbitrary constant, Γ is the defect scaling exponent. $\Gamma = 3$ during early stages of the ordering process and $\Gamma = 5$ during the late stages of the ordering process.

The basic strategy for defect annihilation using superparamagnetic nanoparticles is as follows. Under out of plane magnetic fields, the repulsive dipolar interactions between the nanoparticles force them to form a hexagonal lattice. Due to the long-range nature of the dipolar interactions, the defect concentration in the hexagonal lattice of nanoparticles is lower. Therefore, we envisage employing this long-ranged nature of dipolar interactions to reduce the defect density in the hexagonal lattice formed by the nanodomains of the asymmetric block copolymer. In order to realize faster defect annihilation using this technique, we anticipate sufficient interaction strength between the nanoparticle and the minority block (Vo) as an important requisite for an efficient redistribution or re-ordering of the minority domains around the nanoparticles; provided other parameters such as nanoparticle size, loading etc are chosen appropriately so as to obtain symmetry matching conditions (see chapter 4, section 4.3.2).

For symmetry matching conditions (see chapter 4, section 4.3.2), we use a nanoparticle volume fraction of $\Phi_P \cong 0.06$ in this study, and the nanoparticle size is chosen to be $R_P = 0.5\ R_g$. Under these conditions, we have exactly one nanoparticle per minority nanodomain. The dipolar interaction strength is varied and the defect annihilation scaling is studied. Figure 5.8 shows the effect of dipolar interaction on the defect annihilation of hexagonal morphology. Higher dipolar interaction strength results in faster rate of decrease in the defect concentration.

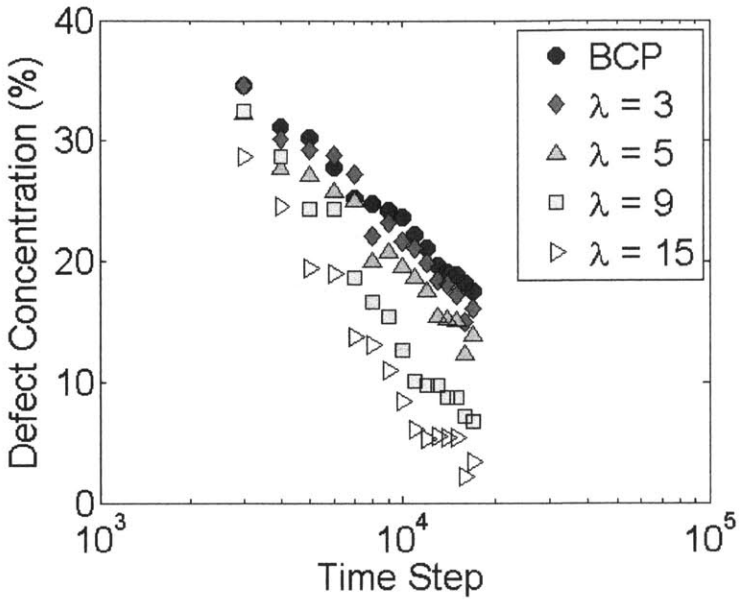

Figure 5.8. Effect of dipolar interaction on the kinetics of defect annihilation in hexagonal morphology, $\Phi_P \cong 0.06$, $V_o = \beta = 0.03$, $f = 0.3$, $\alpha = 0.06$, $\tau = 0.3$, $\sigma = 0.23$, $\upsilon = 0.38$, $D = 0.3$, L = 64 R_g.

5.4.1.2 Effect of Nanoparticle Surface Affinity

The interaction free energy between the nanoparticle and block copolymer in the TDGL model is expressed as (see chapter 2, section 2.2.3),

$$V(\vec{r} - \vec{R}_i) = V_o e^{-\left(\frac{|\vec{r}-\vec{R}_i|}{R_P}\right)} \tag{5.5}$$

We vary the interaction strength V_o and study its effect on the kinetics of defect annihilation. From Figure 5.9 we observe that higher interaction strength V_o results in faster defect annihilation.

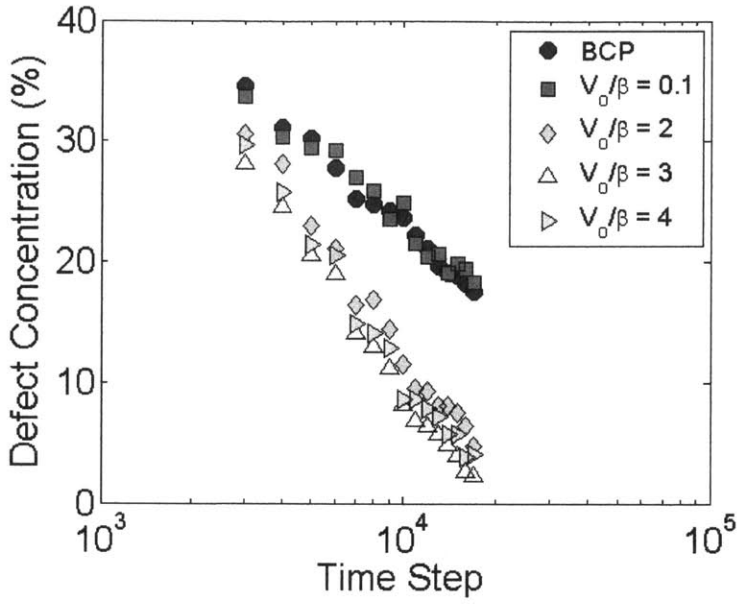

Figure 5.9. Effect of nanoparticle-block copolymer interaction on the kinetics of defect annihilation, the dipolar interaction strength, $\lambda = 9$, $\Phi_P \cong 0.06$, $\beta = 0.03$, $f = 0.3$, $\alpha = 0.06$, $\tau = 0.3$, $\sigma = 0.23$, $\upsilon = 0.38$, $D = 0.3$, L = 64 R_g.

5.5 Conclusions

This chapter provides a preliminary analysis of kinetics of alignment in symmetric block copolymers (using EPD technique) and kinetics of defect annihilation in asymmetric block copolymers (using TDGL model). We observe that dipolar interactions have significant effect on the ordering process. The kinetics of alignment is altered upon introduction of superparamagnetic nanoparticles. The results are obtained for smaller box sizes (16 R_g), nevertheless, they do provide a qualitative picture of rate of alignment and its dependence on the system parameters such as the nanoparticle mobility, the dipolar interaction strength and the

nanoparticle-polymer interaction strength. The EPD technique is employed for the first time to study the dynamics of block copolymer nanocomposites.

5.6 References

1. N. Maurits, J. Fraaije, Mesoscopic dynamics of copolymer melts: From density dynamics to external potential dynamics using nonlocal kinetic coupling. *The Journal of chemical physics* **107**, 5879 (1997).

2. X. He, F. Schmid, Dynamics of spontaneous vesicle formation in dilute solutions of amphiphilic diblock copolymers. *Macromolecules* **39**, 2654-2662 (2006).

3. E. Reister, M. Müller, Formation of enrichment layers in thin polymer films: The influence of single chain dynamics. *The Journal of chemical physics* **118**, 8476 (2003).

4. X. He, F. Schmid, Spontaneous formation of complex micelles from a homogeneous solution. *Physical review letters* **100**, 137802 (2008).

5. S. W. Sides, B. J. Kim, E. J. Kramer, G. H. Fredrickson, Hybrid Particle-Field Simulations of Polymer Nanocomposites. *Physical Review Letters* **96**, 250601 (2006).

6. Y. Oono, S. Puri, Computationally efficient modeling of ordering of quenched phases. *Physical review letters* **58**, 836-839 (1987).

7. Y. Oono, S. Puri, Study of phase-separation dynamics by use of cell dynamical systems. I. Modeling. *Physical Review A* **38**, 434-453 (1988).

8. D. A. Vega, C. K. Harrison, D. E. Angelescu, M. L. Trawick, D. A. Huse, P. M. Chaikin, R. A. Register, Ordering mechanisms in two-dimensional sphere-forming block copolymers. *Physical Review E* **71**, 061803 (2005).

Chapter 6

Scope for Future Work

The main goal of thesis was to study the effect of dipolar interactions on the structure of the block copolymer superparamagnetic nanoparticle composites. We employed a variety of simulation techniques to study the thermodynamics and kinetics of self-assembly occurring in such novel systems wherein external magnetic field can tune the structure formation of one of the components of the composite (i.e. the nanoparticles). This is one of the first studies to exhaustively investigate particle-particle interactions and their effect on the morphologies of the block copolymer nanocomposite. The simulation techniques account for excluded volume interactions between the nanoparticles and the block copolymer and hence capture the OOT accurately.

While this is just a first step towards understanding the role of particle-particle interactions on the structure of block copolymer nanocomposites, we envisage this has tremendous scope for future work. Some of the possible avenues to explore could be:

1. **Role of Nanoparticle Geometry**: We assumed throughout this work, that nanoparticles are hard spheres. While this may be a good first approximation, in reality, the nanoparticles can be of different shapes. It would be interesting to study the effect of nanoparticle shape on the morphology of the nanocomposite.
2. **Role of Nanoparticle Size Distribution**: We assumed that the nanoparticles are monodisperse. In experiments, log-normal distribution of nanoparticles is typically

observed during synthesis of superparamagnetic nanoparticles. All the simulation techniques and methods of analysis mentioned in this thesis could be very easily extended to include nanoparticle size distributions instead of just monodisperse nanoparticles. Important engineering questions could be answered by this study such as what are the allowed particle size distributions that yield good orientational ordering of block copolymers.

3. **Effect of Non-Uniform Magnetic Fields**: We assumed that the external magnetic fields are uniform. Gradation in magnetic fields can result in agglomeration of magnetic nanoparticles causing a high local concentration of nanoparticles, subsequently resulting in a morphological transition locally.
4. **Anisotropic Particle-Polymer Interactions**: We could have anisotropy in the nanoparticle-polymer interactions. Janus nanoparticles with two different surface affinities are well known. It would be interesting to study the effect of dipolar nanoparticles that have anisotropic surface interactions with the block copolymer.
5. **Block Architecture**: All the simulation techniques can be easily extended to different block architectures such as linear tri-block copolymers, star-block copolymers etc. This drastically widens the number of simulation parameters and could be daunting task.